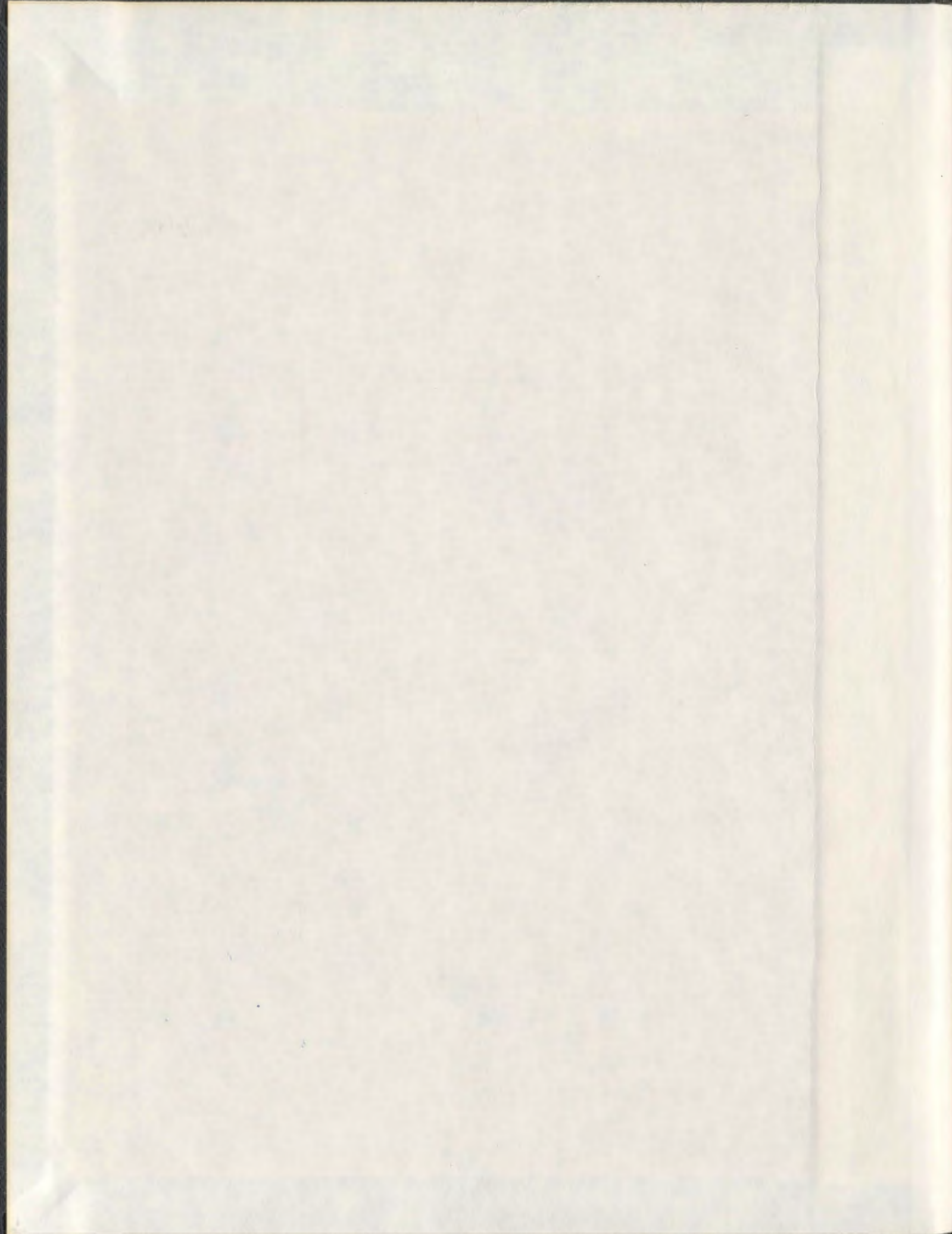


**INVESTIGATING SOIL/PIPELINE INTERACTION
DURING OBLIQUE RELATIVE MOVEMENTS**

NASSER DAIYAN



INVESTIGATING SOIL/PIPELINE INTERACTION DURING OBLIQUE
RELATIVE MOVEMENTS

by

© Nasser Daiyan

A thesis submitted to the School of Graduate
Studies in partial fulfilment of the
requirements for the degree of
Doctor of Philosophy

Faculty of Engineering and Applied Science
Memorial University of Newfoundland

February 2013

St. John's

Newfoundland

ABSTRACT

An understanding of the soil restraint on pipelines due to relative pipe/soil movements is important to assess the pipeline's strain response during large ground displacements. The interaction between soil and pipeline can affect serviceability and integrity of pipelines.

Current engineering practice for pipe/soil interaction is based on an idealized pipeline and soil numerical structural model that evaluates a pipeline's mechanical response using beam elements and soil behavior using discrete spring system. The load-displacement relationships are provided in the state of practice for principal directions (i.e. longitudinal, lateral horizontal, vertical upward and vertical downward).

Recent studies have indicated that in complex pipe/soil relative movements (e.g. axial-lateral or lateral-vertical directions) assuming no interaction among the loads applied to the pipe at different directions is not valid. Therefore, there is a need for more advanced numerical tools and engineering guidelines to assess the pipeline's response in complex loading conditions and reduce technical uncertainty.

This thesis has investigated the complex soil failure processes and load transfer mechanisms during nonlinear, oblique pipeline/soil interaction events associated with large permanent ground deformations. The oblique loading events considered include combined axial-lateral and axial-vertical (upward) relative pipeline/soil displacements in frictional soils, and lateral-vertical pipeline/soil interactions in both frictional and cohesive soils.

A series of centrifuge tests of pipelines displaced in a horizontal plane through sand have been conducted for different relative angles between the pipe longitudinal axis and the transverse lateral loading direction. A three-dimensional continuum finite element model was developed using ABAQUS/Standard (Hibbitt et al. 2005) software. The numerical model is validated against experimental results and is used to extend the physical investigation results through parametric studies.

Interaction diagrams that characterize the coupled soil load-displacement mechanisms were developed and compared with other yield surfaces in the public domain literature. Alternative soil-spring formulations that account for coupled soil deformation mechanisms during oblique pipeline/soil interaction events have been proposed based on interaction diagrams. The effects of this alternative soil-spring formulation on pipelines responses via structural finite element models are shown and discussed in Appendix B of this thesis.

ACKNOWLEDGEMENT

I would like to express my sincere appreciation to those who supported me during my PhD program. Particularly I am greatly thankful to my supervisor Dr. Shawn Kenny for his guidance, support and keen ideas and comments through this research program. I would like to thank Dr. Ryan Phillips, my co-supervisor, for his innovative ideas and insights to the problem and detail reviewing all documents and reports. I would like to express my gratitude to Dr. Radu Popescu, my co-supervisor, for his broad knowledge, detail comments and warm and encouraging words in difficult days. I consider myself a lucky graduate student to benefit from a supervisory committee whose expertise spans from pipeline engineering to experimental and numerical modeling in geotechnical engineering, which covers every aspect of this research program.

I would like to thank C-CORE centrifuge lab team; Mr. Gerry Piercy, Mr. Derry Nickol, Mr. Don Cameron and Mr. Karl Tuff who helped me a lot during the experimental program. Appreciation goes to Mr. John Barrette of C-CORE, who provided me with additional processing capacity during the numerical modeling. I am grateful to my officemates Hiva Mahdavi and Farzad Eskandari for the friendly environment of our office and great discussions.

I wish to acknowledge the funding and awards provided for this research program by C-CORE, MITACS, NSERC DG, NSERC MRS and School of Graduate Studies of Memorial University of Newfoundland. Also I would like to thank the Faculty of

Engineering and Applied Science for the teaching opportunities provided for me as a teaching assistant.

Finally I should thank Marjan, my wife, for her support and patience during my studies and all the ups and downs that we went through throughout these years. I am grateful to my parents' devotion and unconditional love. Their invaluable support has always been pushing me forward in every step of my life. I would like to thank my sister and my brothers for their encouragement and assistance. It was impossible for me to be where I am today, if I did not have such a wonderful family.

Table of Contents

ABSTRACT	II
ACKNOWLEDGEMENT	IV
LIST OF TABLES.....	VIII
LIST OF FIGURES.....	IX
LIST OF ABBREVIATIONS AND SYMBOLS.....	XIII
LIST OF APPENDICES.....	XV
1 INTRODUCTION	1
1.1 BACKGROUND	1
1.2 PROBLEM STATEMENT.....	2
1.3 PURPOSE OF STUDY.....	4
1.4 THESIS OUTLINE.....	5
2 LITERATURE REVIEW	7
2.1 INTRODUCTION.....	7
2.2 CURRENT ENGINEERING PRACTICE.....	7
2.3 COUPLED WINKLER MODELS.....	10
2.4 PIPELINE/SOIL INTERACTION	11
2.4.1 Axial (longitudinal) pipe/soil interaction	11
2.4.2 Lateral (horizontal) pipe/soil interaction	18
2.4.3 Vertical pipe/soil interaction.....	35
2.4.4 Axial-lateral pipe/soil interaction.....	44
2.4.5 Lateral-vertical pipe/soil interaction.....	47
2.5 CONCLUDING REMARKS.....	52
3 CENTRIFUGE TESTS PREPARATIONS AND PROCEDURES	54
3.1 INTRODUCTION	54
3.2 A SUMMARY OF CENTRIFUGE PRINCIPLES AND SCALING LAWS	55
3.3 TEST APPARATUS	56
3.3.1 Load cells.....	57
3.3.2 Displacement transducers	60
3.4 SOIL TEST BED.....	62
3.5 SUMMARY	66
4 EXPERIMENTAL DATA.....	68
4.1 DISPLACEMENT CORRECTION	68
4.2 LATERAL TEST (TEST #1).....	74
4.3 AXIAL TEST (TEST #2).....	78
4.4 OBLIQUE 40° (TEST #3) AND 70° (TEST #4) TESTS.....	80
4.5 SUMMARY	82
5 NUMERICAL MODELING.....	85
5.1 INTRODUCTION	85
5.2 NUMERICAL MODEL PROCEDURES	86
5.3 CONSTITUTIVE MODEL SELECTION FOR SOIL	90
5.4 SOIL PARAMETERS CALIBRATION	90

5.5	COMPARISON WITH EXPERIMENTAL DATA.....	94
5.5.1	<i>Pure lateral loading test</i>	94
5.5.2	<i>Pure axial loading test</i>	97
5.5.3	<i>Oblique loading tests</i>	98
5.6	SUMMARY.....	102
6	PARAMETRIC STUDIES ON OBLIQUE PIPE/SOIL INTERACTION	104
6.1	INTRODUCTION.....	104
6.2	AXIAL-LATERAL PIPE/SOIL INTERACTION.....	104
6.2.1	<i>Ultimate displacements</i>	108
6.2.2	<i>Parametric studies</i>	110
6.3	AXIAL-VERTICAL (UPWARD) PIPE/SOIL INTERACTION.....	115
6.4	LATERAL-VERTICAL PIPE/SOIL INTERACTION	126
6.5	VERTICAL DOWNWARD PIPE/SOIL INTERACTION	133
7	CONCLUSIONS.....	137
7.1	AXIAL-LATERAL PIPE/SOIL INTERACTION.....	137
7.2	AXIAL-VERTICAL PIPE/SOIL INTERACTION	138
7.3	LATERAL-VERTICAL PIPE/SOIL INTERACTION	139
7.4	GENERAL CONCLUSIONS.....	139
8	RECOMMENDATIONS	141
8.1	PRACTICAL RECOMMENDATIONS	141
8.2	FUTURE DIRECTIONS OF RESEARCH.....	141
	REFERENCES.....	143
	APPENDIX A: PARAMETRIC STUDY OF LATERAL-VERTICAL PIPELINE/SOIL INTERACTION IN CLAY.....	154
	APPENDIX B: EXAMPLES OF STRUCTURAL MODELING OF PIPELINE/SOIL INTERACTION CONSIDERING THE EFFECT OF AXIAL-LATERAL PIPE/SOIL INTERACTION	177
B.1	INTRODUCTION.....	178
B.2	EXAMPLE 1: NG LINE.....	180
B.3	EXAMPLE 2: NGL LINE.....	185

List of Tables

Table 2-1: Friction factors for different types of pipe coatings (ALA 2001).	13
Table 3-1: Some common centrifuge scaling relationships	55
Table 3-2: Summary of sand bed parameters.	64
Table 3-3: Summary of equivalent prototype test parameters	65
Table 6-1: Displacement levels at different increments shown in Figure 6-14 (D=400 mm).	123

List of Figures

Figure 2-1: Pipeline modeling approach in current guidelines (ASCE 1984)	9
Figure 2-2: Four commonly used dimensions to characterize buried pipelines: Pipeline diameter (D), cover depth (C), burial depth (H) and embedment depth (h).	12
Figure 2-3: Adhesion factors for buried pipes in cohesive soils (Honegger and Nyman 2004).....	17
Figure 2-4: Main aspects of lateral pipe/soil interaction (Rizkalla et al. 1992).....	19
Figure 2-5: Honegger and Nyman (2004) lateral bearing capacity factors (adapted from Hansen 1961).....	20
Figure 2-6: Comparison of normalized numerical and experimental results in dense sand (Guo and Stolle 2005).....	21
Figure 2-7: Horizontal bearing capacity factor in sand after Trautmann and O'Rourke (1985).....	23
Figure 2-8: Interpretive diagrams of displacement fields during lateral displacement of pipe in medium dense sand with burial depth ratio of $H/D=2$ (a) and $H/D=11.5$ (b) (Trautmann 1983).....	25
Figure 2-9: Proposed design chart for lateral and upward pipe movements (Yimsiri et al. 2004)	25
Figure 2-10: Hyperbolic and bilinear load-displacement relation for lateral pipe/soil interaction.	27
Figure 2-11: Lateral interaction factor contributors (Phillips et al. 2004a)	30
Figure 2-12: Shallow (a), and deep (b) undrained failure mechanisms (Phillips et al. 2004a).....	31
Figure 2-13: Schematic drawing of lateral loading (Karimian 2006).....	32
Figure 2-14: Dependency of soil lateral load on pipe, buried in saturated clay, on displacement rate (Paulin 1998).....	33
Figure 2-15: Ultimate lateral force variation with loading rate (Phillips et al. 2004a).....	34
Figure 2-16: Plotted values of downward bearing capacity factors (Meyerhof 1955).....	36
Figure 2-17: Ranges for vertical uplift factor for clay (Trautmann and O'Rourke-1985).....	38
Figure 2-18: Vertical uplift factor for sands (Trautmann and O'Rourke-1985).....	38
Figure 2-19: lower bound solution for vertical uplift factors of horizontal anchor plates in clay (Merifield et al. 2001)	39
Figure 2-20: Uplift bearing factor for horizontal anchors in sand (Merifield and Sloan 2006).....	41
Figure 2-21: Deformation mechanisms during uplift movement (Cheuk et al. 2008).....	43
Figure 2-22: Axial-lateral oblique angle	45
Figure 2-23: (a) lateral and (b) axial loads on pipe during oblique pipe-soil interaction in loose sand (Hsu et al. 2001).....	45
Figure 2-24: lateral and axial loads on pipe during oblique pipe-soil interaction in dense sand (Hsu et al. 2006)	45
Figure 2-25: Axial-lateral force interaction diagram for two H/D ratios (Phillips et al. 2004b)	47
Figure 2-26: Normalized inclination factor (Nyman 1984).....	49
Figure 2-27: Dimensionless force-displacement curves (left) and Ultimate oblique loads vs. oblique angles (right) for $D=152.4$ mm and $H/D=1.5$ (Hsu 1996).....	50
Figure 2-28: Comparison of oblique resistance on pipes in contractive granular soils (Vanden Berghe et al. 2005).....	50
Figure 2-29: 3D interaction domain (Cocchetti et al. 2009a).....	52
Figure 3-1: Horizontal movement transmission from carriage to stanchions (Lateral test).....	57

Figure 3-2: (a) Plan and (b) elevation view of test box (oblique 40° test).....	58
Figure 3-3: Pipe section before getting buried (lateral test).	59
Figure 3-4: Load cell configuration. after Stroud (1971).	59
Figure 3-5: Load cell dimensions and schematic lateral loads used for calibration.	60
Figure 3-6: Laser sensor and LVDT at one end of the pipe (70° test).....	61
Figure 3-7: Sand raining device at C-CORE.	62
Figure 3-8: Comparison of cone tip resistance and normalized cone tip resistance at different depths	63
Figure 3-9: Location of the crushable foam in front of the stanchion	66
Figure 4-1: Displacement measurements by laser sensors at carriage and dogbone levels (40° test)- laser 1 & 2 are lasers at dogbone level	69
Figure 4-2: In-air set up to measure the actuator compliance.....	70
Figure 4-3: Data points comparing pipe and dogbone level displacements from in-air loading tests	70
Figure 4-4: Comparison of load-displacement curves for oblique 40° test using displacements measured at actuator and dogbone levels and corrected for pipe level.	71
Figure 4-5: Comparison of load-displacement curves for oblique 70° test using displacements measured at actuator and dogbone levels and corrected for pipe level.	72
Figure 4-6: Lateral and axial correction curves as a function of load applied to the pipe.	73
Figure 4-7: Load-displacement curves for lateral test using displacements measured at actuator level and corrected for pipe level.	73
Figure 4-8: Load-displacement curves for lateral test using displacements measured at actuator level and corrected for pipe level.	74
Figure 4-9: Load-displacement relationship from lateral loading test.....	75
Figure 4-10: Vertical displacement measurements during lateral displacement test.....	77
Figure 4-11: Load-displacement relationship from axial loading test	79
Figure 4-12: Soil surface deformation after oblique 40° test.....	81
Figure 4-13: Load-displacement curves from oblique 40° test.....	82
Figure 4-14: Load-displacement curves for oblique 70° test	83
Figure 4-15: Load-displacement curves from all four centrifuge tests.....	83
Figure 4-16: (a) Deformed soil surface after oblique 40° test, (b) Covering the deformed soil surface areas with dark sand and soil surface with filter paper, (c) Filling the upper part of the strong box with gravel, covering the box surface with wood strips and rotating the box by 90°. (d) Excavating the soil layer by layer. (e) Taking pictures of deformed layers of coloured sand in oblique planes.....	84
Figure 5-1: The finite element model geometry	86
Figure 5-2: (a) Typical distribution of axial and lateral loads on the pipe length. during oblique pipe displacement at consecutive increments (b) the middle part of the length of the pipe considered to calculate the loads	89
Figure 5-3: Comparison of numerical and experimental data for triaxial test: (a) deviatoric stress vs. axial strain, (b) volumetric strain vs. axial strain.	92
Figure 5-4: Mobilization of friction and dilation angles inferred from triaxial test data.	93
Figure 5-5: Numerical vs. experimental (Test #1) curves for lateral loading test	95
Figure 5-6: Comparison of numerical analysis with ultimate lateral loads from Guo & Stolle (2005).....	95

Figure 5-7: Soil displacement field in front of the pipe for (a) heavy and (b) light pipe after lateral displacement of 0.3D.	97
Figure 5-8: Numerical vs. experimental (Test #2) curves for axial loading test.....	98
Figure 5-9: Numerical vs. experimental (Test #4) curves-Oblique 70° test	99
Figure 5-10: Numerical vs. experimental (Test #3) curves-Oblique 40° test	99
Figure 5-11: Comparison of failure mechanisms during numerical and physical modeling for oblique 40° test (Test #3)	100
Figure 5-12: Comparison of failure mechanisms during numerical and physical modeling for oblique 70° test (Test #4)	101
Figure 6-1: Lateral (a) and axial (b) load vs. oblique displacement for different oblique angles.....	106
Figure 6-2: Variations of lateral and axial interaction factors with oblique angles	106
Figure 6-3: Axial-lateral pipe-soil interaction curves.....	107
Figure 6-4: Lateral (a) and axial (b) loads vs. lateral and axial displacements respectively, for different oblique angles	109
Figure 6-5: Ratio of normalized ultimate load over normalized ultimate displacement vs. oblique angles	110
Figure 6-6: Mobilization of friction and dilation angles used for parametric studies. ψ_1 , ψ_2 and ψ_3 are dilation angles relevant to peak friction angles of 45°, 40° and 35° degrees respectively.....	111
Figure 6-7: Effect of peak friction angle on axial-lateral pipe/soil interaction (solid lines are based on Eq. 6-1).....	112
Figure 6-8: Effect of interface friction factor on axial-lateral pipe/soil interaction (solid lines are based on Eq. 6-1)	114
Figure 6-9: Effect of burial depth on axial-lateral pipe/soil interaction curve (solid lines are based on Eq. 6-1).....	114
Figure 6-10: Vertical uplift load-displacement curves. (a) effect of burial depth ratio and friction angle, (b) effect of friction factor.	116
Figure 6-11: Comparison of displacement field in soil for H/D=4, d=0.2D.....	119
Figure 6-12: Comparison of displacement field in soil for H/D=2, d=0.15D.....	120
Figure 6-13: Axial (a) and vertical (b) load-displacement curves for different oblique angles: H/D=4, $\varphi_{peak}=40^\circ$, $f=0.8$ ($\mu=0.62$).	121
Figure 6-14: (a) Axial-vertical load-displacement curves for oblique 2°, and (b) normalized axial loads applied at different nodes of pipe at specified increments shown in (a)	123
Figure 6-15: Effect of friction angle on axial-vertical pipe/soil interaction	124
Figure 6-16: Effect of interface friction factor on axial-vertical pipe/soil interaction.....	124
Figure 6-17: Effect of burial depth on axial-vertical pipe/soil interaction	125
Figure 6-18: Lateral-vertical load-displacement curves for H/D=2, $\varphi=40^\circ$, $f=0.5$	126
Figure 6-19: Lateral-vertical load-displacement curves for H/D=4, $\varphi=40^\circ$, $f=0.8$	127
Figure 6-20: Lateral-vertical load-displacement curves for H/D=2, $\varphi=40^\circ$, $f=0.8$	127
Figure 6-21: Summary of normalized interaction factors for lateral-vertical upward pipe/soil interaction.	128
Figure 6-22: Comparison of FE data points with Nyman's interaction curve	129
Figure 6-23: Direction of oblique load vs. oblique movement during lateral-vertical upward pipe/soil interaction	130

Figure 6-24: Comparison of Cocchetti et al. (2009a) yield surface (solid lines) with numerical data points from current study for lateral-vertical pipe/soil interaction (vertical upward +, vertical downward -). 132

Figure 6-25: Comparison of load-displacement curves during downward movement of pipe..... 133

Figure 6-26: Lateral-vertical downward pipe/soil interaction curves for $H/D=2$, $\phi'=40^\circ$, $f=0.8$ 135

List of Abbreviations and Symbols

c'	cohesion of soil
c_u	undrained shear strength of soil
D	pipe external diameter
D_r	relative density
D_{ref}	reference diameter
E	soil elastic modulus
E_0	soil elastic modulus at reference pressure, p_0
f	pipe external surface friction factor
H	soil cover depth to the pipe centerline
K_0	coefficient of lateral earth pressure at rest
K_a	coefficient of active lateral earth pressure
L	pipe length
N_{ch}, N_{qh}	lateral interaction (bearing capacity) factors for cohesive and frictional effects, respectively
N_{cv}, N_{qv}	vertical interaction (bearing capacity) factors for cohesive and frictional effects, respectively
$N_{qh(90)}$	lateral interaction factor for pure lateral pipe/soil interaction
N_t	axial interaction factor
N_c, N_q, N_γ	Bearing capacity factors for horizontal strip footings, vertically loaded in downward direction
p	mean effective stress
p_0	atmospheric (reference) pressure
q	deviatoric stress
q_c	cone tip resistance
T, P, Q	soil forces applied to unit length of pipeline in axial, lateral and vertical directions, respectively

T_u, P_u, Q_u, Q_{ud}	ultimate soil forces applied to unit length of pipeline in axial, lateral, vertical upward and vertical downward directions, respectively
t	pipe wall thickness
W_p	pipe selfweight
x, y, z	relative pipe/soil displacements in axial, lateral and vertical directions, respectively
x_u, y_u, z_u, z_{ud}	ultimate relative displacements in axial, lateral, vertical upward and vertical downward directions, respectively
X_u, Y_u	ratio of ultimate relative displacements in axial and lateral directions over pipe diameter
γ'	effective unit weight of soil
δ	interface friction angle between pipeline and soil
ε^{pl}	plastic strain tensor
ε_m^{pl}	plastic strain magnitude
θ	axial-lateral oblique angle of movement
μ	pipe/soil interface friction coefficient
ρ	density of soil
ϕ'	effective friction angle of soil
ϕ'_{cv}	effective constant volume friction angle of soil
ϕ'_{peak}	effective peak friction angle of soil
ψ	dilation angle of soil

List of Appendices

Appendix A: Parametric Study of Lateral-Vertical Pipeline/Soil Interaction in Clay. N.Daiyan, S.Kenny, R.Phillips and R.Popescu. CSCE 2009 Annual Conference.	154
Appendix B: Examples of Structural Modeling	177

1 Introduction

1.1 Background

In the oil and gas industry, energy pipelines systems are critical transportation elements for the transmission of hydrocarbon products over long distances. In Canada, more than 580,000 km of pipelines deliver natural gas and petroleum products from field development areas to market (www.cepa.com).

One of the challenges in designing buried pipelines is the effects of geohazards on the pipelines. Large permanent ground deformations caused by geohazards such as landslides, seismic faulting and large subsidence, are imposed on segments of the pipeline system with other sections restrained. The relative displacement between the buried pipeline and the surrounding soil will impose geotechnical loads into the pipe. This will increase the level of stress and strain in the pipeline, which may affect pipeline operations and mechanical integrity. A report of the European Gas pipeline Incident Data Group (EGIG 2005) has indicated that ground movement represents the fourth major cause of gas pipeline failures where almost half of these incidents resulted in pipe rupture.

In engineering practice, avoiding areas prone to geohazards should be considered if alternative options exist when selecting pipeline route. Avoiding lands with possibility of geohazards is getting more difficult because of issues such as land ownership or environmental restrictions. Therefore, the risks of geohazards must be managed where they cannot be avoided. Pipeline integrity management strategies to mitigate geohazards

consists of: (1) design measures that improve the pipeline resistance to the geohazards, (2) measures that reduce the severity of geohazards, (3) monitoring ground displacement or pipe response to identify conditions that require mitigation (Honegger et al. 2010). Advancement of the understanding of pipe/soil interaction will lead to improved engineering designs to enhance pipeline resistance to geohazards, reduced uncertainty, greater safety and improved economy for the oil and gas pipeline industry.

1.2 Problem statement

Engineering guidelines (e.g. Honegger and Nyman 2004; ALA 2001), provide an engineering model for the analysis of pipe/soil interaction events, based on the beam on elastic subgrade model, with structural beam elements for the pipe and spring elements for the soil. Soil behaviour is modeled using discrete springs in three orthogonal (axial, lateral and vertical) directions. Load-displacement relationships for springs are generally defined by bilinear or hyperbolic functions. The main parameters to define soil springs are the ultimate load and relative soil displacement at ultimate load for each orthogonal loading axes. Several theoretical, numerical and experimental investigations have been conducted on buried pipelines and analogue systems (e.g. piles, anchor plates) to study the soil load-displacement relationships to define the springs at each direction. Depending on the type of soil and loading condition, these relationships use total or effective stress parameters.

The load-displacement relationships for the three orthogonal soil springs are usually considered independent and without coupling. A number of experimental (e.g. Hsu et al. 2001 and 2006), theoretical (e.g. Cocchetti et al. 2009a, 2009b; Nyman 1984) and numerical (e.g. Phillips et al. 2004b) studies have been conducted to investigate the pipe/soil interaction during an oblique pipe/soil relative movement. Also, there are several studies investigating foundations or buried structures under combined loadings, which include Taiebat and Carter (2000) on shallow foundations, Martin and Houlsby (2000) on spudcan foundations, and Aubeny et al. (2003) on suction caissons. These studies show the significance of considering the coupling between the loads in different directions on a buried structure such as pipeline.

Phillips et al. (2004b) investigated the axial-lateral pipe/soil interaction in clay using numerical continuum modeling and showed that axial soil load increased during oblique pipeline/soil interaction events for low angles of attack. Also, some studies (e.g. Cocchetti et al. 2009a; Nyman 1984) have indicated the importance of lateral-vertical pipe/soil interaction. Calvetti et al. (2004) and Cocchetti et al. (2009a) have shown that the downward movement of pipe increases the lateral soil restraint on the pipeline. None of these coupling effects are considered in the current state of practice. Therefore, more investigations on complex loading conditions are needed to enhance the numerical tools and engineering guidelines that are used to assess the pipeline's response in a three-dimensional pipe/soil interaction event.

1.3 Purpose of study

This study is focused on pipe/soil interaction in the axial-lateral, axial-upward and lateral-upward oblique planes in sand. Some observations on pipe/soil interaction during downward movement are included. Also a paper investigating lateral-vertical pipe/soil interaction in clay is included as Appendix A. The main objectives of the study are:

- Conducting physical model tests to investigate axial-lateral pipe/soil interaction and use the experimental data to validate the numerical model.
- Developing a continuum numerical model and validating the numerical model using experimental data.
- Developing interaction curves for pipeline/soil interaction in axial-lateral, axial-vertical and lateral-vertical oblique planes.
- Conducting parametric studies to investigate the effect of soil burial depth, pipe/soil interface friction angle and soil shear strength parameters on oblique pipeline/soil interaction.
- Developing alternative soil-spring relationships and implementing the new relationship in structural modeling to account for the interaction effect.

A series of centrifuge tests have been conducted on pipe/soil axial-lateral interaction in dense sand with the test procedures and results reported. Continuum finite element modeling procedures were developed using ABAQUS/Standard (Hibbitt et al. 2005) and validated using the centrifuge test results. Mohr-Coulomb plasticity model implemented in ABAQUS/Standard (Hibbitt et al. 2005) is customized to account for progressive mobilization of shear strength of soil using triaxial test data. Numerical parametric studies were conducted to develop a limit load interaction curve for axial-lateral pipe/soil interaction in sand. The same numerical model was used to investigate axial-vertical and lateral-vertical pipe/soil interaction through parametric studies and propose relevant interaction curves for each oblique plane. The proposed interaction curves can be used to define enhanced soil springs for use in conventional structural based finite element modeling procedures simulating pipeline/soil interaction events.

1.4 Thesis outline

This thesis is organized in eight Chapters. Chapter two includes a literature review on pipeline/soil interaction. Current state of practice and previous studies on pipeline/soil interaction and similar systems are discussed in this Chapter. Chapter three describes centrifuge test procedures and preparations. Details of the test setup and measurement devices are described in this Chapter. Centrifuge test results for four different oblique angles in axial-lateral plane are presented and discussed in Chapter four. The numerical continuum model development is discussed in Chapter five. The procedure to calibrate

mechanical properties of soil is explained and numerical model predictions are compared with experimental data from centrifuge tests. Chapter six comprises parametric studies using the validated numerical model for pipeline/soil interaction in axial/lateral, axial/vertical and lateral/vertical planes. The effects of some major parameters on pipe/soil interaction curves in different oblique planes are investigated and discussed. Conclusions of the thesis are summarized in Chapter seven and some recommendations for further studies on oblique pipe/soil interaction are presented in Chapter eight.

A paper including continuum finite element analysis on lateral-vertical pipe/soil interaction in clay is presented in Appendix A. Some examples of considering the coupling between axial and lateral soil springs within structural (beam-spring) modeling and investigating the effect on pipe strains are presented in Appendix B.

2 Literature review

2.1 Introduction

Any relative displacement between a buried pipeline and the surrounding soil will impose some load in typically the direction of relative displacement to the pipe. This will happen when soil withstands the motion of the pipeline or when the pipeline resists the motion of the surrounding soil (e.g. landslides).

Permanent Ground Deformations (PGD) resulting from landslides, large subsidence, ground deformations due to deep excavations or tunnelling, and soil liquefaction or surface faulting due to earthquakes can exert a large amount of displacement in a complex direction to any buried structure like pipelines.

This Chapter presents a literature review on the current state of pipeline/soil interaction modeling in engineering practice. The previous works on assessing the soil load on pipelines and analogous systems such as anchor plates are discussed. Other investigations on oblique pipe/soil interaction are reviewed and the shortcomings of the current state of practice are indicated.

2.2 Current Engineering Practice

Many problems in geotechnical engineering involve soil-structure interaction. In such problems, the deformations of structure and soil are inter-dependent. A proper subgrade model that provides a balance between theoretical accuracy and ease of use in engineering practice should be used to account for this dependency.

In current pipeline engineering practice, to account for pipe/soil interaction, pipelines are generally modeled using structural beam and spring elements, which are based on Winkler (1867) beam on elastic subgrade model.

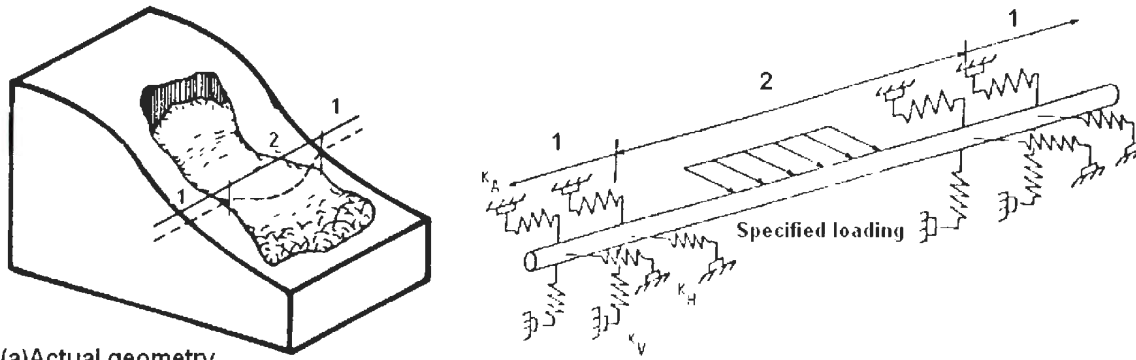
Numerical continuum soil/pipeline modeling provides a better tool than structural beam-spring modeling to account for different aspects of pipe/soil interaction such as shear transfer through soil; however, it is not generally used for analyzing long pipelines as it demands a high amount of computational effort, time and cost. A combination of using continuum modeling in the large ground movement region and structural modeling in the anchor length of pipeline (e.g. Kenny et al. 2004 and Nobahar et al. 2007) can be used in engineering practice to benefit from the accuracy of continuum modeling and the relative simplicity of structural modeling.

In the current pipeline engineering guidelines (e.g. Honegger and Nyman 2004), Winkler type springs are defined in three perpendicular directions: longitudinal (axial), transverse horizontal (lateral) and transverse vertical directions to represent the soil restraint on the pipe (Figure 2-1). In this kind of analysis, it is important to have knowledge of load-displacement behaviour of soil during relative movement between soil and pipe. The general form of the load-displacement relations for the soil springs can be expressed as the following functions:

Eq. 2-1

$$T = f(x), P = g(y), Q = h(z)$$

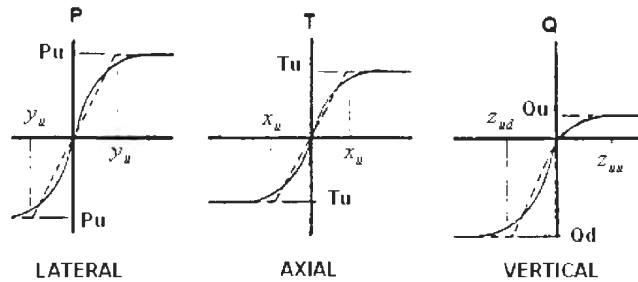
where T , P and Q are soil forces applied to the unit length of the pipelines and x , y and z are relative displacements between pipe and soil in longitudinal, lateral (horizontal) and vertical directions respectively.



(a) Actual geometry

1=Section of pipeline restrained by soils (burial or friction)
2=Section of pipeline loaded by soil slide

(b) Idealized structural model



(c) Bilinear soil springs in lateral, axial and vertical directions used to represent soil forces on pipe

Figure 2-1: Pipeline modeling approach in current guidelines (ASCE 1984)

The force-displacement relationships during pipeline/soil interaction are nonlinear and can be defined by bilinear or hyperbolic functions, which are proposed in guidance documents for pipeline engineering (e.g. American Lifeline Alliance 2001; Honegger and Nyman 2004) and from other analogous systems such as pile engineering. Bilinear

relationships are usually used for simplicity (Figure 2-1.c). Numerous theoretical, numerical and experimental investigations have been conducted to define load-deformation relationships in soils caused by lateral movement of piles, horizontal, vertical or inclined movement of rigid strip anchor plates and axial, lateral, vertical or oblique movement of fully buried pipelines that are summarized in the next sections of this Chapter.

2.3 Coupled Winkler Models

Winkler (1867) single-parameter (i.e. coefficient of subgrade reaction) model does not replicate all shearing modes that occur within subgrade material. Several multiple-parameter methods that include subgrade shear effects have been developed such as Pasternak/Loof method and Reissner's simplified continuum model which are more advanced and more accurate than Winkler's hypothesis. Multiple-parameter models can be developed from both a mechanical approach using assemblages of springs, shear layers and other physical elements, and a simplified-continuum approach that is based on the theory of linear elastic continuum (for a comprehensive comparison of different methods refer to Horvath 2002). These models are mostly derived for mat foundations and in pipeline engineering can be used to account for mechanical interaction between individual springs at adjacent nodes which is out of scope of the current study.

Cocchetti et al. (2009a) presented a numerical method to consider the coupling among loading components in a structural model. In this method, the pipeline is modeled using beam elements and soil reactions are lumped at the nodes using macro-elements with

coupled elastoplastic constitutive relationships. Cocchetti et al. (2009a) and other studies that propose to consider coupling among load components using coupled constitutive relationships for soil springs (e.g. Guo 2005; Hodder and Cassidy 2010) have only considered the coupling between lateral and vertical load components on the pipelines. The results of this thesis can be used to improve the constitutive relationships for soil springs (or macro-elements) in these models. This method will be discussed in the next section.

2.4 Pipeline/Soil Interaction

2.4.1 Axial (longitudinal) pipe/soil interaction

Honegger and Nyman (2004) suggested the ultimate axial load on pipelines in cohesionless soils be calculated as:

Eq. 2-2

$$T_u = 0.5\pi \cdot D \cdot \gamma' \cdot H \cdot (1 + K_0) \cdot \tan \delta$$

x_u = 3 to 5 mm for dense to loose sand

Where:

x_u : Ultimate relative displacement in axial direction

K_0 : Coefficient of lateral earth pressure at rest

D : Pipe external diameter

H : Soil depth to the center of pipeline (Figure 2-2)

γ' : Effective unit weight of soil

δ : Interface friction angle between soil and pipeline

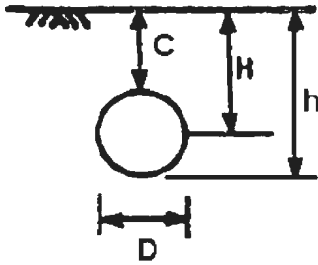


Figure 2-2: Four commonly used dimensions to characterize buried pipelines: Pipeline diameter (D), cover depth (C), burial depth (H) and embedment depth (h).

Eq. 2-2 applies for at rest condition and will underestimate axial forces on the pipe when lateral and axial relative displacements between pipe and soil exist at the same time. This issue was pointed out by Kennedy et al. (1977). They increased the axial soil load on the length of the pipeline which was subjected to high lateral loads. This effect will be discussed in more detail in next Chapters of this thesis.

Two key governing parameters in longitudinal soil restraint on the pipeline in a cohesionless soil are coefficient of interface friction (μ) and normal stress distribution on the pipeline circumference.

2.4.1.1 Effect of interface friction angle

The coefficient of pipe/soil interface friction is a function of soil friction angle and the type of pipe coating. The interface friction angle ($\delta = \tan^{-1}(\mu)$) can be expressed as:

Eq. 2-3

$$\delta = f \cdot \phi'$$

where ϕ' is the internal friction angle of soil and f is the friction factor which depends on the type of pipe external coating. The values of friction factors for a range of pipe coatings are presented in Table 2-1 (ALA 2001). Friction factors may vary from 0.5 to 1.0 depending on the characteristics of the pipe coatings.

Table 2-1: Friction factors for different types of pipe coatings (ALA 2001).

PIPE COATING	f
Concrete	1.0
Coal Tar	0.9
Rough Steel	0.8
Smooth Steel	0.7
Fusion Bonded Epoxy	0.6
Polyethylene	0.6

A value of $f=1$ is used for bare metal pipelines which have been buried for many years or oxidized and soil particles became cemented or bonded to the pipe, where shear occurs in soil close to the pipe surface (e.g. O'Rourke 1989). This happens mostly for civil pipelines rather than energy pipelines.

The interface friction angle δ can also be taken equal to ϕ' for wrapped pipelines with soft wrapping. For a pipeline surface with smooth, relatively hard coating, resistant to weathering, δ can be reduced to $0.5 \phi'$ to $0.7 \phi'$. Long term creep of wrap or insulation may significantly reduce the axial interface loads.

Pipe coating with lower friction factors can be used as a mitigation method to reduce the soil load on the pipelines. Scarpelli et al. (1999) indicated that to minimize the friction between pipe and surrounding soil, hard and smooth coatings are preferred to soft and rough ones by conducting some direct shear box tests of different pipe/soil interfaces.

Wijewickreme et al. (2005) has reported four axial pullout tests on geosynthetic-wrapped and bare steel pipes in very dense, dry sand. Comparing the results of two different interface conditions (bare steel with $\delta=38^\circ$ and geotextile with $\delta=21^\circ$) it is indicated that using two layers of woven geosynthetic wrapping reduces the axial load on pipe and can be used as a mitigation method. This method can be used for mitigating soil loads on limited length of pipelines or improving the performance of existing pipelines at vulnerable parts. They have suggested that geosynthetic wrapping contributed to reducing the normal soil pressure on the pipe. This effect has been attributed to reducing the dilation of dense sand in the shear zone around the pipe.

2.4.1.2 Effect of normal stress distribution on the pipe surface

Coefficient of lateral earth pressure at rest –when there is no lateral strain (K_0) - is a parameter that significantly influences the normal stresses and as a result the axial soil restraint on the pipe. Current guidelines (e.g. Honegger and Nyman 2004, ALA 2001) use this coefficient in equations like Eq. 2-2 but they do not propose any method to calculate it. For loose sand and normally consolidated clay, Jacky's (1944) relation can be used:

Eq. 2-4

$$K_0 = 1 - \sin \phi'$$

where ϕ' is the effective friction angle of soil.

For dense sand, taking into account the effect of density, the empirical relation of Sherif et al. (1984) can be used:

Eq. 2-5

$$K_0 = 1 - \sin \phi' + 5.5(\gamma_d / \gamma_{d\min} - 1)$$

where γ_d is dry unit weight and $\gamma_{d\min}$ is minimum dry unit weight of sand.

Experimental works on piles (e.g. Jardine and Overy 1996) and buried pipes (e.g. Karimian 2006, Wijewickreme et al. 2009) have indicated that confined dilation in sheared dense sand can increase the normal stress distribution on the pile or pipe during axial movements. The normal stresses about the circumference of pipeline are not uniform. Wijewickreme et al. (2009) proposed an equivalent lateral earth pressure coefficient between K_0 and 2.5, to be used in Eq. 2-2, to represent an average normal stress distribution on the pipe to account for the effect of constrained dilation during axial pipe/soil relative displacements in compacted sand backfill.

Pipe selfweight is another important factor that affects the normal stresses applied to the pipe surface. Eq. 2-2 does not include the pipe selfweight effect. For large diameter pipelines, the weight of the pipeline and its contents may have a significant effect on the friction load acting on the pipeline. Schaminee et al. (1990) used the following equation

to estimate the axial resistance of a buried pipe considering the normal stresses on the top, bottom and sides of an equivalent square:

Eq. 2-6

$$T_u = 0.25[\gamma.H + 2K_a.\gamma.(H + \frac{D}{2}) + \gamma.H + \frac{W_p}{D}].\mu.\pi.D$$

Where K_a is the active lateral soil pressure coefficient and W_p is pipe's selfweight.

2.4.1.3 Axial load on pipelines buried in cohesive soil

Honegger and Nyman (2004) guidelines suggested the ultimate axial soil load on unit length of pipeline buried in cohesive soil be considered similar to axial resistance used in pile engineering as:

Eq. 2-7

$$T_u = \pi.D.\alpha.c$$

with $x_u = 8-10$ mm for stiff to soft clay

where:

c : backfill soil cohesion

α : adhesion factor (Figure 2-3) $= 0.608 - 0.123c - \frac{0.274}{c^2 + 1} + \frac{0.695}{c^3 + 1}$, c is in ksf or kPa/100

The adhesion factors in Figure 2-3 are significantly scattered specially for small shear strengths. It may be attributed to small misalignment or slightly bent pipe length (Phillips et al. 2004b) or difference in test methods (field condition or laboratory controlled condition), rate of loading, pipe coatings and soil conditions (such as water content and developing positive or negative pore pressures) in different experimental studies.

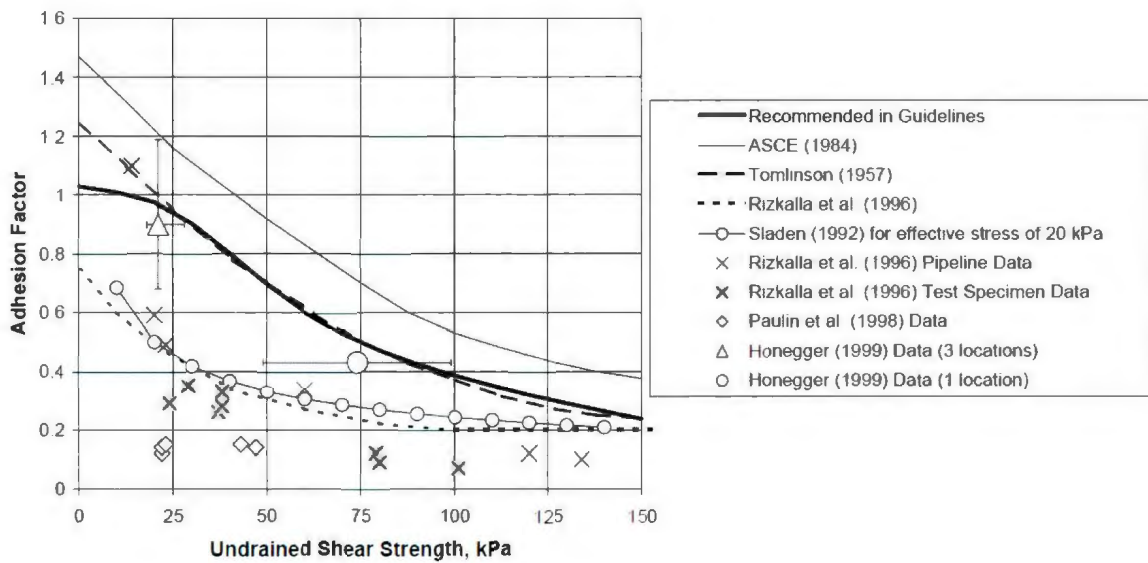


Figure 2-3: Adhesion factors for buried pipes in cohesive soils (Honegger and Nyman 2004)

The adhesion factor α recommended by Honegger and Nyman (2004) guidelines are based on field observations by Honegger (1999). The pipe tests of Rizkalla et al. (1996), Sladen (1992) and Paulin et al. (1998) resulted in much lower α values (Figure 2-3). Phillips et al. (2004b) suggested that this discrepancy is partly because of a small misalignment during the axial tests which can significantly increase the mobilized axial force. This is more likely for field test conditions and can be tracked in Figure 2-3 where all small values for adhesion factor (points below Rizkalla et al. 1996 line) are resulted from laboratory tests in controlled condition. This issue will be discussed in the next Chapters of this thesis in more detail. Furthermore, desiccated soil such as reported by Honegger (1999) can increase the axial resistance and the α value.

Rate of loading can be important for overconsolidated soil, where rapid shear may result in negative pore pressure and increase the axial restraint and result in large α values. The

values of α more than one are not practical as the shear strength on the interface exceeds the shear strength of surrounding soil and failure will happen in the soil mass instead of on the interface.

For cohesive soils, Finch et al. (2000) proposed a decision has to be made regarding drained or undrained behavior. When the operational loads develop relatively slowly, both sands and clays can be treated as drained for axial loading. For undrained conditions, such as seismic events, Eq. 2-7 is proposed. Finch (1999) suggested that for clays with low shear strength, values of α should be 1.0 for peak resistance and about $1/S_r$ for residual strength where S_r is the sensitivity of the soil. The sensitivity of clay is defined as the ratio of undisturbed peak undrained shear strength to totally remolded undrained shear strength.

2.4.2 Lateral (horizontal) pipe/soil interaction

Lateral soil restraint represents the load on the pipe by surrounding soil due to any horizontal lateral pipe/soil relative displacement. Most of the early studies on lateral pipe/soil interaction are based on experimental or numerical studies on vertical anchor plates moving horizontally in the soil (e.g. Mackenzie 1955, Rowe and Davis 1982a & 1982b, Neely et al. 1973). Also they used analogous test conditions and response of retaining walls and shallow pipelines, or laterally loaded piles and deep strip footing and deeply buried pipes. The main aspects of lateral pipe/soil interaction can be presented as Figure 2-4.

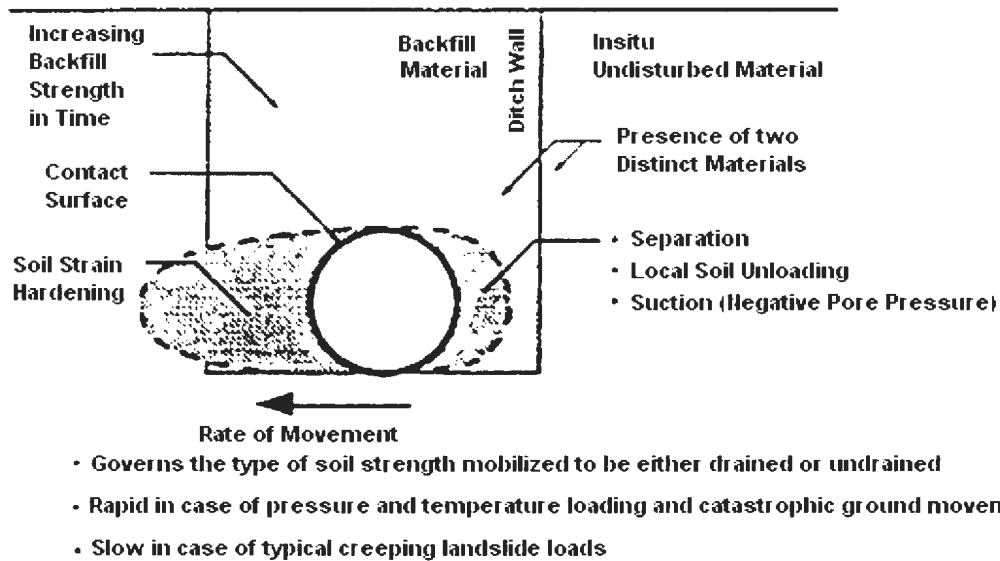


Figure 2-4: Main aspects of lateral pipe/soil interaction (Rizkalla et al. 1992)

The PRCI guidelines (Honegger and Nyman 2004) and ALA (2001) consider the contribution of both soil friction and cohesion in lateral soil resistance as:

Eq. 2-8

$$P_u = \gamma' HDN_{qh} + N_{ch}cD$$

Where:

N_{qh} : Lateral bearing capacity factor for frictional effects (0 for $\phi' = 0$)

N_{ch} : Lateral bearing capacity factor for cohesive effects (0 for $c = 0$)

Polynomials fitted to curves based on Hansen's (1961) model (Figure 2-5) are proposed in the guidelines for N_{qh} and N_{ch} .

The displacement at ultimate load is proposed as:

Eq. 2-9

$$y_u = 0.04(H+D/2)$$

but not more than 0.10 to 0.15D.

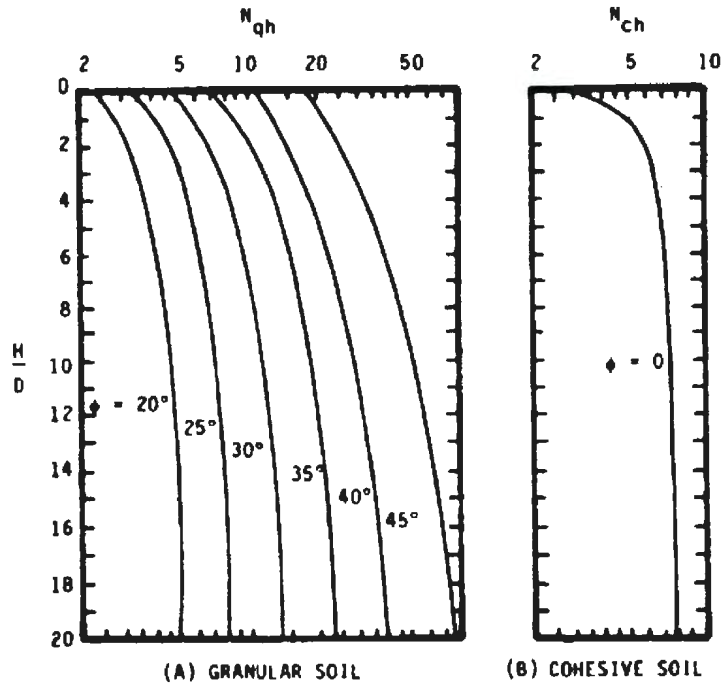


Figure 2-5: Honegger and Nyman (2004) lateral bearing capacity factors (adapted from Hansen 1961)

2.4.2.1 Lateral pipe/soil interaction in granular soils

Honegger and Nyman (2004) adopted the lateral bearing capacity factors (N_{qh}) of Hansen (1961) which are consistent with Audibert & Nyman (1977) experimental results. This approach estimates bearing capacity factors that are higher than those suggested by other studies on pipes or vertical anchor plates (e.g. Trautmann 1983, Murray & Geddes 1989, Dickin 1988, Paulin et al. 1998).

Guo and Stolle (2005) referred to the wide range of predicted maximum soil forces on buried pipelines in sand. They reviewed the experimental studies on lateral pipe-soil interaction and vertical anchor plates in sand and noticed the sensitivity of lateral bearing capacity factor to pipe diameter and model scale. They referred to the combination of these two effects as “scale effect”. A parametric study based on finite element method was conducted to investigate the scale effect and also the effect of burial depth (H) and stress level in soil, on pipe response. The study successfully explained the difference between most of the available experimental data where other parameters are the same. A unique relation was established that matches the experimental data in the literature (Figure 2-6.b). The authors suggested this equation can be incorporated into the current guidelines to account for the scale and burial depth effects.

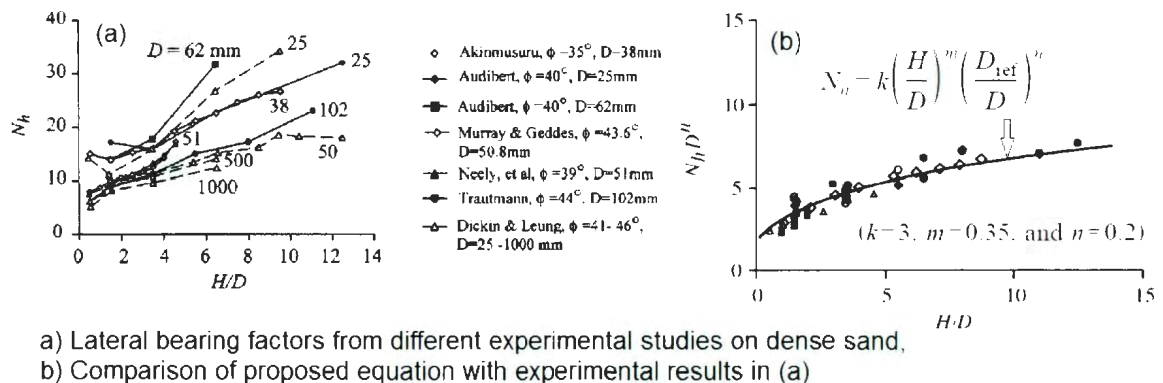


Figure 2-6: Comparison of normalized numerical and experimental results in dense sand (Guo and Stolle 2005)

Another factor that contributes to higher ultimate lateral loads from Hansen (1961) method is the effect of vertical restraint. Hansen’s (1961) model has been developed for lateral capacity of rigid piles. This model is based on a shallow failure mechanism, a deep

failure mechanism and an intermediate function. At the ground surface, Hansen assumed, laterally loaded piles behave as rough, horizontally translating retaining walls. For larger depths he assumed that piles behave as deep strip footings. Hansen (1961) assumed full vertical restraint for piles. For shallow buried pipelines equilibrium must be satisfied between the weight of the pipe and the vertical component of soil pressure. Since shallow buried pipelines can move upward with the passive wedge of soil in front of the pipe, the assumption of vertical restraint results in over prediction of forces applied to the pipe. In Audibert and Nyman (1977) tests which reported good agreement with Hansen's model, the vertical movement of pipes were restrained too. Audibert and Nyman's (1977) study is one of the pioneering experimental works on pipe/soil interaction. They conducted small scale 1g tests in sand to investigate the lateral pipe/soil interaction.

Trautmann (1983) conducted a series of field-scale laboratory tests on laterally loaded pipes in sands to investigate their load-displacement behavior. He found lateral bearing capacities (Figure 2-7) up to 200% lower than what was reported by Hansen's method. Trautmann (1983) suggested that vertical restraint can double the load on the pipeline. The experimental results of Trautmann show good agreement with Ovesen (1964) model that was developed for vertical anchor plates where no vertical displacement boundary condition was imposed.

A rigorous finite element limit analysis by Merifield and Sloan (2006) on vertical anchor plates, which were vertically restrained, shows Hansen's results are close to or more than upper bound solutions for shallow depths ($H/D < 3$) while for the case of deep anchors ($H/D > 5$) they are in the range of lower bound solutions.

It seems the future guidelines should consider using lateral bearing capacities in sand from methods similar to Guo and Stolle (2005), as Hansen (1961) and Audibert and Nyman (1977) results are compromised by vertical restraint and scale effects.

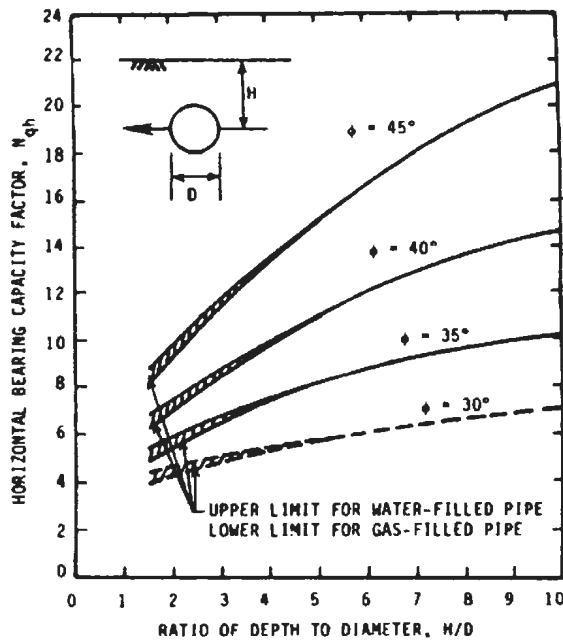


Figure 2-7: Horizontal bearing capacity factor in sand after Trautmann and O'Rourke (1985)

Trautmann (1983) also indicated that if the model pipe and the loading system are relatively heavy, whereby the model weight becomes a significant fraction of the weight of the soil passive wedge in front of the pipe, the normal stress on the failure surface will increase and result in higher loads on the pipeline during the test. In typical pipeline systems, the pipe self-weight is not significant in comparison with the soil self-weight. A comparison of lateral bearing capacity for water filled and gas filled pipes is shown in

Figure 2-7. Increasing the pipe weight increases the lateral bearing capacity at shallow burial depth where the failure mechanism consists of a passive wedge in front of the pipe.

Trautmann (1983) noted that during horizontal loading loose sand densifies and the friction angle increases by compaction. Therefore the resulting force on pipeline is consistent with that of sand with a higher initial density. For this reason in Figure 2-7 the curve corresponding to loose sand ($\phi=30^\circ$) is shown by dashed line to show caution should be exercised in assuming low lateral force on pipes buried in loose sand should large ground movements occur.

Lateral bearing capacity of pipe, as it is shown in Figure 2-5 and Figure 2-7, increases by increasing the soil friction angle and burial depth ratio. Numerical finite element parametric studies of Guo and Stolle (2005) on buried pipelines and Rowe and Davis (1982b) on buried anchor plates concluded that increasing soil dilatancy increases the lateral bearing capacity, particularly at moderate depths ($H/D>3$) where volume increase in sheared soil increases the normal stress on the pipe or anchor plate. The effect of soil dilatancy is not considered in the current guidelines.

Audibert and Nyman (1977) showed for shallow to intermediate burial depths a front passive wedge bounded by a logarithmic failure surface was observed. For deeper burial depths a confined zone of soil, flowing around pipe was reported. Deep punching failure mechanism was observed at cover ratios from 12 to 24 which is in agreement with what was found later by other researchers in sand (e.g. Trautmann 1983 and Yimsiri et al. 2004).

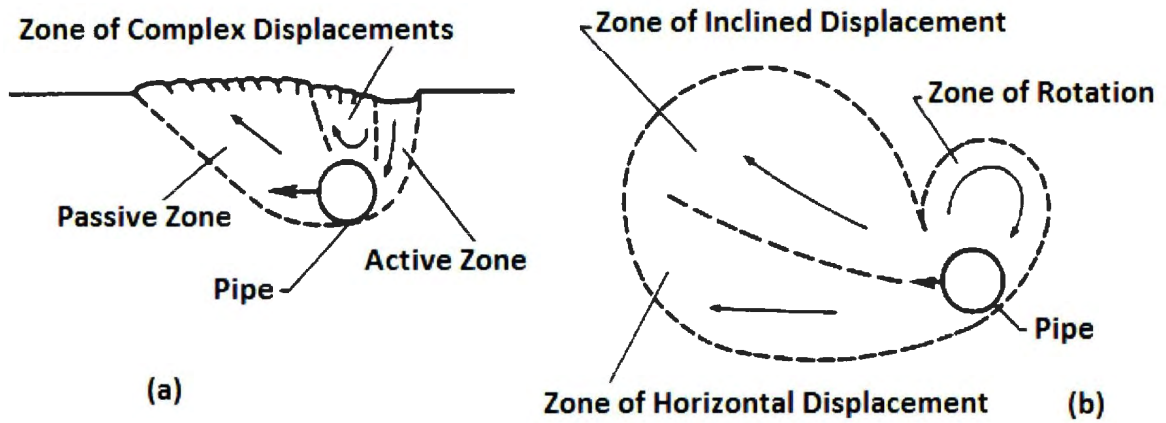


Figure 2-8: Interpretive diagrams of displacement fields during lateral displacement of pipe in medium dense sand with burial depth ratio of $H/D=2$ (a) and $H/D=11.5$ (b) (Trautmann 1983).

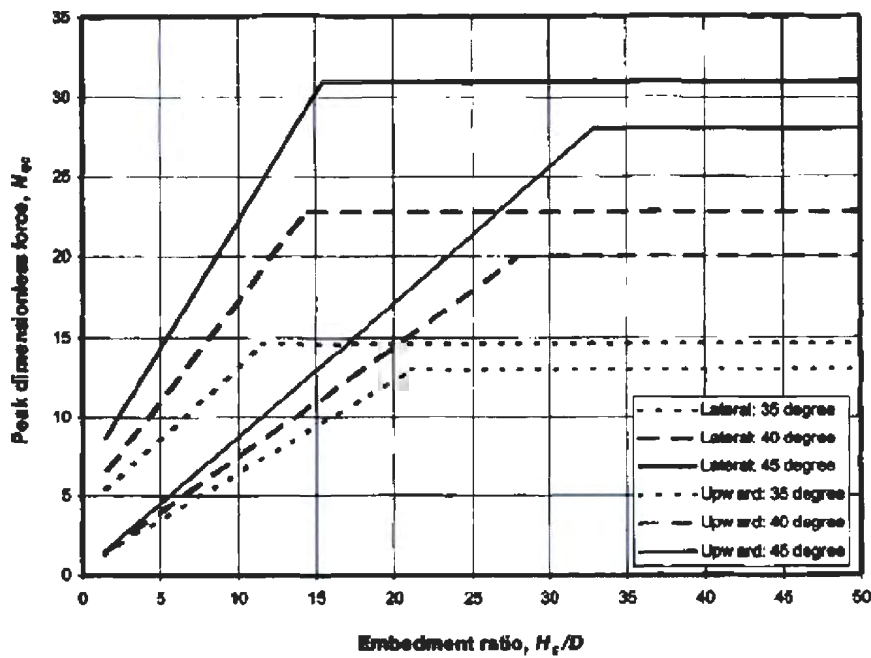


Figure 2-9: Proposed design chart for lateral and upward pipe movements (Yimsiri et al. 2004)

Trautmann (1983) found the transition between shallow and deep failure mechanisms took place at H/D of 8.5 to 11.5 for loose and medium dense sand. For dense sand, the transition took place at H/D more than 11.5. A comparison of shallow and deep

mechanisms observed during Trautmann (1983) experimental studies is shown in Figure 2-8. Yimsiri et al. (2004) conducted a series of finite element analysis to investigate the transition burial depth and to calculate the peak forces induced on deeply buried pipelines in medium to dense sand. The authors used two different soil models (Mohr-Coulomb and Nor-Sand) and calibrated their numerical models by Trautmann (1983) large scale tests. While two soil models yielded similar results the authors suggested a design chart (Figure 2-9) to be used for estimating the critical embedment depth and dimensionless forces on the pipeline buried in sand with ϕ'_{peak} of 35, 40 and 45° and for H/D up to 50.

A hyperbolic load-displacement relationship for pipeline lateral displacement in sand can be used based on Audibert and Nyman (1977) and Trautmann (1983) test results:

Eq. 2-10

$$P = \frac{y/y_u}{A + B y/y_u} P_u$$

where $A=0.145$, $B=0.855$, P_u is the ultimate lateral load imposed on the pipe corresponding to an ultimate displacement y_u . A similar equation was proposed by Das and Seeley (1975) for vertical anchor plates in sand.

In engineering practice a bilinear load-displacement relationship is usually used for simplicity. Both hyperbolic and bilinear relationships are shown in Figure 2-10 schematically.

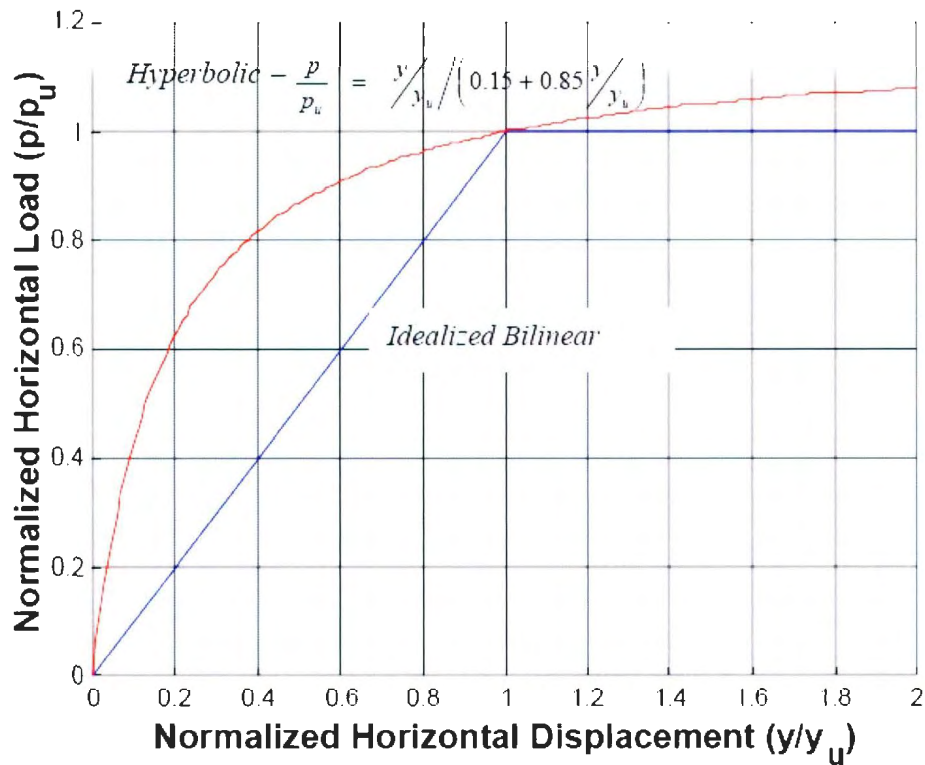


Figure 2-10: Hyperbolic and bilinear load-displacement relation for lateral pipe/soil interaction.

The ultimate displacement can be found from Eq. 2-9. Trautmann (1983) found the ultimate displacement y_u to reach the ultimate lateral load P_u to be 0.13h, 0.08h, and 0.03h (for h see Figure 2-2) for loose, medium and dense sand respectively. Audibert and Nyman (1977) recommended a value of 1.5% to 2% of embedment depth as the ultimate lateral displacement y_u .

2.4.2.2 Lateral pipe/soil interaction in cohesive soil

Most early studies on lateral pipe/soil interaction in clay are based on experimental studies of vertical anchor plates moving horizontally in soil (e.g. Mackenzie 1955). They also include some analogy between the response of retaining walls and shallow pipelines, or similarities between laterally loaded piles or deep strip footings and deeply buried pipes (e.g. Hansen 1961). Several experiments on lateral pipe/soil interaction have been reported such as Wantland et al. (1982), Rizkalla et al. (1992), Paulin et al. (1998), and Paulin (1998).

Based on experimental investigations by Wantland et al. (1982) and numerical studies by Rowe and Davis (1982a) and comparing with the theoretical model suggested by Audibert and Nyman (1977), Honegger and Nyman (2004) adopted the lateral bearing capacity factors (N_{ch}) of Hansen (1961) in clay (Figure 2-5).

Ng (1994) conducted some field tests and numerical analysis of buried pipelines subjected to lateral displacements in clay. He concluded that Hansen's model can be adopted for lateral bearing capacity (N_{ch}). A relation similar to what is proposed by Audibert and Nyman (1977) for sand (Eq. 2-10) was suggested for nonlinear P-y curve in clay as:

Eq. 2-11

$$P = \frac{y/y_u}{A + By/y_u} P_u$$

where $A=0.16$, $B=0.84$, and P_u is the ultimate lateral load imposed on the pipe. Ng (1994) noted that the effect of backfilled trench should be considered in obtaining P_u and y_u .

Phillips et al. (2004a) investigated the lateral pipe/soil interaction in clay using continuum finite element modeling. Von-Mises failure criterion has been used to model the undrained clay behavior. They suggested that lateral interaction factor in clay can be represented as following equation to include the soil weight and be capped for deep burial behavior:

Eq. 2-12

$$N_{ch} = \min \left(N_{ch}^* + \beta \frac{\gamma H}{c_u}, N_{ch}^{\max} \right)$$

where:

N_{ch}^* : Lateral interaction factor associated with soil strength

$\beta \frac{\gamma H}{c_u}$: Factor to account for the soil weight which is related to the vertical stress level

(Figure 2-11)

N_{ch}^{\max} : Upper limit of the lateral interaction factor associated with deep burial depth.

c_u : Undrained shear strength of soil

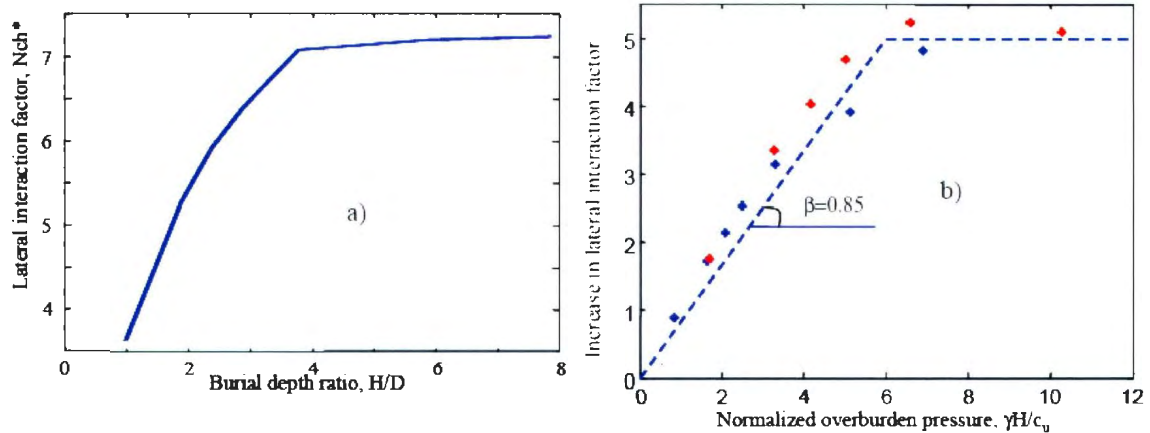


Figure 2-11: Lateral interaction factor contributors (Phillips et al. 2004a)

In Figure 2-11, β equal to one seems to be more acceptable. Rowe and Davis (1982a) presented a similar equation to Eq. 2-12. They indicated that coefficient β is a function of overburden ratio ($\frac{\gamma H}{c_u}$) and burial depth ratio (H/D) and presented different curves over a range of H/D ratios which cap at different $\frac{\gamma H}{c_u}$. Merrifield et al. (2001) calculated upper and lower bound solutions for lateral and vertical capacity of anchor plates in clay using finite element limit analysis method and proposed different curves for various H/D ratios with $\beta=1$ where all curves cap at a constant value of $\beta \frac{\gamma H}{c_u}$. This topic is discussed in more detail in Appendix A of this thesis. The paper presented in Appendix A includes a numerical parametric study of lateral pipe/soil interaction in cohesive soil which resulted in β values as a function of burial depth ratio and overburden ratio.

Figure 2-12 indicates undrained failure mechanisms for shallow and deep pipelines resulted from numerical modeling by Phillips et al. (2004a). The occurrence of deep failure mechanism is a function of both burial depth ratio (H/D) and overburden ratio ($\frac{\gamma H}{c_u}$). It seems pipeline engineering guidelines need to adopt a more updated solution that gives the lateral bearing capacity of pipelines in clay as a function of both burial depth and overburden ratio. An example of such a solution is presented in Appendix A of this thesis.

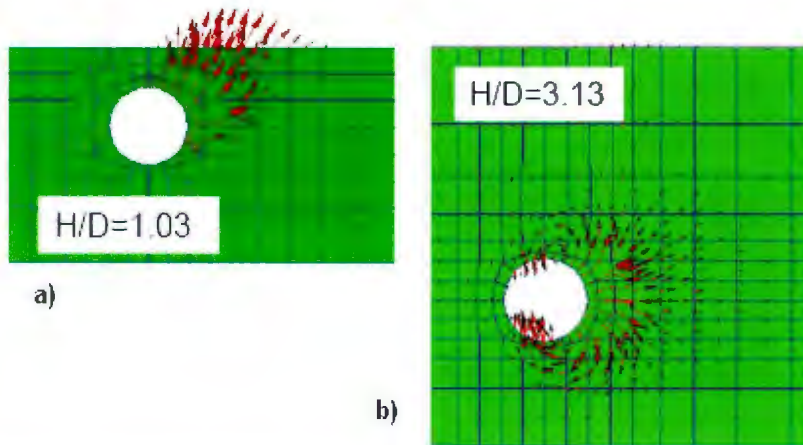


Figure 2-12: Shallow (a), and deep (b) undrained failure mechanisms (Phillips et al. 2004a)

2.4.2.3 Trench effect

Rizkalla et al. (1992) conducted some centrifuge tests on lateral pipe/soil interaction in clay. They noticed a significant effect from trench geometry on load transferred to buried pipe and proposed more investigation to be performed on construction related issues, like trench geometry and backfill soil properties. Phillips et al. (2004a) investigated the trench effects using numerical modeling and experimental tests by Paulin (1998) in saturated

clay. They indicated that the response of a pipe in a trench with a wall inclination of 60° was similar to a pipe in vertical trench, and a wall inclination of 45° is required to mitigate the load on pipeline. It was shown that increasing the trench width mitigates the load on pipe due to upward movement of pipe before reaching the trench wall. A tri-linear curve was recommended to predict the load displacement response of a trenched pipeline.

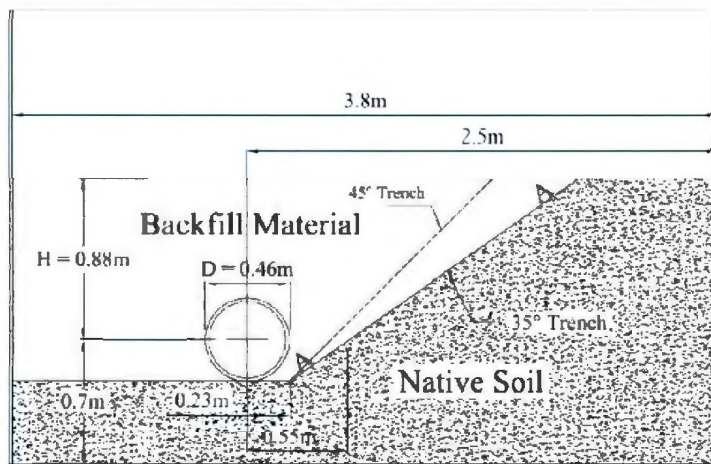


Figure 2-13: Schematic drawing of lateral loading (Karimian 2006)

Karimian (2006) conducted eight large scale tests on steel pipes buried in trenches with dry and moist sand as backfill soil materials (Figure 2-13). The effectiveness of lining the trench slope with two layers of geotextiles as a method of reducing soil loads was investigated.

The test results suggested that lining of trench slopes with geotextile layers can reduce soil loads on the pipe by about 20% only when the native soil material is significantly stiffer than backfill material (e.g. pipe buried in glacial till-like material or bedrock).

2.4.2.4 Effect of loading rate

Paulin (1998) performed a series of centrifuge tests on pipes with 0.95m prototype diameter moving laterally in clay to investigate the effects of trench geometry, soil preconsolidation stress, pipe displacement rate and backfill type on pipeline/soil interaction. A significant effect of loading rate was observed. It was shown that by decreasing the loading rate (partial drainage) the soil load on pipe increased (Figure 2-14). In undrained conditions (high loading rate) Paulin's (1998) experimental study of the effect of embedment depth indicated that as H/D increased from 1 to 2.4 the normalized lateral load increased. For higher H/D ratios, the effect of burial depth was not obvious. The experimental results were in good agreement with Rowe and Davis (1982a) numerical analysis for vertical anchor plates in clay.

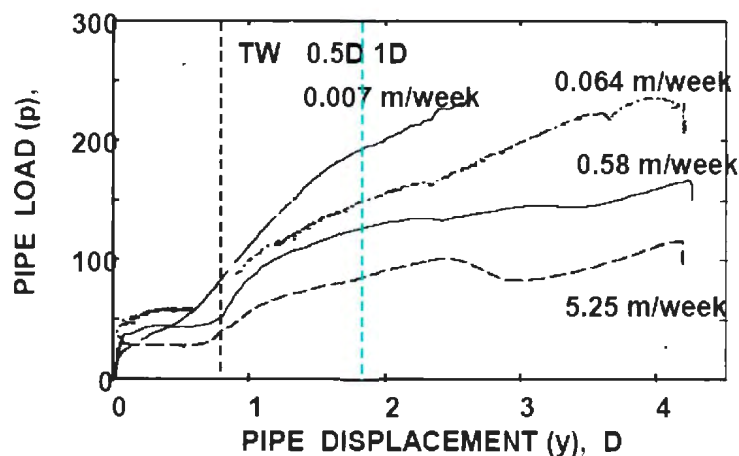


Figure 2-14: Dependency of soil lateral load on pipe, buried in saturated clay, on displacement rate (Paulin 1998)

Phillips et al. (2004a) investigated the effect of loading rate using coupled finite element analysis in clay. The authors illustrated the transition from undrained through partially drained to drained behavior using normalized displacement rate, $V=vD/c_v$, where D is pipe diameter and c_v is the coefficient of consolidation (Figure 2-15). Numerical results are compared to experimental findings of Paulin (1998).

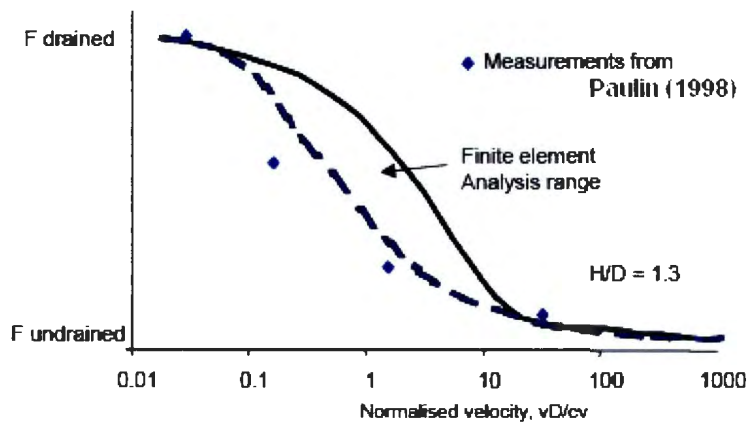


Figure 2-15: Ultimate lateral force variation with loading rate (Phillips et al. 2004a)

Centrifuge experiments by Krstelg (1996) on saturated dilative sand (60% relative density) indicated that the soil load increased with increase in loading rate. This effect can be attributed to dilative behavior of soil materials. The volume increase during shear in dilative soils results in negative pore pressure and larger effective stresses which causes larger loads on pipeline.

2.4.3 Vertical pipe/soil interaction

Unlike pipe-soil interaction in longitudinal and lateral directions, pipe-soil interaction in vertical direction is generally asymmetric. Soil failure mechanisms and ultimate resistances and displacements are different for downward and upward vertical pipe/soil differential displacements.

2.4.3.1 Vertical downward pipe/soil interaction

Soil resistance against pipelines moving downward can be estimated from bearing capacity of cylindrical strip foundations. ALA (2001) and PRCI Guidelines (Honneger and Nyman 2004) present the ultimate soil resistance per unit length of pipelines as:

Eq. 2-13

$$Q_{ud} = c N_c B + \gamma' H N_q B + 1/2 \gamma B^2 N_\gamma$$

where:

N_c, N_q, N_γ : Bearing capacity factors for horizontal strip footings, vertically loaded in downward direction, based on Meyerhof (1955)

(Figure 2-16– equations fitted to the curves are presented in ALA 2001)

c: Soil cohesion (or undrained shear strength)

γ : Total unit weight of soil

γ' : Effective unit weight of soil

B: Projected width of contact area of pipeline with soil; B=D for pipelines buried at least halfway in the soil

D: Pipeline diameter

The ultimate displacement is considered to be in the order of 0.1D for granular soils and 0.2D for cohesive soils.

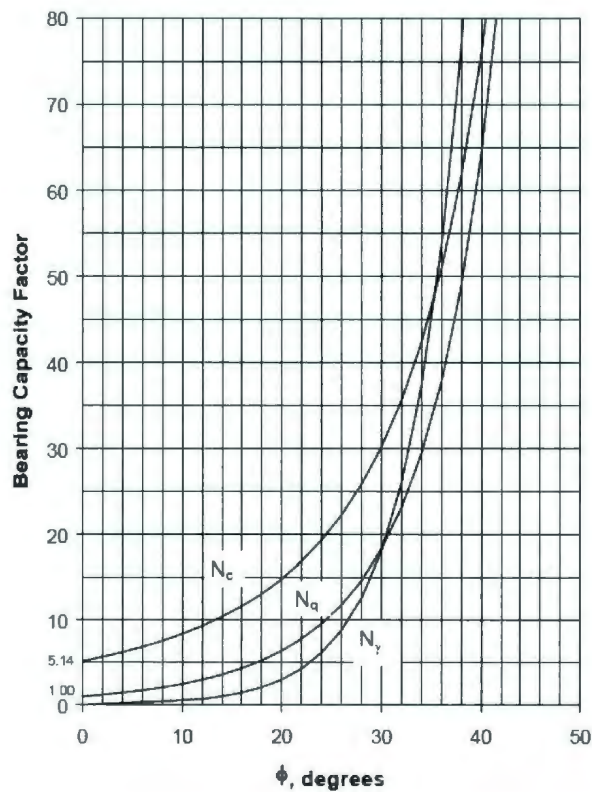


Figure 2-16: Plotted values of downward bearing capacity factors (Meyerhof 1955)

Numerical modeling by Calvetti et al. (2004) using distinct element method shows the ultimate downward load on pipe is consistent with the ultimate load calculated from Eq. 2-13; however the ultimate displacement is in the range of 1 to 1.5 D which is much larger than what is proposed by guidelines. The numerical data from a limited number of

vertical downward pipe/soil interaction analysis presented in Chapter 6 of this thesis confirm the range of ultimate displacements suggested by Calvetti et al. (2004). It seems the ultimate displacements proposed by the guidelines for vertical downward movements of pipes in soil, need to be revised.

2.4.3.2 Vertical upward pipe/soil interaction

PRCI Guidelines (Honegger and Nyman 2004) suggested a general expression for vertical upward pipe/soil interaction in granular and cohesive soils which is similar to what is proposed by Reese and Casbarian (1968) and Vesic (1971):

Eq. 2-14

$$Q_u = c N_{cv} D + \gamma' H N_{qv} D$$

where N_{cv} and N_{qv} are vertical uplift interaction factors for clay and sand respectively which are plotted in Figure 2-17 and Figure 2-18 and are based on experimental and numerical works of Vesic (1971), Rowe and Davis (1982a, 1982b) and Trautmann (1983).

Ultimate displacements of 0.01 to 0.02H (< 0.1D) for dense to loose sand and 0.1 to 0.2 H (< 0.2D) for stiff to soft clay are proposed by the guidelines.

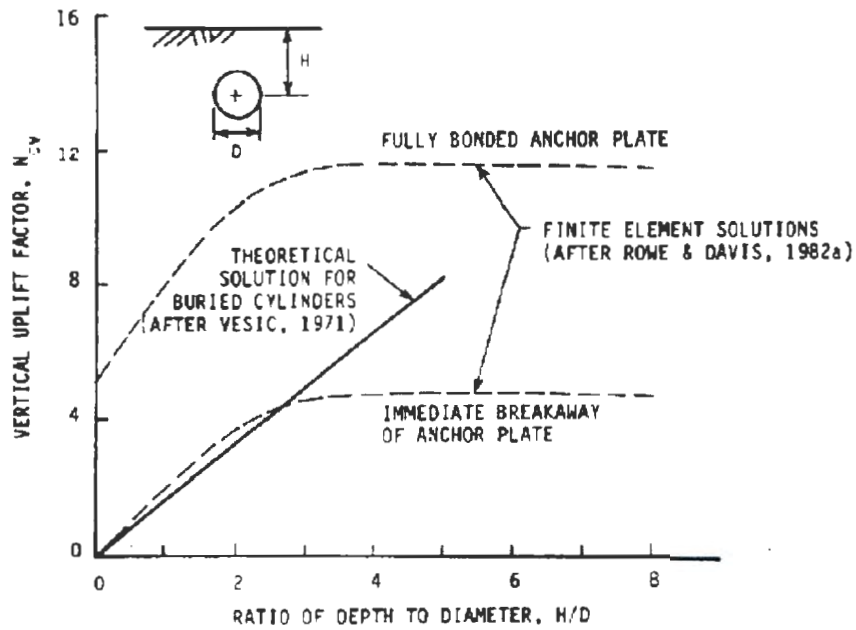


Figure 2-17: Ranges for vertical uplift factor for clay (Trautmann and O'Rourke-1985)

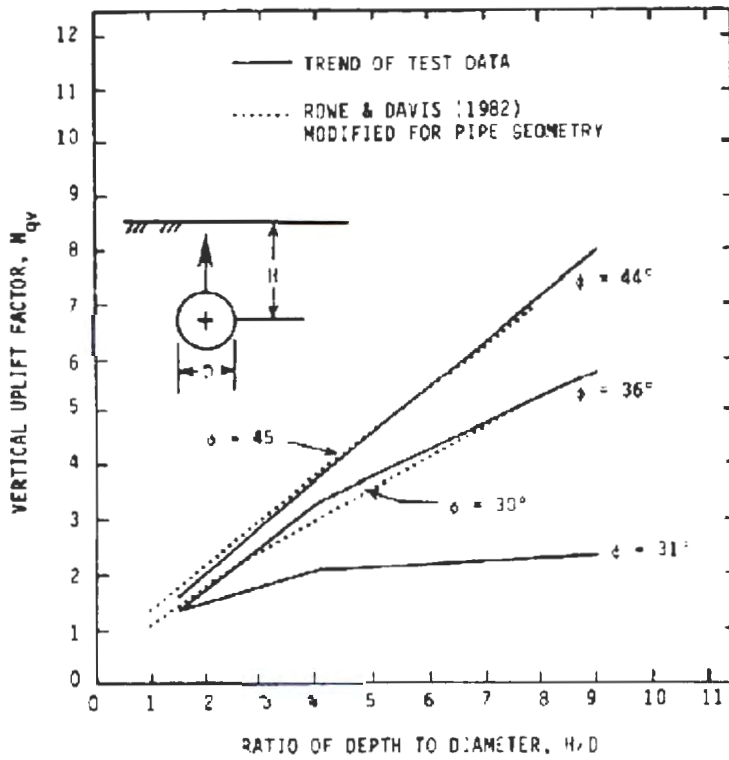


Figure 2-18: Vertical uplift factor for sands (Trautmann and O'Rourke-1985)

2.4.3.2.1 Vertical upward pipe/soil interaction in cohesive soil

In Figure 2-17 Vesic (1971) theoretical solution is compared with Rowe and Davis (1982a) numerical solution in cohesive soils. Vesic (1971) calculated the upward bearing capacity factor for buried horizontal cylinders (like pipes) as well as circular and strip anchor plates for H/D from 0.5 to 5 based on cavity expansion model. Rowe and Davis (1982a) conducted numerical elasto-plastic finite element analysis of uplift loading of strip anchors with H/D ranging from 1 to 8. The numerical modeling showed a significant difference between fully bonded and immediate break away conditions. It is also indicated that the anchor uplift capacity in clay increases up to a critical H/D of about three and after that it remains almost constant.

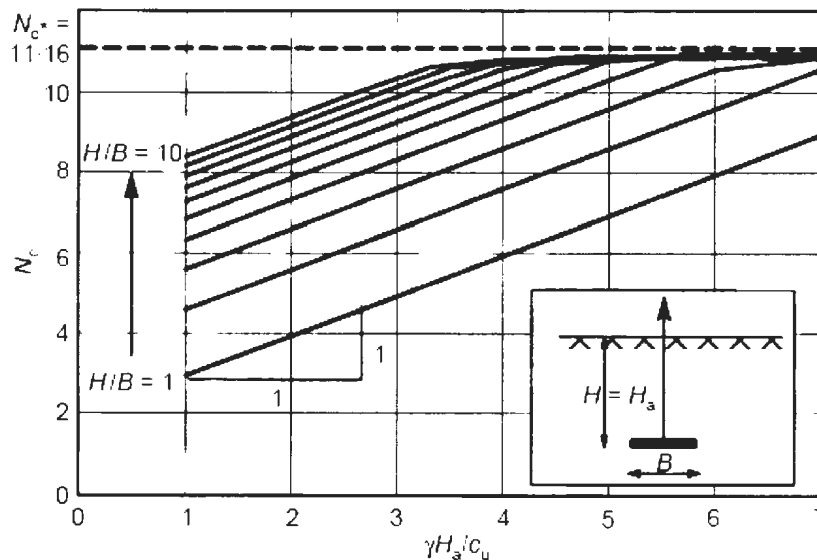


Figure 2-19: lower bound solution for vertical uplift factors of horizontal anchor plates in clay (Merifield et al. 2001)

Figure 2-17 gives a wide range for vertical uplift factor which is consistent with most of other experimental and numerical works in the literature, but it is not a straight forward method to find the upward bearing factor in engineering practice with an acceptable level of accuracy. Merifield et al. (2001) using finite element limit analysis proposed an equation similar to Eq. 2-12 for horizontal anchor plates in clay and showed the upward capacity of anchors is a function of burial depth ratio and overburden ratio. It seems pipeline engineering guidelines need to adopt more accurate and updated solutions such as Figure 2-19. A similar solution for pipelines, based on finite element continuum modeling, is presented in Appendix A of this thesis.

2.4.3.2.2 *Vertical upward pipe/soil interaction in granular soil*

In Figure 2-18, experimental results of Trautmann (1983) on pipelines are compared to Rowe and Davis's (1982b) numerical results for no dilation and no anchor surface friction case. Test results for loose sands ($\phi=31^\circ$) do not agree well with numerical models. Trautmann (1983) suggested it can be used if field conditions are appropriate for the steady migration and collapse of loose sand into the void beneath the pipe. Both experimental and numerical data in Figure 2-18 are lower than what is proposed by Merifield and Sloan (2006) (Figure 2-20).

Trautmann and O'Rourke (1983) test results indicated an ultimate pull out resistance is obtained at displacements ranging from 0.5 to 1.5% of H for 100mm diameter pipelines buried in dense to loose sand. Dickin (1994) reported larger ultimate displacements for

1m strip anchor plate in centrifuge tests which is about 1 to 2% of H in dense sand and about 1 to 5% of H in loose sand for H/D from 1 to 8.

These observations suggest a scale effect, similar to the scale effect reported by Guo and Stolle (2005) for lateral movement of pipes in granular materials, may have affected the vertical soil resistance on pipes or horizontal anchor plates. This issue needs to be investigated in the future.

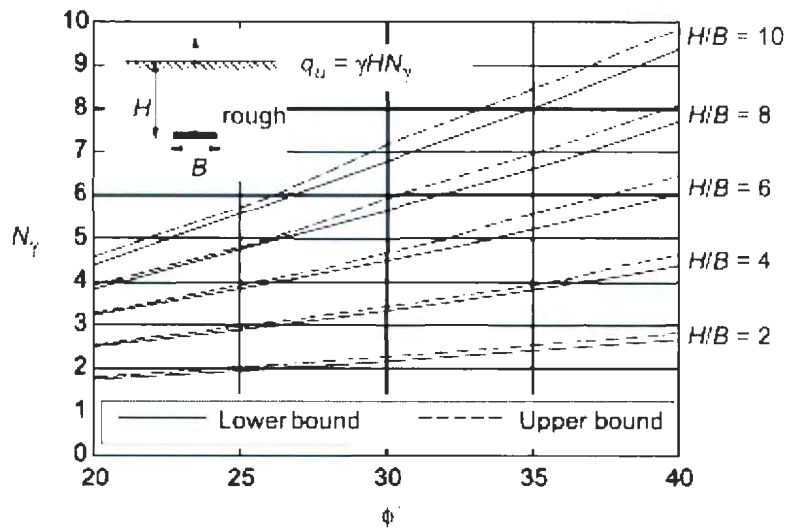


Figure 2-20: Uplift bearing factor for horizontal anchors in sand (Merifield and Sloan 2006)

The analysis by Rowe and Davis (1982b) showed soil dilatancy had a significant effect on deep anchor's uplift capacity and little effect on shallow anchors. It was found that the initial soil stress state and anchor roughness had little effect on the uplift capacity at any depth which is consistent with what was found by Merifield and Sloan (2006).

Trautmann and O'Rourke (1983) presented the vertical upward force-displacement relationship as a hyperbolic equation from large scale tests on upward motion of pipes buried in dry, uniform sand:

Eq. 2-15

$$Q = z / (A'' + B'' \cdot z)$$

where $A'' = 0.07 z_u / Q_u$ and $B'' = 0.93 / Q_u$.

Q_u is the ultimate uplift resistance and z_u is the ultimate displacement at which Q_u is mobilized.

Trautmann (1983) concluded that the transition between shallow and deep failure mechanisms depends on the sand density. For loose sand, the transition occurred at H/D of about four. For medium and dense sand, the ultimate resistance increased linearly with depth for H/D from 1.5 to 13, so the transition was not observed for H/D as large as 13 (Figure 2-18). Vesic (1971) theoretical solutions are limited to H/D=5 and Rowe and Davis (1982b) numerical solutions are limited to H/D=8 and neither of them indicated the depth of deep behavior for dense sand. Dickin (1988) experimental results are limited to H/D=8 and indicated a transition H/D of 5 for loose sand and suggested a transition H/D in the range of 10 for dense sand. Yimsiri et al. (2004) conducted FE analysis of pipelines buried in medium to dense sand with H/D up to 100. They showed the transition occurs at H/D of 21, 28 and 33 in sands with ϕ'_{peak} of 35, 40 and 45° (Figure 2-9).

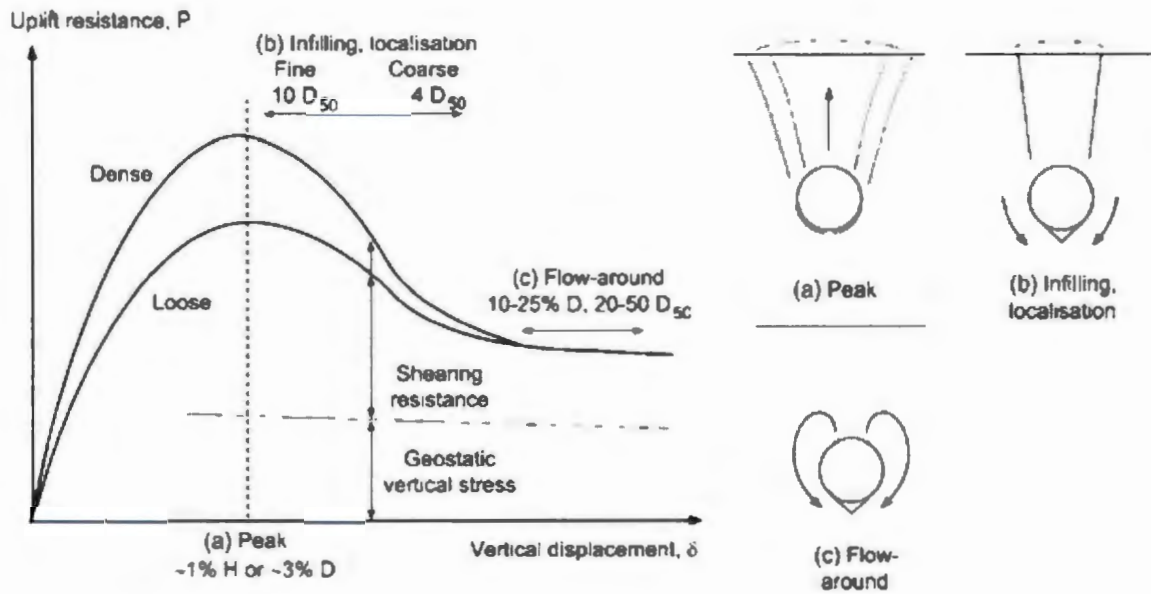


Figure 2-21: Deformation mechanisms during uplift movement (Cheuk et al. 2008)

Cheuk et al. (2008) used PIV (particle image velocimetry) technique to study the mechanism relevant to peak uplift resistance through four model tests of pipes in dry sand. Two grain sizes (fine and coarse) and two relative densities (about 30 and 90%) were used for sand. Pipes' diameter were 100mm and were buried to a springline burial depth of $H/D=3$. Different stages were noticed during uplift movement including: peak resistance, infilling, shear band formation and flow around (Figure 2-21). The authors noticed a curved shear zone whose average inclination depends on soil dilatancy and concluded vertical slip surface assumption (e.g. Schaminee et al. 1990) cannot get the correct deformation at peak resistance. Also it was found that the flow rule on the shear zone does not obey normality; therefore, assuming an associated flow rule (e.g. Ng and Springman 1994) will lead to an overestimation of shear zone inclination and peak uplift resistance.

2.4.4 Axial-lateral pipe/soil interaction

Unlike the simplifications used in engineering practice, the relative movement between pipelines and soil during a ground movement incident may occur in axial, lateral and vertical directions at the same time. For instance, it is rare to have pure axial pipe/soil relative displacement without any lateral or vertical displacements. While there are many studies in the literature investigating the lateral-vertical pipe/soil interaction, there are a limited number of studies on axial-lateral pipe/soil interaction and there is almost no study on axial-vertical pipe/soil interaction.

Kennedy et al. (1977) noted that the lateral soil pressure on the pipe affects the effective axial soil resistance on the pipe. They considered this effect by using different pipe/soil friction factors in places with and without large lateral forces on pipe.

Hsu et al. (2001) and Hsu et al. (2006) investigated the axial-lateral pipe-soil interaction for shallow buried pipes in loose and dense sand respectively. Medium scale tests were conducted for 10 different angles of movement (θ) between 0° and 90° (Figure 2-22), three different diameters and three different H/D ratios.

The authors concluded that the longitudinal and lateral soil restraints on the pipe during oblique pipe-soil interaction can geometrically be obtained from the vector components of the soil load on the pipe in the direction of movement. They presented theoretical analysis based on modified Meyerhof theory of logarithmic spiral failure surface for pure lateral pipe movement and compared it with experimental results (Figure 2-23 and Figure

2-24). Minor scale effect due to pipe diameter was observed for pipe diameters ranging from 152.4 to 304.8 mm.

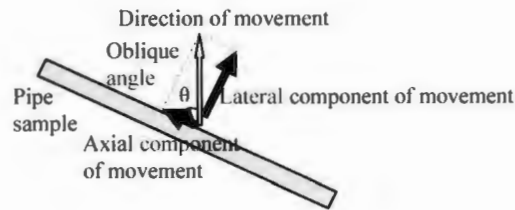


Figure 2-22: Axial-lateral oblique angle

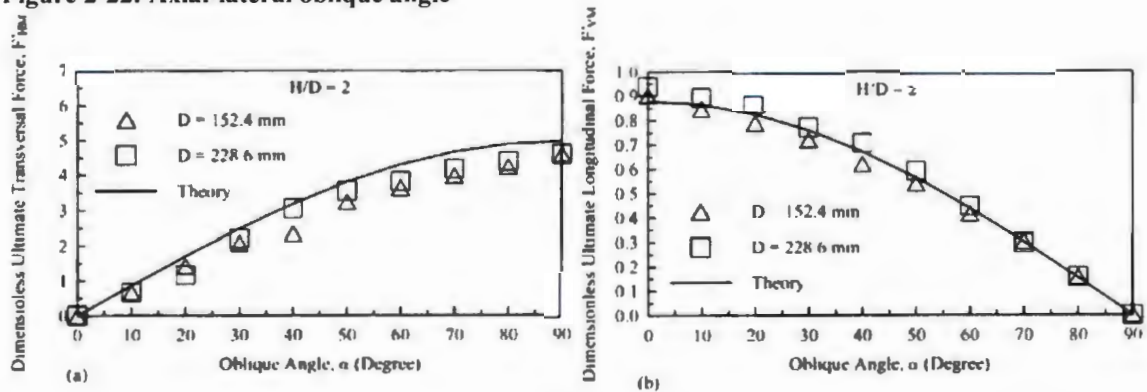


Figure 2-23: (a) lateral and (b) axial loads on pipe during oblique pipe-soil interaction in loose sand (Hsu et al. 2001)

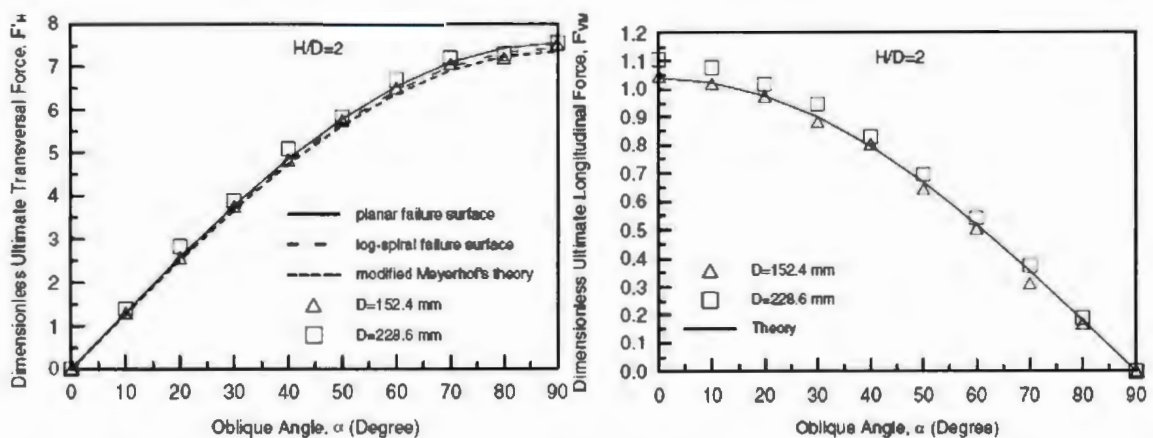


Figure 2-24: lateral and axial loads on pipe during oblique pipe-soil interaction in dense sand (Hsu et al. 2006)

Phillips et al. (2004b) presented a parametric study using continuum finite element analysis on axial-lateral pipe/soil interaction in cohesive soil. They suggested that the soil failure mechanism under axial loading is restrained within a very thin layer of soil surrounding the pipe which will involve more soil if there is any lateral displacement. Although conducted in cohesive soil, this is consistent with Wijewickreme et al. (2009) full scale test observations of a shear zone thickness of 5 to 12 times the mean particle size for axial pipe/soil interaction. Phillips et al. (2004b) developed an interaction diagram (Figure 2-25) and the following equation for combined axial-lateral loading:

Eq. 2-16

$$N_x^2 + 3N_z^2 = N_{x90}^2 \quad , \quad N_z < \alpha\pi$$

where:

$$N_x = \frac{F_x}{c_u DL} \quad , \quad F_x \text{ is the maximum lateral force on pipe}$$

$$N_z = \frac{F_z}{c_u DL} \quad , \quad F_z \text{ is the maximum axial force on pipe}$$

N_{x90} : Lateral interaction factor under pure lateral loading condition

The interaction curve in Figure 2-26 accounts for two failure mechanisms during axial-lateral pipe/soil interaction events. For small oblique angles, failure occurs by sliding along the pipe/soil interface. At larger angles, the soil failure mechanism is dominated by shear and bearing. The limiting oblique angles for the linear criterion are independent of pipe burial depth or soil shear strength or pipe/soil interface friction

angle. The curved part represents the shear failure in the soil media that is relevant to larger angles of attack up to 90°.

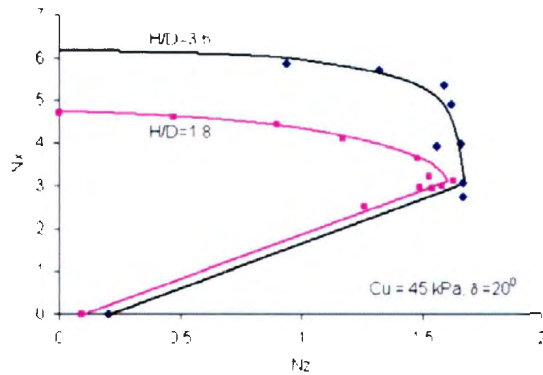


Figure 2-25: Axial-lateral force interaction diagram for two H/D ratios (Phillips et al. 2004b)

2.4.5 Lateral-vertical pipe/soil interaction

There are several studies that have made comparisons between loads and displacements in lateral and vertical directions on pipelines (e.g. Trautmann 1983, Dickin 1988, Yimsiri et al. 2004) as discussed in previous sections of this Chapter. In this section studies on oblique lateral-vertical pipe movements in soil or inclined strip anchor plates are reviewed.

Nyman (1984) performed an implicit limit equilibrium analysis on pipes buried in cohesionless soils based on Meyerhof (1973) limit equilibrium model for inclined anchor plates. Nyman used a failure mechanism including a passive wedge with planar failure surfaces which is acceptable for shallow burial depths. The ultimate soil restraint on the pipe in the oblique direction is presented as (Figure 2-26):

Eq. 2-17

$$P_{u-oblique} = i Q_u$$

where:

Eq. 2-18

$$i = 1 + \left(\frac{0.25\alpha}{90^\circ - 0.75\alpha} \right) (i_u - 1)$$

$i_u = P_u / Q_u$ is the ratio of ultimate horizontal restraint to ultimate vertical restraint and α is the angle of oblique lateral-vertical pipe movement with the vertical axis. Nyman proposed the ultimate oblique displacement as 0.015H to 0.025H for dense to loose materials, respectively.

Experimental results by Das (1985) from small scale tests on anchor plates in clay and by Hsu (1996) from large scale tests on pipes in loose sand indicate good agreement with Eq. 2-17.

Hsu (1996) conducted a series of large scale tests to investigate the lateral-uplift pipe/soil interaction for pipes buried in shallow depths in dry loose sand (friction angle=33°, relative density=21%). Four different pipe diameters with ten angles of attack from 0 to 90° were tested in two H/D ratios of 1.5 and 3.5. Typical force displacement curves and ultimate loads vs. oblique angles are presented in Figure 2-27 which indicate soil ultimate oblique restraint increases with oblique angle where most of increase happens from 45 to 90°. Hsu (1996) has indicated that the experimental results are in good agreement with Nyman (1984) limit equilibrium model for pipes and Murray and Geddes (1989) experimental results on inclined anchor plates. Hsu's results also compare well with Vanden Berghe et al. (2005) numerical analysis for lateral-vertical movement of pipes in

very loose sand (Figure 2-28). The trend of the results by Vanden Berghe et al. (2005) and Hsu (1996) on pipes in loose sand are consistent with Das (1985) experimental results for anchor plates in clay that states the oblique (lateral-vertical) restraint does not change greatly for angles from zero to 45°.

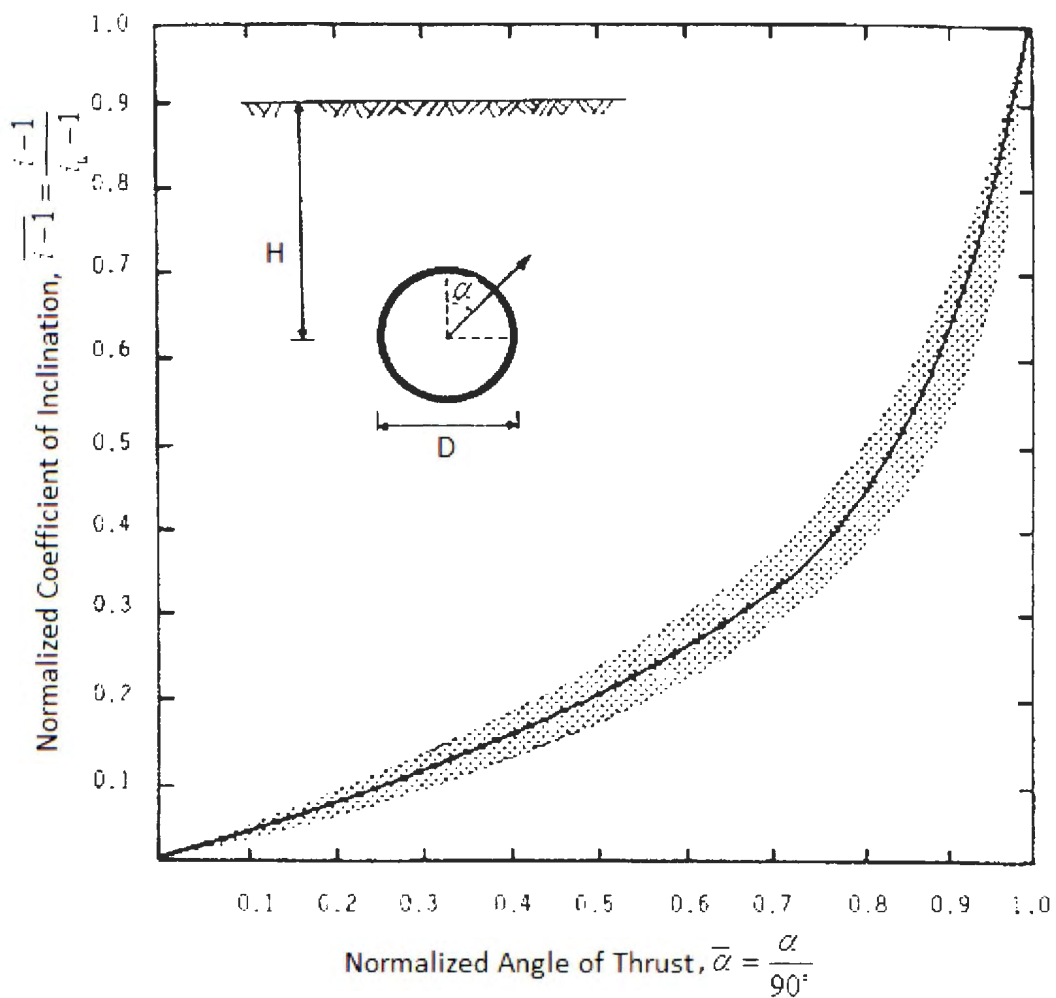


Figure 2-26: Normalized inclination factor (Nyman 1984)

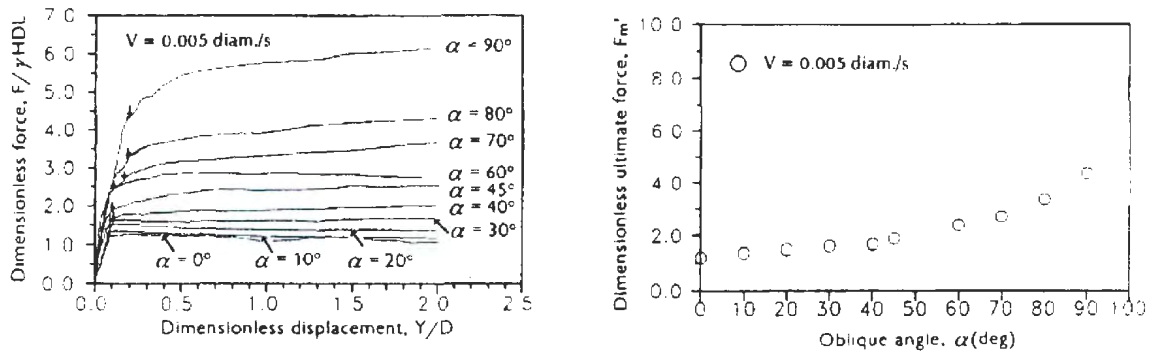


Figure 2-27: Dimensionless force-displacement curves (left) and Ultimate oblique loads vs. oblique angles (right) for $D=152.4$ mm and $H/D=1.5$ (Hsu 1996)

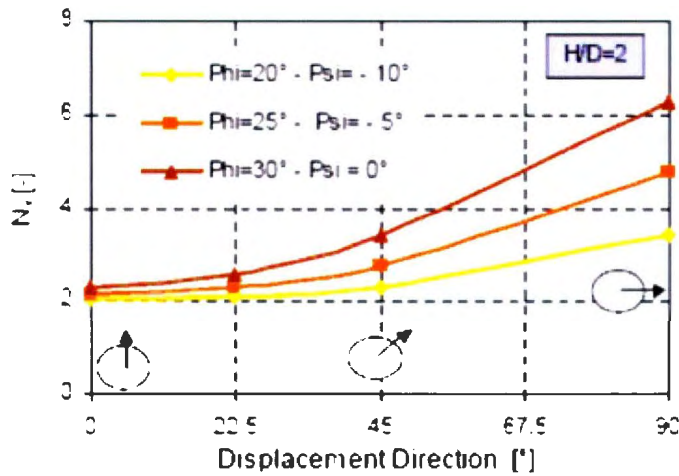


Figure 2-28: Comparison of oblique resistance on pipes in contractive granular soils (Vanden Berghe et al. 2005)

Several researchers presented the lateral-vertical pipeline/soil interaction using a plasticity model. These models consist of a failure locus or interaction curve which relates the lateral and vertical ultimate loads and an associated (e.g. Guo 2005) or non-associated (e.g. Calvetti et al. 2004) flow rule to determine the plastic displacement increments. Failure loci from some studies are discussed here.

Guo (2005) developed an associative hardening elastoplastic constitutive model for lateral-vertical upward pipe/soil interaction in clay. A circular relationship between lateral and vertical loads normalized by pure lateral and pure vertical soil restraints respectively was used as failure locus. He indicated good agreement between his model's predictions and his numerical model's results as well as Hsu's (1996) experimental results. Guo's failure surface compared well with the results of numerical modeling for clay in Appendix A of this thesis.

Zhang et al. (2002) presented the following interaction curve for lateral-vertical pipe/soil interaction for shallow buried (or half-buried) pipelines in sand (sea bed):

Eq. 2-19

$$P - \mu(Q_{ud} - Q) \left(\frac{Q}{Q_{ud}} - \frac{Q_u}{Q_{ud}} \right) = 0$$

Where P and Q are lateral and vertical components of soil load on the pipeline and μ is the coefficient of pipe/soil interface friction. Hodder and Cassidy (2010) presented a similar study on shallow buried pipes in clay.

Cocchetti et al. (2009a) proposed a three-dimensional failure criterion (Figure 2-29) for pipelines buried in sand, but they assumed no interaction in axial-lateral and axial-vertical planes. The general form of the proposed interaction domain is:

Eq. 2-20

$$\left(\frac{P}{P_u} \right)^{\alpha_1} + \left(\frac{T}{T_u} \right)^{\delta} - \left(\frac{Q_u - Q}{Q_u} \right)^{2\gamma_1} \left(\frac{Q_{ud} - Q}{Q_{ud}} \right)^{2\beta} = 0$$

where α_1 , γ_1 , δ and β define the shape of the domain. These curves are compared and discussed in Chapter six of this thesis.

Numerical studies by Cocchetti et al. (2009a) and Calvetti et al. (2004) shows a considerable interaction between lateral and vertical downward soil restraints on the pipe. As indicated in Figure 2-29, the lateral soil restraint on the pipeline may increase dramatically when downward relative displacement between pipe and soil exists. This interaction effect is not considered in the current guidelines as well.

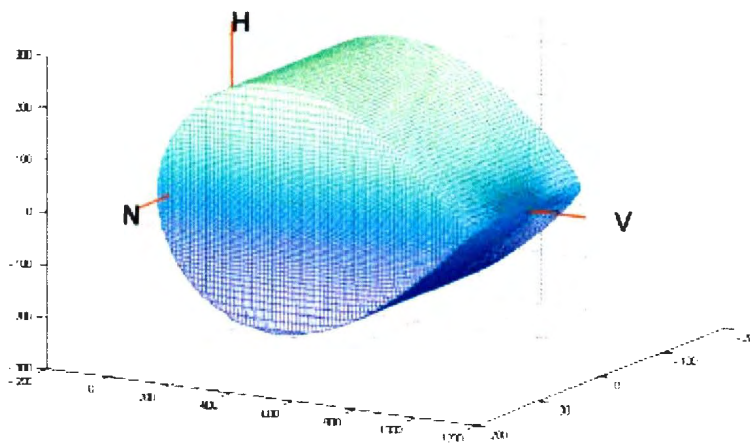


Figure 2-29: 3D interaction domain (Cocchetti et al. 2009a)

2.5 Concluding Remarks

A summary of the state of the art and practice on pipe/soil interaction is presented in this Chapter. The proposed methods by guidelines to calculate the ultimate loads and displacements during relative displacements between pipe and soil in different directions are discussed. Recent studies in the literature are reviewed and it is shown that the current

guidelines need to be revised to consider new findings in the literature. Also the previous studies on oblique pipe/soil interaction are discussed. It is shown that there is a need for more investigations on oblique pipe/soil interactions particularly in axial-lateral and axial-vertical directions which will be discussed in detail in this thesis.

3 Centrifuge tests preparations and procedures

3.1 Introduction

Centrifuge modeling is an efficient method to study gravity dependent problems in geotechnical engineering. Considering the cost and difficulties associated with large scale modeling and uncertainties relevant to scale effect in the results of small scale 1-g tests, geotechnical centrifuge usually provides an efficient option. It has been used in several studies (e.g., Dickin 1988; Paulin et al. 1995) to investigate different aspects of pipe/soil interaction.

A series of centrifuge tests have been conducted in this study to investigate the effect of obliquity in pipe/soil relative displacements on the load applied to the pipe in axial and lateral directions. The experimental data are also used to validate a numerical model to extend the investigations through numerical parametric studies (details of comparisons are discussed in Chapter 5).

Four tests were conducted under similar conditions except for the oblique angles of movement (Figure 2-22). The angles of movement for tests number one to four were 90° (pure lateral), 0° (pure axial), 40° and 70° respectively. All tests were performed under a centrifugal acceleration of 12.3g and a displacement rate of 0.04 mm/s.

3.2 A summary of centrifuge principles and scaling laws

In centrifuge modeling technique the gravitational effects in prototype scale are replicated in a small scale model using centrifugal acceleration. The centrifugal acceleration is applied to the model by spinning it at a prescribed angular velocity. By increasing the centrifugal acceleration by N times of the gravitational acceleration (g), the model dimensions can be reduced N times with respect to the prototype dimensions while the stress level remains identical.

Certain scaling laws apply during construction of the model and also interpreting the results in prototype scale. These scaling laws can be derived from dimensional analysis or from governing equations. Some scaling relationships relevant to this thesis are presented in Table 3-1 (Taylor 1995).

Table 3-1: Some common centrifuge scaling relationships

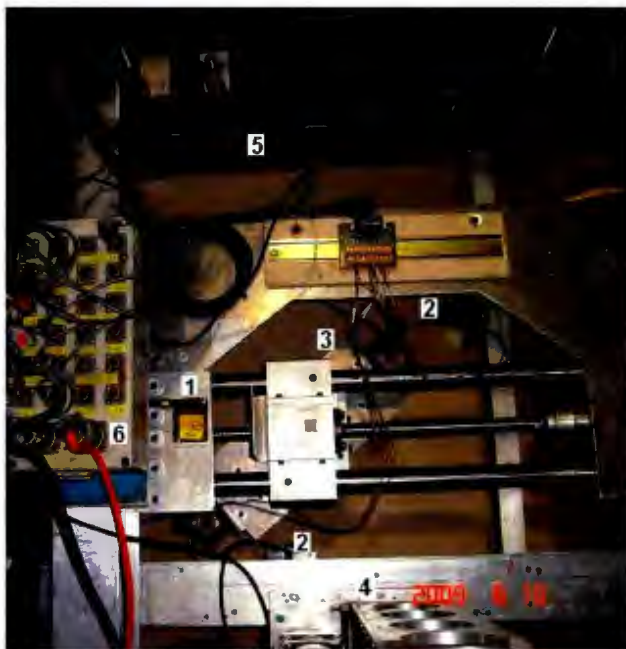
Parameter	Scale factor (Prototype: Model) at Ng
Length	1: $1/N$
Stress	1: 1
Strain	1: 1
Density	1: 1
Unit weight	1: N
Force	1: $1/N^2$
Time (inertial events)	1: $1/N$

The centrifuge facility at C-CORE includes an Acutronic 680-2 machine which is capable of testing models at up to 200 g. It has a radius of 5.5 m to the surface of the swinging platform and its maximum capacity is 220 g-tones at 100g.

3.3 Test apparatus

The centrifuge strong box inner dimensions were 1180 mm x 940 mm x 400mm. The model steel pipe was 41mm in outer diameter (minimum diameter required for the load cells) with 6.35mm wall thickness. This provided a rigid pipe mechanical response, but the pipe weight influenced the pipe/soil interaction response. As this study is concentrated on finding the load-displacement relationship and the ultimate loads and displacements in soil, a rigid pipe is considered in both experimental and numerical modeling. The pipe was buried to a cover depth of 61.5mm that corresponds to a pipe springline burial depth to pipe diameter ratio (H/D) of 2. The pipe length was 328 mm that gives a length over diameter ratio of eight ($L/D=8$). Previous experimental studies (e.g. Das 1985, Dickin 1988) have shown that a length equal to eight times pipe diameter or anchor width provides a condition like strip anchor plate or continuous pipeline.

The buried pipe was moved in a horizontal plane using a leadscrew actuator. The horizontal motorized carriage was connected to two ball races via guiding plate (Figure 3-1). The angle between the pipe longitudinal axis and the direction of movement (oblique angle) could be adjusted using the guiding plate. The guiding plate configuration during oblique 40° test is shown in Figure 3-2.



- 1-Top laser displacement sensor
- 2-Bottom laser displacement sensor
- 3-Guiding plate
- 4-Vertical actuator set up for CPT
- 5-Strong box
- 6-Signal conditioning box

a) Plan view



- 1-Dog bone
- 2-Stanchion
- 3-Ball races
- 4-Guiding plate
- 5-CPT probe

b) Elevation view

Figure 3-2: (a) Plan and (b) elevation view of test box (oblique 40° test).

There was cross sensitivity between axial and lateral strain gauges when lateral load was applied to the load cell, so that during pure lateral loading strains were recorded on both lateral and axial strain gauges. Therefore the load cells were calibrated for axial load and two sets of lateral loads with different lever arms, using a coupled calibration matrix. The lateral load (F) and its lever arm (L) used during load cell calibration are shown

schematically in Figure 3-5. The axial load measured (dA) during lateral loading causes the cross sensitivity. Coupled calibration matrix was used to establish this effect. In air pipe loading tests were conducted to confirm the load cells measurements.



Figure 3-3: Pipe section before getting buried (lateral test).

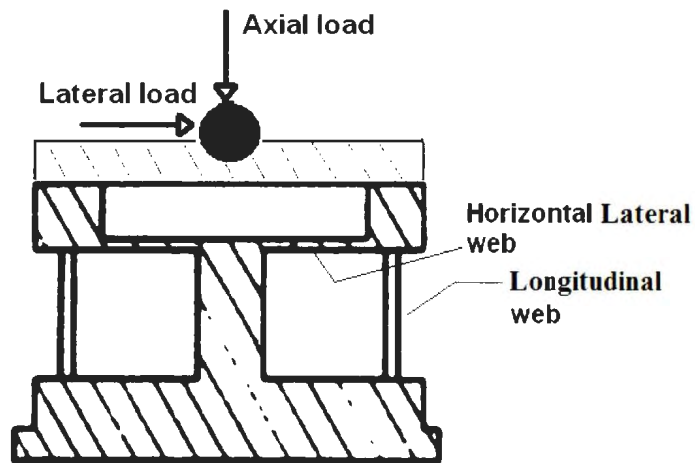


Figure 3-4: Load cell configuration, after Stroud (1971).

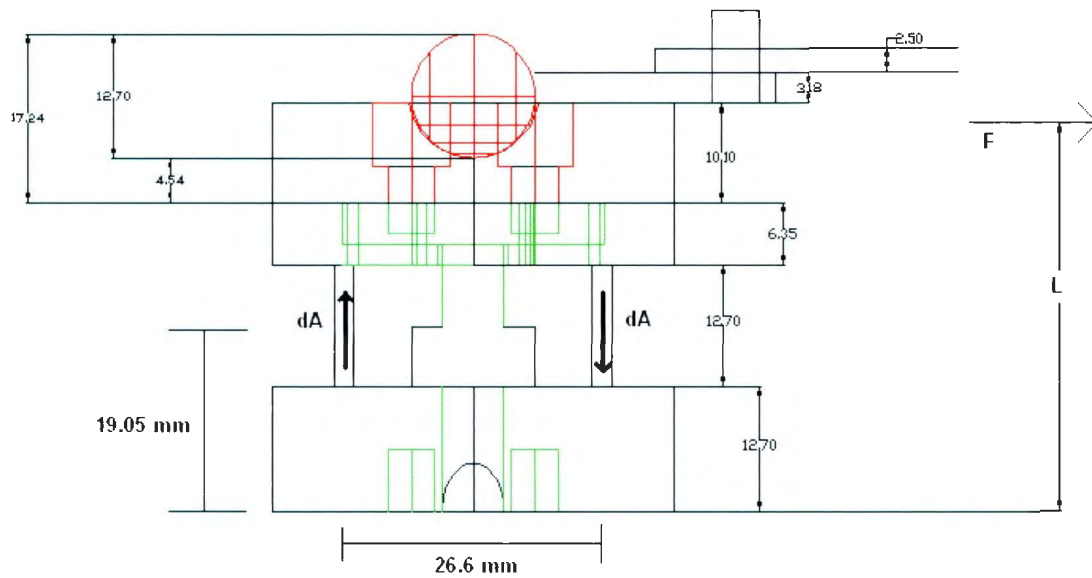


Figure 3-5: Load cell dimensions and schematic lateral loads used for calibration.

3.3.2 Displacement transducers

Vertical movements of pipe were measured by two LVDTs (linear variable differential transformer) at the two ends of the dog bone. LVDTs were secured on ball races (Figure 3-6).

Lateral and axial pipe displacements during pure lateral and pure axial loading tests, were measured using a laser displacement sensor (#1 in Figure 3-2.a) on top of the horizontal actuator. For the two oblique loading cases (40° and 70°) two laser sensors (#2 in Figure 3-2.a and Figure 3-6) were added at a lower elevation to measure the displacement at the dogbone level. These added sensors allowed capturing differences

in measured displacements at actuator and dogbone level and perform relevant corrections on pipe displacements.



Figure 3-6: Laser sensor and LVDT at one end of the pipe (70° test)

An actuator compliance effect was observed during the centrifuge tests due to a slight rotation of the loading system. To account for the actuator compliance, a series of in-air tests were conducted to find the relationship between the applied load to the pipe and the corresponding stiffness of the loading system. The displacement measurements at actuator and dog bone levels were corrected to address the actuator compliance which is discussed in more detail in the next Chapter. The corrected pipe displacements were used for the final load-displacement curves.

3.4 Soil Test Bed

Dry fine silica sand with specific gravity of 2.65, and the minimum and maximum void ratios of 0.60 and 0.93, respectively, was used. An average relative density of 0.82 was obtained in the four test beds using sand raining procedure. All test beds were prepared under the same sand raining conditions i.e. height, aperture size and funnel moving speed. Sand raining device at the C-CORE centrifuge lab is shown in Figure 3-7.



Figure 3-7: Sand raining device at C-CORE.

Cone Penetration Tests (CPT) were conducted on test bed, for 40 and 70 degrees oblique tests, to ensure that repeating the sand raining procedure gives similar sand beds. The CPT test was run after reaching the desired acceleration (12.3g) level and before starting pipe movement. The depths of cone penetration were almost 140 and 150 mm from the

soil surface for 40° and 70° tests respectively. Figure 3-2.a shows the location of the vertical actuator for CPT test (#4) and Figure 3-2.b shows the position of the CPT probe (#5) with respect to pipe. The cone diameter was 11.28 mm with the section area of 100 mm² and the cone angle of 60°.

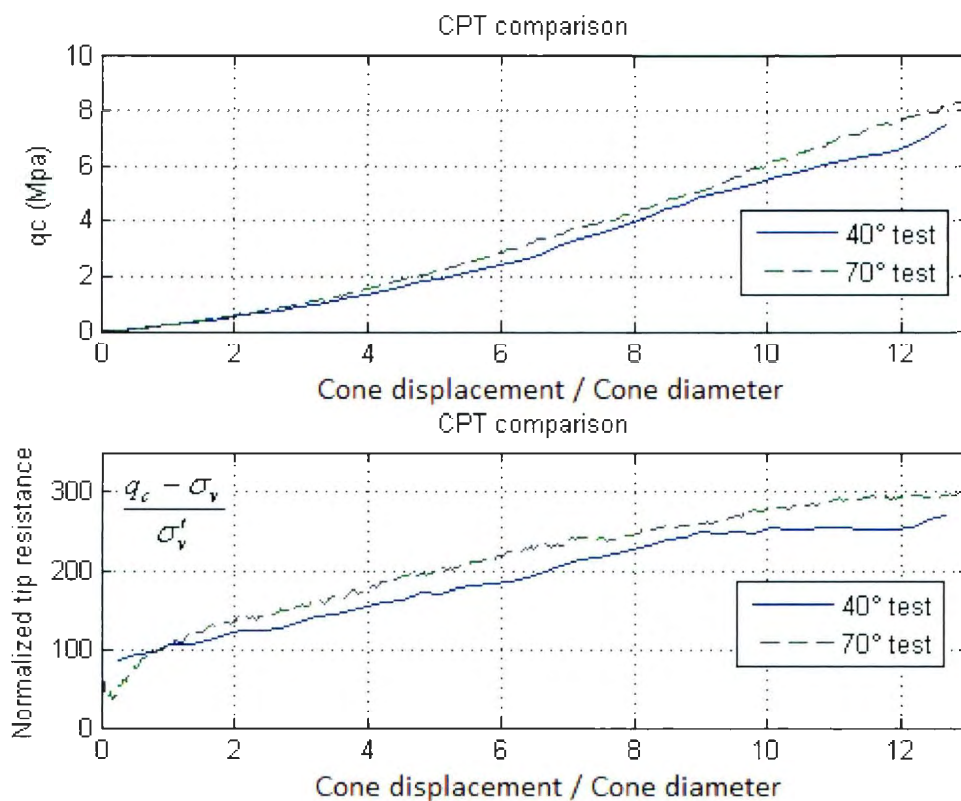


Figure 3-8: Comparison of cone tip resistance and normalized cone tip resistance at different depths

Figure 3-8 compares the cone tip resistances (q_c) and normalized tip resistances for the two oblique loading tests. The CPT test results confirm the repeatability of the raining method and similarity of the sand bed at different depths. A slightly higher resistance for 70° test comes from a slightly higher relative density (Table 3-2).

A summary of sand bed parameters for all four tests is presented in Table 3-2.

Table 3-2: Summary of sand bed parameters.

Parameters	Angle of movement ($^{\circ}$)(Figure 2-22)			
	90	0	40	70
ρ (kg / m^3)	1598	1596	1596	1600
Dr (relative density %)	82.5	82	82	83

Direct shear tests under normal stresses of 16 to 65 kPa resulted in the peak friction angle of 43° , constant volume friction angle of 33° and pipe/soil interface friction coefficient of 0.44. The pipe/soil interface coefficient of friction was evaluated by using pipe material and soil, in the bottom and top parts of the direct shear box, respectively. Kulhawy et al. (1983) indicated that the interface friction angle δ between sand and smooth steel varies from $0.5\phi'$ to $0.7\phi'$ which is consistent with $\delta=0.55\phi'$ found from direct shear tests in this study for steel pipe with smooth surface. They also indicated that δ between sand and rough steel varies from $0.7\phi'$ to $1.0\phi'$. In Chapter 6 two values of 0.5 and 0.8 for pipe surface friction factor are used for parametric studies which are relevant to smooth and rough surface for steel pipelines.

The pipe bedding layer was 100 mm of sand, which was equivalent to 2.4 pipe diameters.

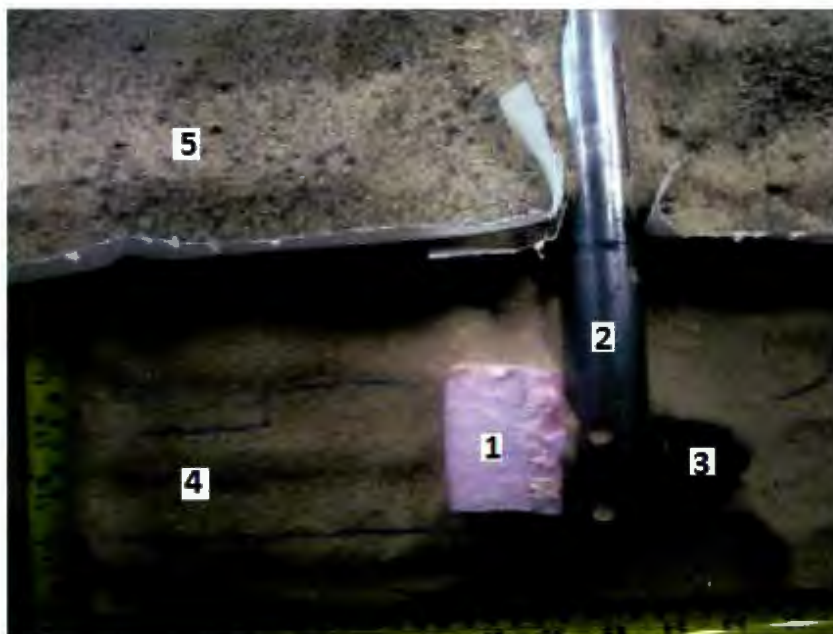
The prototype soil parameters are summarized in Table 3-3.

Crushable foams were used in front of the stanchions in axial and oblique loading tests to reduce the effect of end bearing on the axial component of the load on the pipe. The foams were placed during sand raining. Figure 3-9 shows the location of the crushable foam in front of the stanchion, after excavation, at the end of the oblique 45° centrifuge test. The stanchions moved into the foam during pipe displacements to avoid failing the soil which could change the stress conditions around the near end of the pipe.

Table 3-3: Summary of equivalent prototype test parameters

Parameters	Values
Pipe diameter-D (mm)	504
Embedment depth to the pipe centerline-H (mm)	1008
Pipe length over diameter-L/D	8
Average dry density of sand- ρ (kg/m ³)	1598
Peak sand internal friction angle- ϕ'_{peak}	43°
Constant volume friction angle- ϕ'_{cv}	33°
Pipe/soil interface friction coefficient- μ	0.44
Cohesion- c'	0

Several unloading-reloading cycles were conducted during each centrifuge test to have a measure of the elastic response of the soil to compare with numerical modeling results.



- 1- Crushable foam**
- 2- Stanchion**
- 3- Loadcell and pipe sample**
- 4- Sand**
- 5- Gravel (added before excavation)**

Figure 3-9: Location of the crushable foam in front of the stanchion

3.5 Summary

- Main parts of the test apparatus and major steps required for test preparations are discussed in this Chapter,
- Test box dimensions were 1180 mm × 940 mm × 400 mm,
- The model pipe diameter was 41 mm, with a length over diameter ratio (L/D) of 8,
- All tests were carried out for a burial depth ratio (H/D) of 2,
- Loading system included:
 - Horizontal carriage to move the pipe in soil,
 - Guiding plate to connect the carriage to ball races in the desired oblique angle,
 - Two ball races to let the pipe holding system to move freely in vertical

direction.

- Two stanchions to connect the two ends of the pipe to ball races.
- A dogbone to keep the stanchions and the pipe in a vertical plane.
- Measurement devices included:
 - Two load cells fixed to the ends of the stanchions and connected to both ends of the pipe using two small bearings.
 - One laser displacement sensor for lateral and axial loading tests and three laser sensors for oblique loading tests, to measure the pipe displacements in horizontal plane.
 - vertical displacements were measured by two LVDTs at the two ends of the dogbone.
- All tests were performed in sand test bed with 0.82 relative density. Cone Penetration Tests were carried out to control the repeatability of the test bed preparation procedures.

4 Experimental data

In this Chapter, the load-displacement data resulted from centrifuge tests are presented and briefly discussed. A more detailed discussion along with comparison with numerical data is presented in Chapter 5.

As it is mentioned in Chapter 3, actuator compliance was observed during centrifuge tests. During oblique 40° and 70° tests, the displacements were measured at top carriage (actuator) and dog bone levels, but for pure axial and pure lateral tests the displacements were measured at the top carriage level. All measured displacements were corrected for actuator compliance and estimated for pipe level. A brief explanation of displacement correction procedure is presented in the following section.

4.1 Displacement correction

Figure 4-1 shows the displacement measurements by three laser sensors during the oblique 40° test. The measured displacements by the laser sensor which is fixed at the carriage level (#1 in Figure 3-2.a) are larger than the displacements measured at dogbone level due to actuator compliance. To account for the actuator compliance, a series of in-air tests were conducted. It was found that actuator compliance occurs because of rotation of the loading system including stanchions, ball races, guiding plate and carriage (Figure 3-1) along a point at the center of the carriage. Figure 4-2 shows one of the setups used for in-air tests. In this figure a lateral load is applied at the middle of the pipe and

displacements at carriage and top ball race level and rotation of the guiding plate are measured.

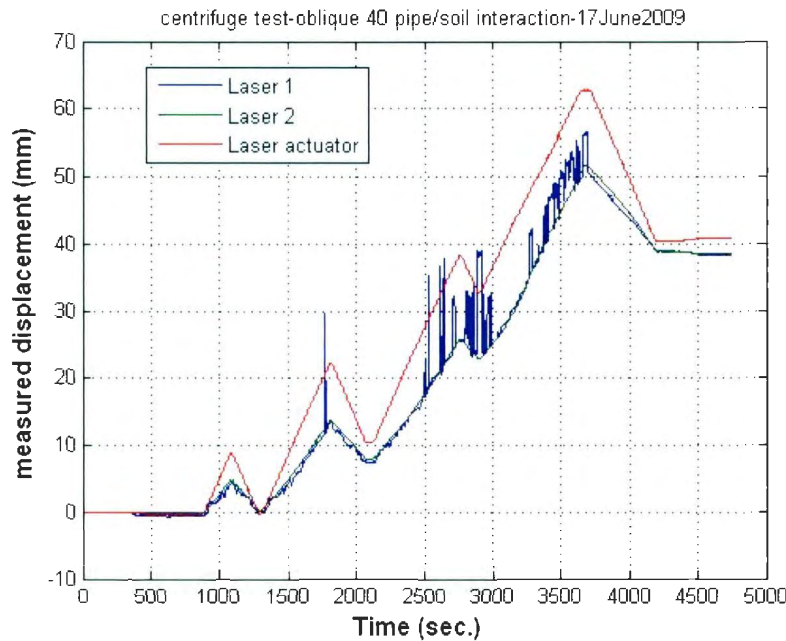


Figure 4-1: Displacement measurements by laser sensors at carriage and dogbone levels (40° test)- laser 1 & 2 are lasers at dogbone level

Figure 4-3 presents data points from in-air lateral and axial loading tests. Axial and lateral loads up to the maximum loads applied to the pipe during centrifuge tests, are exerted to the pipe and the displacements at pipe and dogbone levels are compared. Data points are very close to the line of $y=1.5x$, which means the measured displacements at pipe level are about 1.5 times the measured displacements at dogbone level. The ratio of the distance from pipe centerline to the center of carriage (325mm) over the distance from dogbone to the center of carriage (215mm) is equal to 1.51. This is consistent with the rotation of the loading system around a point at the center of the carriage.



Figure 4-2: In-air set up to measure the actuator compliance

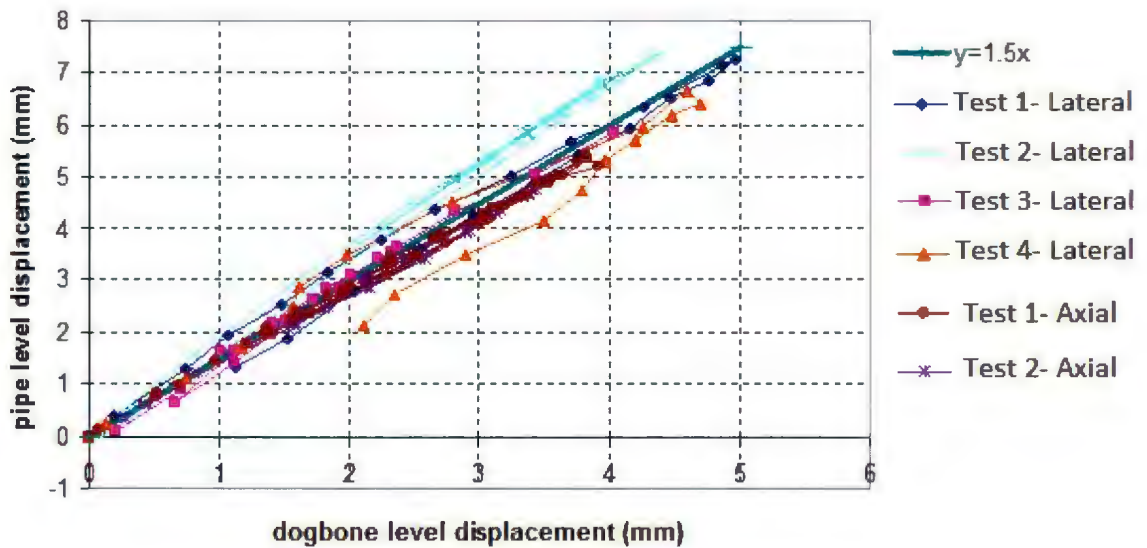


Figure 4-3: Data points comparing pipe and dogbone level displacements from in-air loading tests

To obtain the displacements at pipe level from oblique loading test data, the dogbone and actuator level measurements during centrifuge tests were used:

Eq. 4-1

$$d_{\text{pipe}} = d_{\text{actuator}} - 1.5(d_{\text{actuator}} - d_{\text{dogbone}})$$

where d_{pipe} is the calculated displacement at pipe level and d_{actuator} and d_{dogbone} are the measured displacements at actuator and dogbone levels respectively.

Figure 4-4 and Figure 4-5 compare the corrected load-displacement curves for oblique 40° and 70° tests with the load-displacement curves based on displacements measured at actuator and dogbone levels during centrifuge tests.

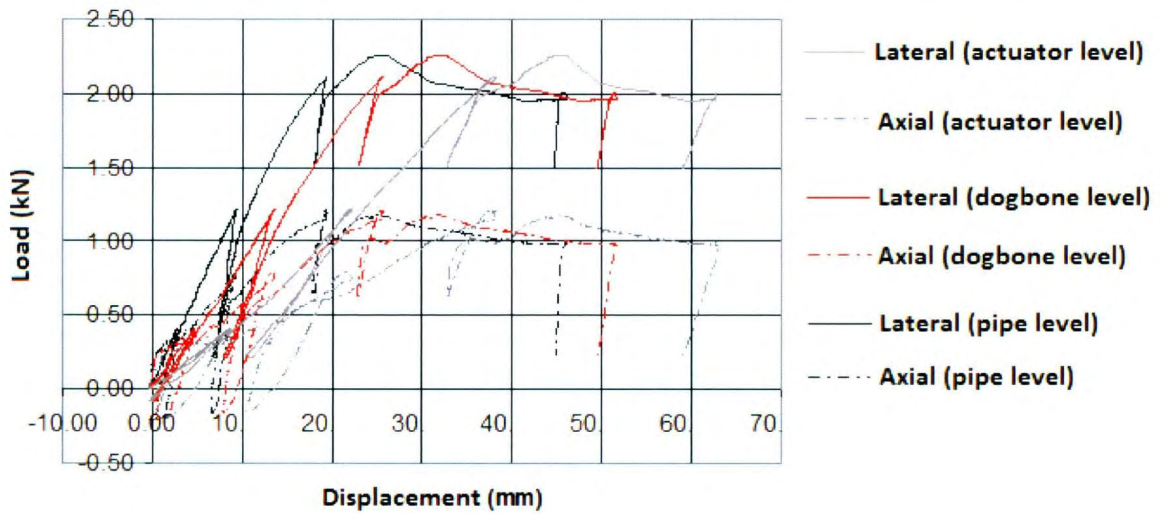


Figure 4-4: Comparison of load-displacement curves for oblique 40° test using displacements measured at actuator and dogbone levels and corrected for pipe level.

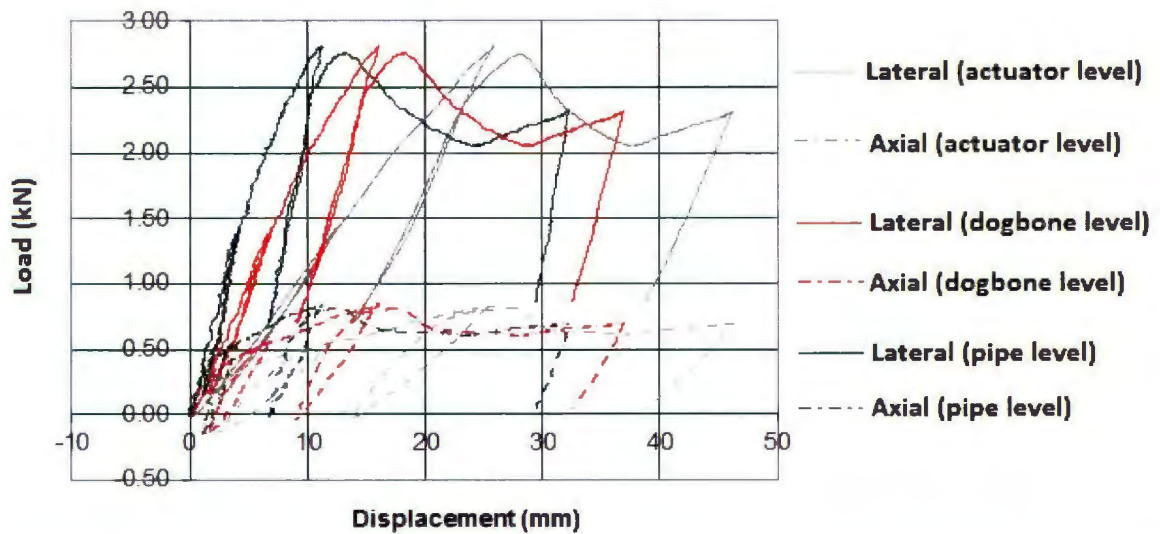


Figure 4-5: Comparison of load-displacement curves for oblique 70° test using displacements measured at actuator and dogbone levels and corrected for pipe level.

For pure lateral and pure axial tests, the displacements were measured at actuator level during centrifuge tests. The measured displacements were corrected using bilinear relationships that relate the differential displacements in the loading system to the load applied to the pipe. Using data from in-air loading tests (Figure 4-6), the measured lateral and axial load-displacement curves are corrected for displacements at pipe level, as shown in Figure 4-7 and Figure 4-8.

All displacements reported in the following sections of this thesis are corrected displacements at pipe level. The first unloading cycles are removed from the corrected curves for the sake of clarity.

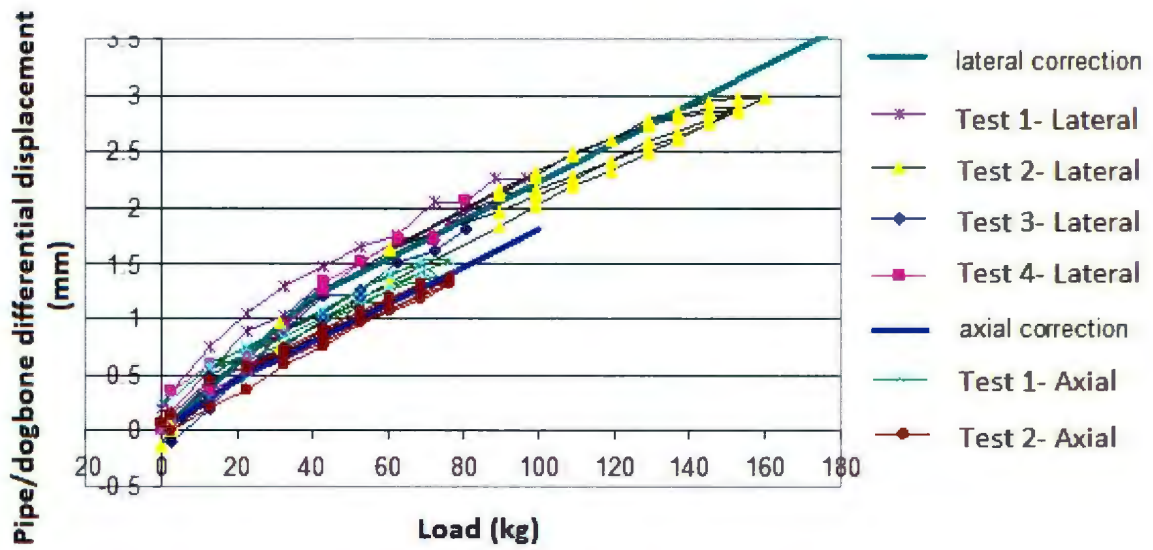


Figure 4-6: Lateral and axial correction curves as a function of load applied to the pipe.

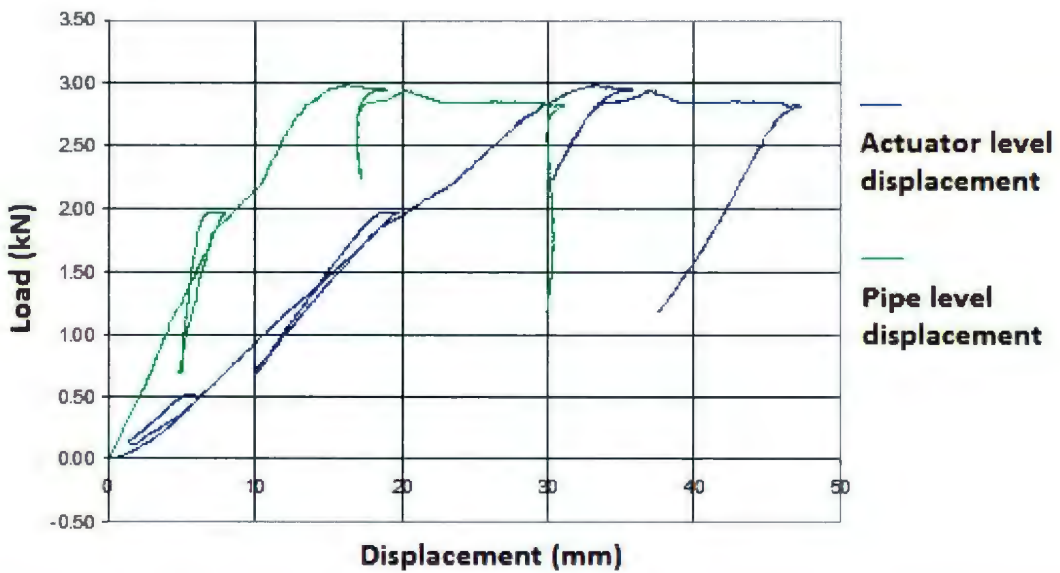


Figure 4-7: Load-displacement curves for lateral test using displacements measured at actuator level and corrected for pipe level.

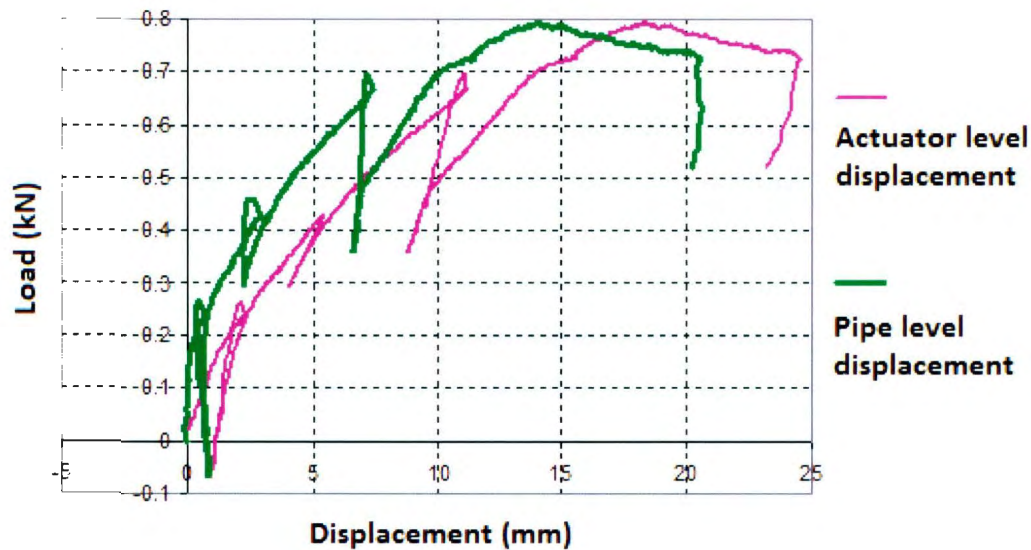


Figure 4-8: Load-displacement curves for lateral test using displacements measured at actuator level and corrected for pipe level.

4.2 Lateral test (Test #1)

Figure 4-9 shows the load-displacement relationship resulted from pure lateral loading centrifuge test. Horizontal axis represents the nondimensional lateral displacement and the vertical axis represents the nondimensional lateral load on the unit length of the pipe. The irregular shape observed during the initial segment of the unloading curve was associated with actuator compliance as discussed in Chapter 4.

Ultimate load and ultimate displacement are general terms used in pipeline design guidelines. In this study, as it is concentrated on dense sand, peak loads are used as ultimate loads. The pipe/soil relative displacements at peak loads are referred to as ultimate displacements. Using the peak load as ultimate load a lateral interaction factor of 14 is obtained from Figure 4-9. The lateral interaction factor is defined as:

Eq. 4-2

$$N_{qh} = \frac{P_u}{\gamma' \cdot H \cdot D}$$

where P_u is the ultimate lateral load obtained from the load-displacement curve and was chosen as peak load in this study. P is the lateral load applied to the unit length of the pipeline.

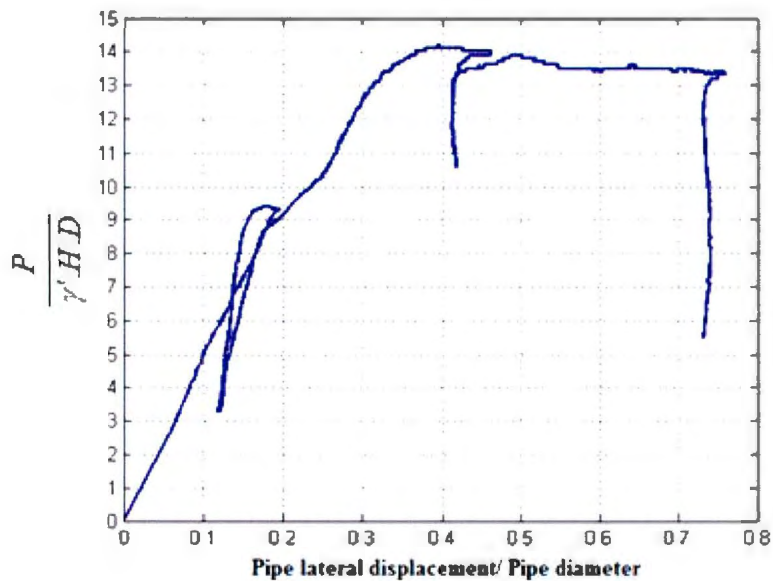


Figure 4-9: Load-displacement relationship from lateral loading test

As mentioned in Chapter two, Honegger and Nyman (2004) suggested the lateral bearing capacity factors (N_{qh}) of Hansen (1961) to be used for pipe/soil interaction in sand. This approach (Figure 2-5) estimates bearing capacity factors (e.g. $N_{qh} = 21$ for $H/D=2$ and $\phi' = 43^\circ$) that are significantly higher than those suggested by other studies. Trautmann

(1983) experimental results (Figure 2-7) are consistent with Ovesen (1964) theoretical model with estimates of $N_{qh}=8.5$ for the same condition.

Guo and Stolle (2005) presented the following equation to consider the scale effect:

Eq. 4-3

$$N_{qh} = k \left(\frac{H}{D} \right)^m \left(\frac{D_{ref}}{D} \right)^n$$

where $D_{ref}=1$ m. For $\phi=43^\circ$ the authors suggested $k=6$, $m=0.35$ and $n=0.2-0.25$ that results in a bearing capacity factor of 8.8 to 9.1 which is lower than what is resulted in this study ($N_{qh}=14$).

The main factor that increases the lateral bearing capacity in the current experimental study is the pipe selfweight. As mentioned in Chapter two, Trautmann (1983) indicated that relatively heavy model pipe and loading system will result in higher loads on the pipeline during the test. In this study the weight of the centrifuge model pipe and supporting system i.e. stanchions and dog bone (Figure 3-3) was 24.7 kN/m in prototype scale which is about eight times higher than that of an oil filled pipe (assumed to be about 3.1 kN/m). Although vertical motion was unrestrained during centrifuge testing, the recorded vertical movement was negligible. Figure 4-10 shows the vertical displacement measurement at the two ends of the pipe during lateral centrifuge test. The maximum displacement of 0.24 mm in model scale, with an acceleration level of 12.3g, results in a vertical displacement of about 3 mm in prototype scale. This amount of vertical displacement is very small compared to a pipe diameter of 504 mm.

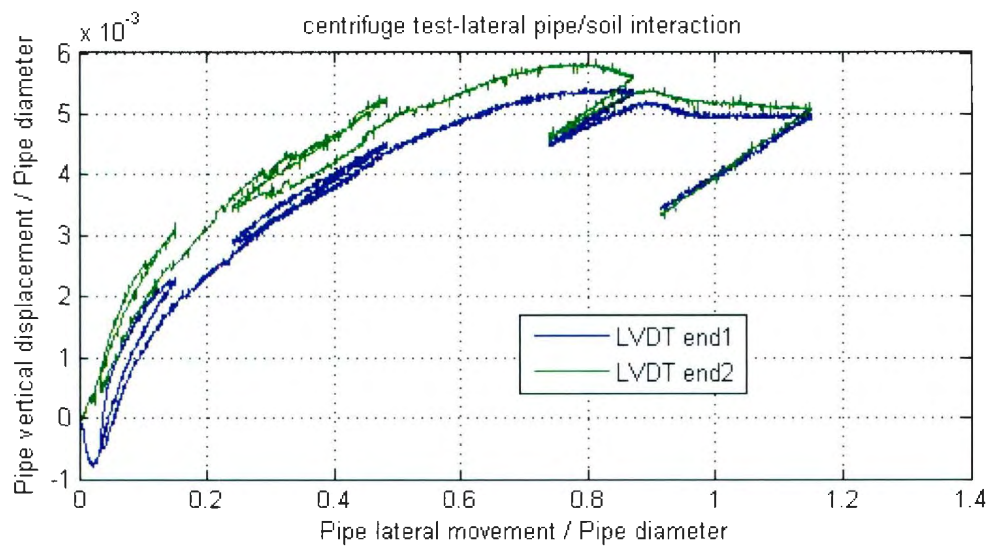


Figure 4-10: Vertical displacement measurements during lateral displacement test

The effect of pipe selfweight, observed from experimental data, are discussed in Chapter five by means of numerical modeling.

The ultimate lateral displacement, defined as the lateral displacement at peak load, from the centrifuge test (0.4D) (Figure 4-9) is higher than similar experimental results reported in the literature. The ultimate displacements from Trautmann (1983) large scale tests were in the range of 0.05 to 0.075D. Hsu et al. (2006) reported an ultimate displacement of 0.25 for $H/D=1$ in dense sand during full scale tests. Dickin (1988) reported ultimate displacements in the range of 0.2D in dense sand during 40g centrifuge tests. This inconsistency between the ultimate displacements in centrifuge tests and full scale tests has been observed in previous studies (e.g. Palmer et al. 2003).

There may be several reasons that explain this result. Test bed construction disturbance (i.e. change in density around pipe during sand pluviation) can cause an effect similar to the trench effect and increase the ultimate displacement during centrifuge tests.

The ultimate displacement is further discussed in Chapter 5 in comparison with numerical modeling results.

4.3 Axial test (Test #2)

Figure 4-11 shows the load-displacement curve resulted from pure axial centrifuge test. In this figure, T is the axial load applied to the unit length of the pipeline. Several unloading-reloading cycles were conducted during the centrifuge test. The experimental load-displacement curve shows the axial interaction factor increases with axial displacement to approximately $0.34D$ (14 mm at model scale). According to Honegger and Nyman (2004) pure axial friction should be mobilized at very small displacements of about 3 mm for dense sand.

Eq. 2-5, which is developed for dense sands, with a choice of $\gamma_d=15.66 \text{ kN/m}^3$, $\gamma_{dmin}=13.47 \text{ kN/m}^3$ and $\phi'=43^\circ$ results in a K_0 value of 1.2, and Eq. 2-2 results in an axial interaction factor of 1.52. The axial interaction factor is defined as:

Eq. 4-4

$$N_t = T_u / \gamma' \cdot H \cdot D$$

where T_u is the ultimate axial load that is equal to the peak load in this study.

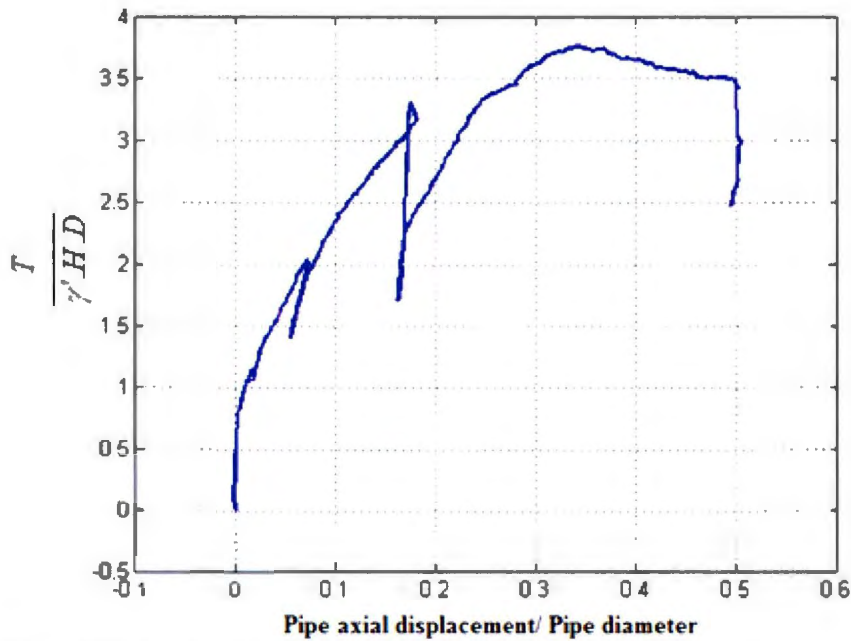


Figure 4-11: Load-displacement relationship from axial loading test

Eq. 2-2 does not consider the effect of pipe selfweight. Eq. 2-6 considering the pipe selfweight (24.7 kN/m) gives an axial interaction factor of 1.94 that is lower than the axial interaction factor of 3.75 from the centrifuge test (Figure 4-11).

The large value for the axial resistance during centrifuge test can be attributed to a small amount of pipe misalignment in vertical plane. It is shown later in this study that a small amount of pipe misalignment in horizontal plane causes this kind of increase in the soil axial resistance.

Wijewickreme et al. (2009) presented results of full scale axial tests in dense sand and reported an increase in the axial restraint on the pipeline due to confined shear induced dilation. Wijewickreme et al. (2009) referred to this phenomenon as the effect of confined

dilation. The increased axial resistance in this study can also be a result of confined dilation in the sheared sand at the pipe/soil interface, which is equivalent to an increase in the coefficient of lateral earth pressure at rest (K_0). Shearing dense sand in confined condition increases the normal load on the pipe circumference and consequently increases the axial load on the pipe.

These two effects, discussed in the previous paragraphs, both require larger axial displacements of pipe in the soil to reach the peak load, than in the case of pure axial friction.

4.4 Oblique 40° (Test #3) and 70° (Test #4) tests

For oblique loading tests, the pipe's position was adjusted to make the specified oblique angle with the direction of movement. Figure 4-12 shows the pipe position with respect to the direction of movement at the end of the oblique 40° test.

Figure 4-13 and Figure 4-14 show the load-displacement curves for oblique angles of 40° and 70°, respectively. In comparison with the lateral loading test, the unload/reload curves from oblique loading tests exhibit improvement and no irregular shape is observed. This improvement was due to the addition of two bottom laser displacement sensors (#2 in Figure 3-2.a) during oblique loading tests that resulted in an improved correction basis for estimating the actuator compliance. Small negative axial loads are recorded at the end of unloading curves in Figure 4-13 and 4-14. These negative values show at some point during unloading the direction of load on the pipe has changed.

A comparison of all experimental load-displacement curves is presented in Figure 4-15. The ultimate lateral load increases by increasing the oblique angle from zero to a maximum at 90° . The ultimate axial load increases by increasing the oblique angle from 0° to 40° and then decreases to zero at 90° . This observation is discussed in detail in Chapter six.

For the two oblique loading tests, the failure surfaces in front of the pipe were examined using layers of coloured sands. The general configuration of failure surfaces from experimental and numerical modeling are compared in Chapter five. In Figure 4-16 the main steps to find the failure surfaces in soil after centrifuge tests are shown.



Figure 4-12: Soil surface deformation after oblique 40° test.

4.5 Summary

- Centrifuge tests were conducted for lateral, axial and oblique 40° and 70° pipe/soil relative displacements,
- Experimental data resulted from four centrifuge tests are reported in this Chapter,
- The displacements were corrected for actuator compliance,
- The effect of pipe selfweight on the ultimate loads on the pipe is discussed. This effect will be assessed in more detail in Chapter 5,
- The purpose of experimental program was to provide data to validate the numerical model which will be discussed in the next Chapter.

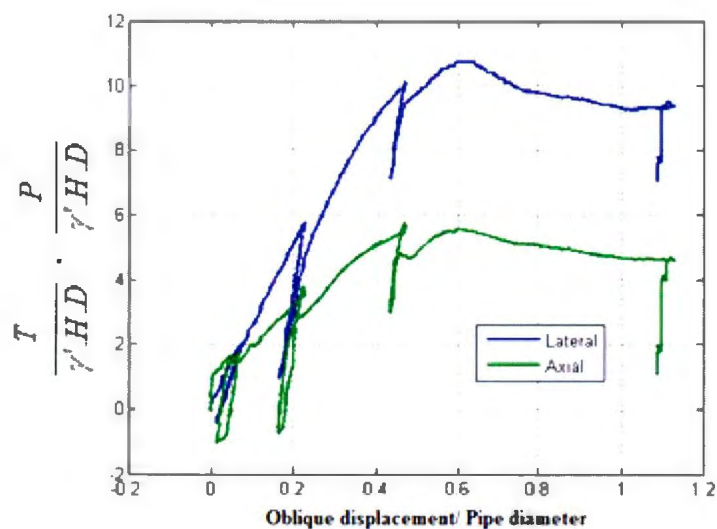


Figure 4-13: Load-displacement curves from oblique 40° test

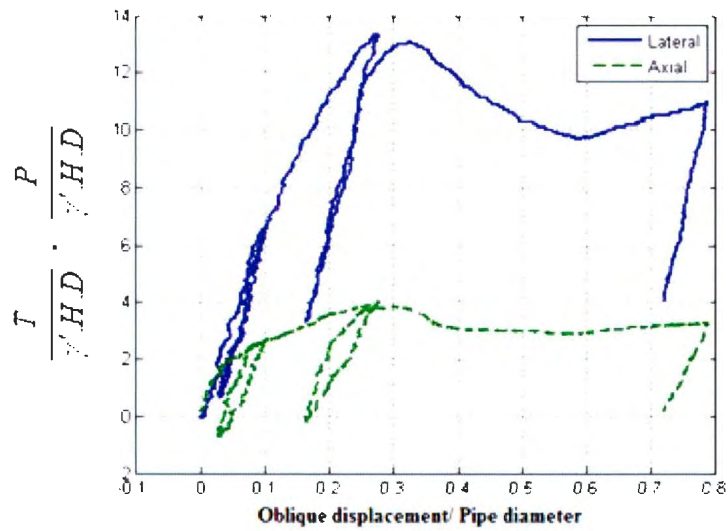


Figure 4-14: Load-displacement curves for oblique 70° test

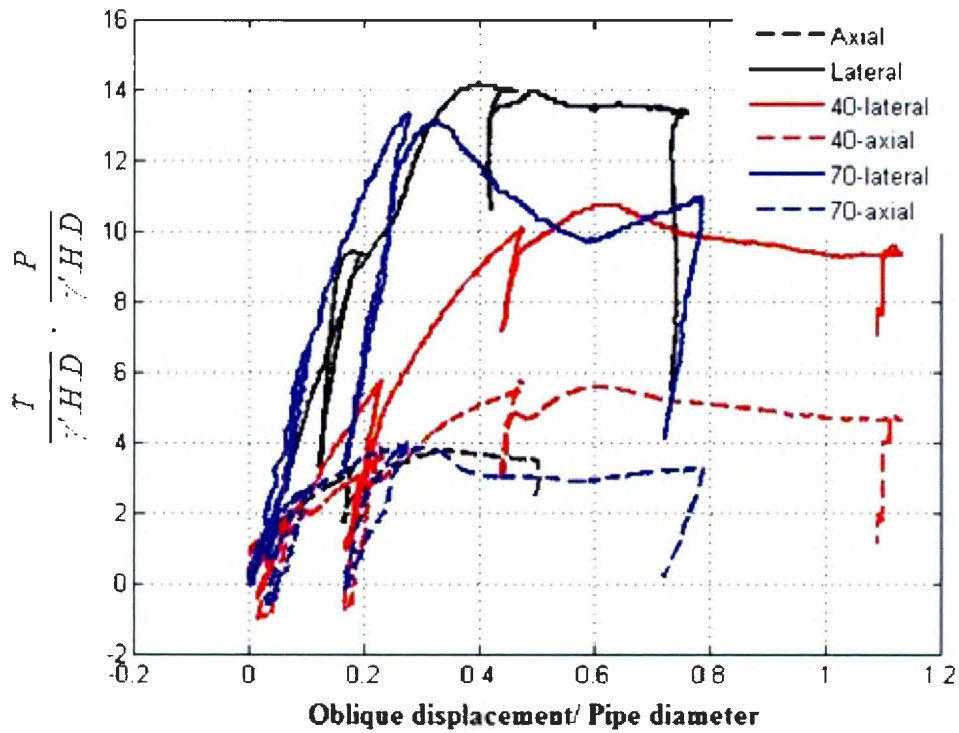


Figure 4-15: Load-displacement curves from all four centrifuge tests.

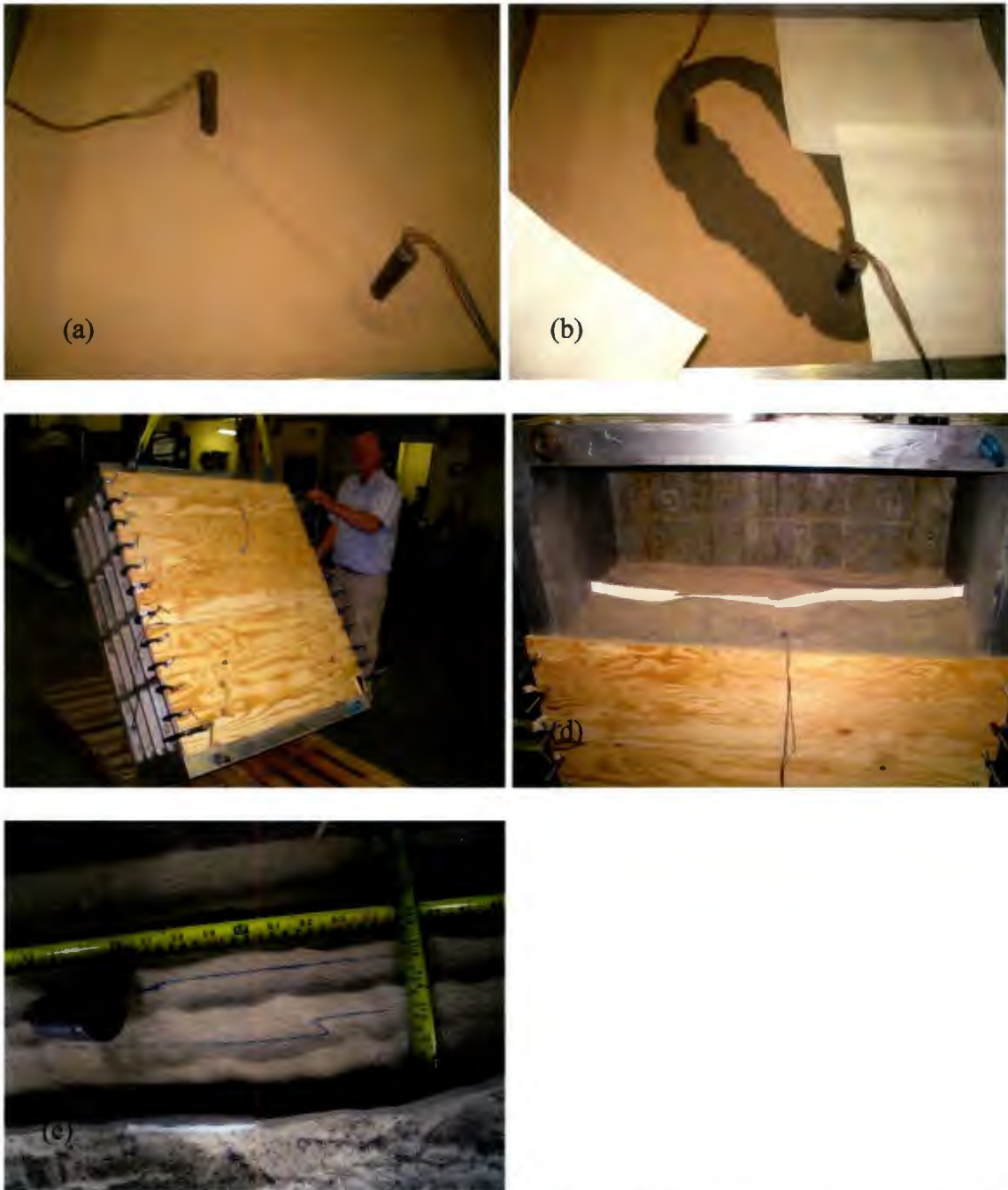


Figure 4-16: (a) Deformed soil surface after oblique 40° test, (b) Covering the deformed soil surface areas with dark sand and soil surface with filter paper, (c) Filling the upper part of the strong box with gravel, covering the box surface with wood strips and rotating the box by 90°, (d) Excavating the soil layer by layer, (e) Taking pictures of deformed layers of coloured sand in oblique planes.

5 Numerical modeling

5.1 Introduction

The finite element (FE) method is by far the most widely used technique to simulate solid deformation problems. Most of previous numerical studies on pipe/soil interaction, as shown in Chapter 2, have been conducted using the finite element method. Several numerical investigations (e.g. Popescu et al. 1999, Phillips et al. 2004a, 2004b, Guo and Stolle 2005 and Yimsiri et al. 2004) have indicated that continuum finite element modeling provides a reliable tool to solve soil/structure interaction problems by addressing nonlinearities from material behaviour, large deformations and pipe/soil contact behaviour. In numerical continuum modeling, pipe and soil are usually discretized to 2D or 3D elements and are connected using contact elements or surfaces.

The load deformation behaviour of soil during pipe/soil interaction depends on the type and properties of soil. While in loose sand or normally consolidated clay the load deformation curves are almost hyperbolic, in dense sand or overconsolidated clay a peak followed by load decrease (strain softening) is observed. Also soil behaviour is dependent on stress history (e.g. overconsolidation). Soil constitutive models should be able to address these complex behaviours of soils.

5.2 Numerical model procedures

The numerical modeling procedures to simulate pipeline/soil interaction events were developed using the finite element software package ABAQUS/Standard (Hibbitt et al. 2005). A three-dimensional continuum model (Figure 5-1) was developed for the centrifuge tests at prototype scale. Dimensions of the modeled soil domain were selected to minimize boundary effects on the predicted soil load, displacement and failure mechanisms. The bedding distance from the pipe centerline used in the numerical simulations was consistent with the centrifuge experiments ($2.5D$). For the node sets located on the front, back and two side faces of the numerical model of soil, the displacement degrees of freedom perpendicular to the relevant faces are restrained. All three displacement degrees of freedom of the nodes on the bottom face are restrained.

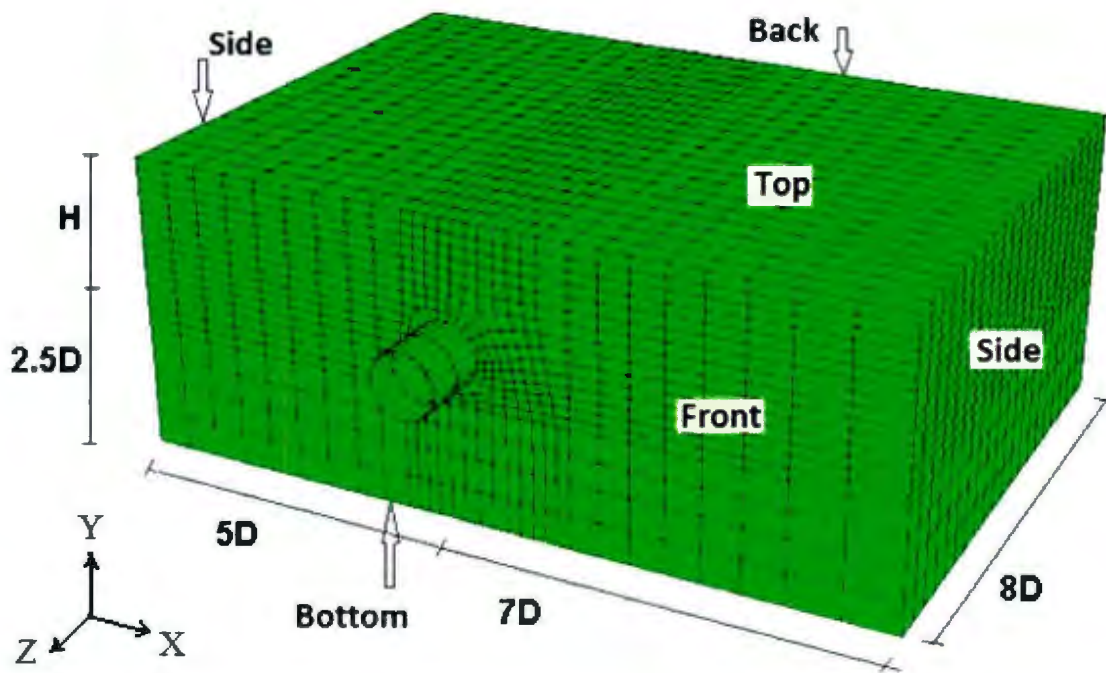


Figure 5-1: The finite element model geometry

Eight node continuum linear (brick) elements with reduced integration and hourglass control (C3D8R) are used to discretize the soil domain. This type of solid elements can be used for nonlinear problems involving large deformations. Using reduced integration elements prevents volumetric locking during solving problems involving large plastic strains.

Conventional four node linear shell elements (S4R5) are used to model the pipeline. As the main purpose of the study was the load-displacement relationship in the soil, a rigid pipe was used during the physical tests. In the numerical model the pipe displacement is applied to all nodes of the pipe to simulate a rigid pipe.

To minimize the end effects of the model front and back boundaries (Figure 5-1) on the pipe, only the central region having uniform stress distributions was examined for all numerical analyses. Each curve in Figure 5-2a represents the load distribution on the pipe length at one specific displacement increment. Each point on the curves shows the sum of the loads on the nodes located on a transverse section of the pipe. The variations in the loads at the ends of the pipe are caused by boundary conditions; however the load values in the central section of the pipe are quite uniform. As it is shown in Figure 5-2b about one-third of the pipe length, with a length equal to $2.8D$, at the middle was considered to calculate the soil load on the unit length of the pipe.

The pipe/soil interface is simulated using the contact surface approach implemented in ABAQUS/Standard (Hibbitt et al. 2005). This approach allows for separation and sliding with finite amplitude and arbitrary rotation of the contact surfaces. The Coulomb friction

model is used for the frictional interface between pipe and dry sand. In this method, the friction coefficient (μ) is defined between the pipe and the soil. Sliding occurs after the shear stress on the contact surface exceeds the critical shear stress. The critical shear stress is the product of friction coefficient (μ) and the contact pressure.

During the centrifuge modeling, the weight of the model pipe and other parts of the test apparatus (i.e. stanchion and dogbone) connected to it, affected the ultimate soil restraint applied to the pipe. In the numerical model the weight of the connecting parts (stanchions and dogbone) were included in the pipe selfweight.

The analysis was conducted in two main steps. The first step was a geostatic stress step that accounted for the effects of pipe and soil weight to determine the initial stress state in the soil. The second step was to impose the pipe displacement in the specified direction (i.e. loading angle).

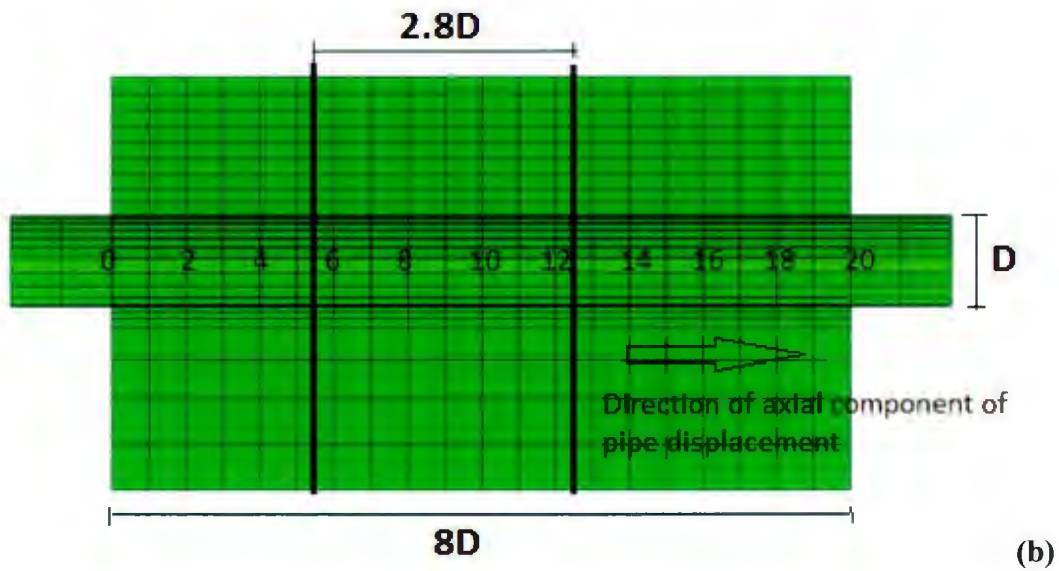
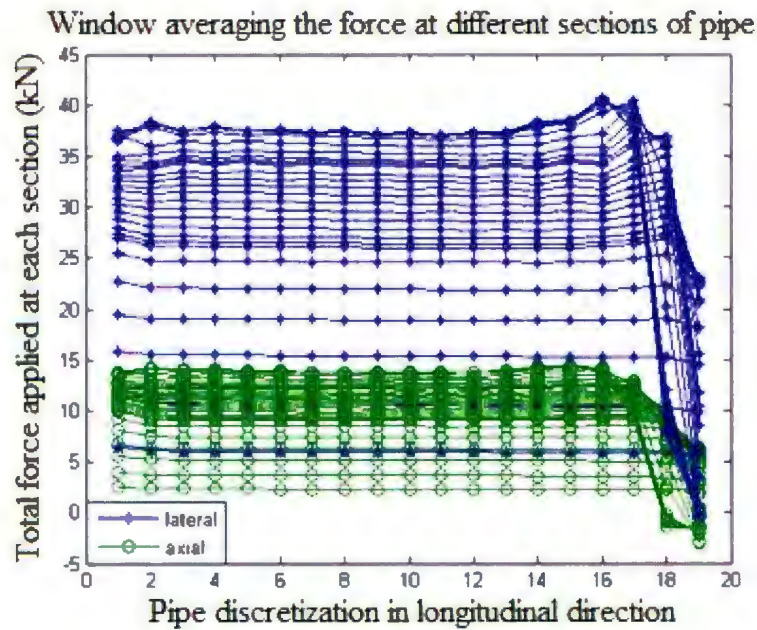


Figure 5-2: (a) Typical distribution of axial and lateral loads on the pipe length, during oblique pipe displacement at consecutive increments (b) the middle part of the length of the pipe considered to calculate the loads

5.3 Constitutive model selection for soil

A variety of constitutive models have been used for surrounding soils in pipe/soil interaction problems. Linear elastic behavior is the simplest one which is applicable for small strain problems and cannot be used for large ground deformation problems.

The Mohr-Coulomb (MC) plasticity model implemented in ABAQUS/Standard is intended for pressure-dependent materials. Popescu et al. (1999) and Yimsiri et al. (2004) indicated that non-associated Mohr-Coulomb model implemented in ABAQUS/Standard with isotropic hardening-softening provides acceptable results in medium to dense sand. Hardening-softening trend can be defined using the procedure presented in Nobahar et al. (2000) via a user defined subroutine to update the friction and dilation angles as a function of plastic strain magnitude. The pressure dependency of elastic modulus of soil was also added via a user subroutine.

Only non-negative values are allowed for the dilation angle in Mohr-Coulomb plasticity in ABAQUS/Standard, therefore the model cannot account for shear induced plastic compaction and cannot predict the compactive behavior of loose sands.

5.4 Soil parameters calibration

The soil elastic modulus was defined using the following relation to simulate its dependence on effective confining pressure, p :

Eq. 5-1

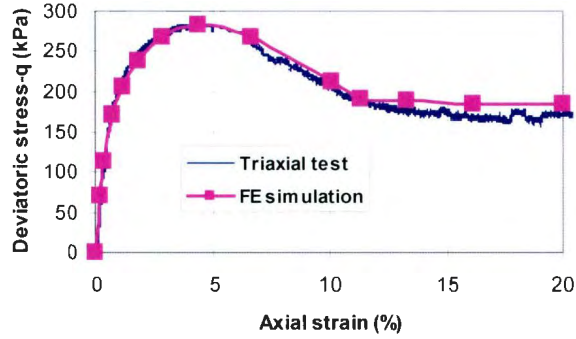
$$E = E_0 \left(\frac{P}{P_0} \right)^n$$

In Eq. 5-1, p_0 is a reference pressure equal to the atmospheric pressure ($p_0 = 100$ kPa), E_0 is the soil elastic modulus at the reference pressure and n is the power exponent ($n = 0.5$). The elastic modulus at the reference pressure ($E_0 = 15000$ kPa) was calibrated against the triaxial test data (Figure 5-3.a). The Poisson's ratio was assumed to be 0.3. A small value of cohesion of 4 kPa was assigned to soil to achieve numerical convergence in pipe/soil interaction model. Similar experiences are reported by other studies such as Popescu et al. (1999) and Guo and Stolle (2005). As the numerical model is validated against experimental results, the effect of a small value of 4 kPa is assumed to be minor.

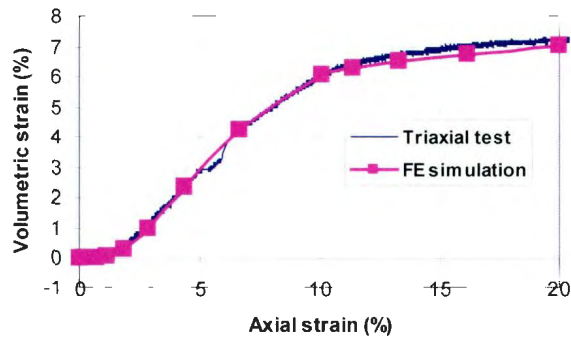
The non-associated Mohr-Coulomb plasticity model implemented in ABAQUS/Standard was used. Comparison of Mohr-Coulomb and Norsand as soil models by Yimsiri et al. (2004) has shown the Mohr-Coulomb model provides reasonable results in the case of pipe/soil interaction. This model has also been successfully used for other studies on pipe/soil interaction involving large soil deformations such as Popescu et al. (2002) and Guo & Stolle (2005).

Dense sand exhibits a strain hardening and softening response with shear induced dilative behavior. Nobahar et al. (2000) described a method to estimate the progressive mobilization of soil shear strength parameters using direct shear test data. Similar procedures have been used in this study to define the soil internal friction angle and

dilation angle as a function of plastic strain magnitude as a state parameter using triaxial data.



(a)



(b)

Figure 5-3: Comparison of numerical and experimental data for triaxial test: (a) deviatoric stress vs. axial strain, (b) volumetric strain vs. axial strain.

The plastic strain magnitude, ε_m^{pl} was defined as:

Eq. 5-2

$$\varepsilon_m^{pl} = \sqrt{\frac{2}{3} \varepsilon^{pl} : \varepsilon^{pl}} = \sqrt{\frac{2}{3} ((\varepsilon_{11}^{pl})^2 + 2(\varepsilon_{33}^{pl})^2)}$$

where ε^{pl} is the plastic strain tensor, and ε_{11}^{pl} , ε_{33}^{pl} are the axial and radial plastic strains in triaxial test. The plastic strains were calculated by subtracting the elastic strains from

the total strains. The modulus of elasticity as shown in Eq. 5-1 was used to evaluate the elastic strains.

The deviatoric stress and volumetric strain vs. axial strain data from a triaxial test and numerical simulation are presented in Figure 5-3. The soil sample was made of the same type of the sand which was used during the centrifuge tests and had 75% relative density with peak friction angle of 41° . The effective cell pressure during triaxial test was 70 kPa.

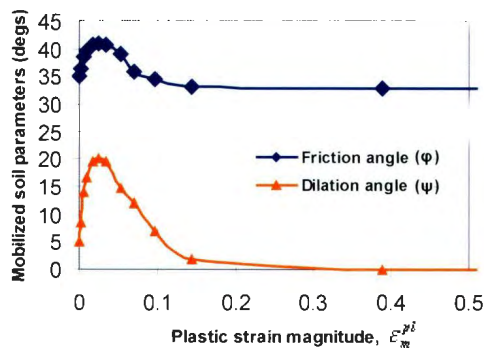


Figure 5-4: Mobilization of friction and dilation angles inferred from triaxial test data.

The progressive mobilization of soil strength parameters (Figure 5-4) was implemented in the finite element simulation through a user subroutine. The range of dilation angles in Figure 5-4 is higher than what is expected from literature (e.g. Bolton 1986). The type of sand used for this study has shown high volumetric strains in laboratory tests; therefore, it was decided to calibrate the dilation angle against the triaxial test rather than using data from literature.

For numerical simulation of pipe/soil interaction the hardening rule in Figure 5-4 was modified to a peak friction angle of 43° corresponding to centrifuge test conditions (Table

3-3). The modification was established through a simplified approach by multiplying the ratio of $(\phi'_{peak} - \phi'_{cv})$ for two cases to $(\phi' - \phi'_{cv})$ for the relationship illustrated in Figure 5-4 to modify the peak friction angle while keeping the constant volume friction angle the same.

5.5 Comparison with experimental data

5.5.1 Pure lateral loading test

Figure 5-5 presents a comparison between the numerical and experimental load-displacement curves during lateral pipe/soil interaction. The ultimate displacements from experimental and numerical simulations do not compare well. The higher ultimate displacements from experimental data, as discussed in Section 4.2, can be attributed to test bed construction disturbance which resulted in placement of lower density sand in the immediate vicinity of the pipe sample.

The numerical simulations estimated the ultimate lateral load favourably compared with experimental data. The slopes of the unloading-reloading curves from numerical and experimental modeling are generally consistent which confirms the similarity in elastic behaviour of numerical and experimental data. The weight of model pipe and supporting system is considered in the numerical simulation.

Figure 5-6 shows the load-displacement curve based on numerical simulation with the same parameters as the numerical model in Figure 5-5 except for the pipe selfweight. The analysis presented in Figure 5-6, is relevant to a gas filled steel pipe, regularly used in

practice, with a pipe diameter to wall thickness ratio (D/t) of 50 and selfweight of 1.16 kN/m. This pipe is about 20 times lighter at prototype scale than the heavy pipe (24.7 kN/m as mentioned in Section 4.2) presented in Figure 5-5. The ultimate load from numerical modeling compares well with the range of ultimate load according to Eq. 4-3 from Guo and Stolle (2005) which is based on numerous experimental works in the literature.

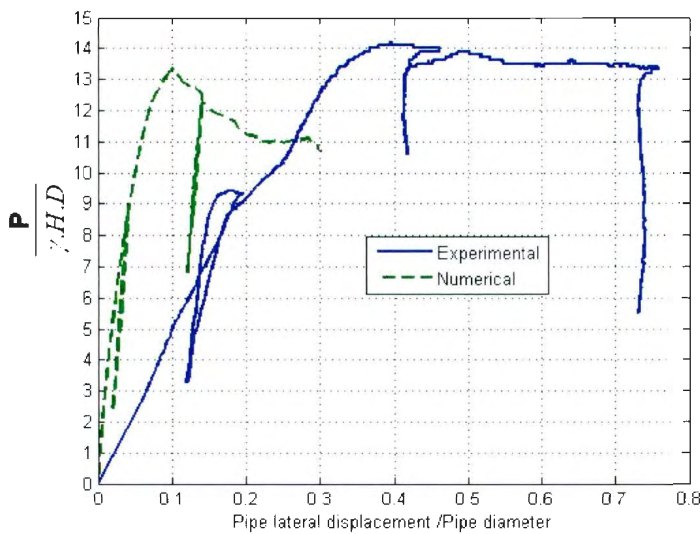


Figure 5-5: Numerical vs. experimental (Test #1) curves for lateral loading test

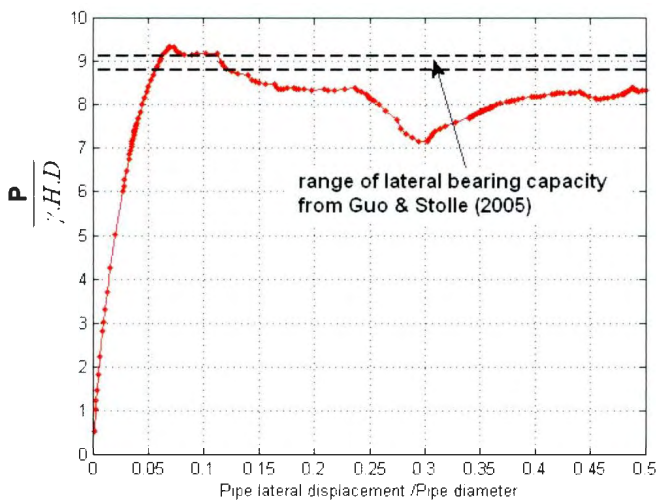


Figure 5-6: Comparison of numerical analysis with ultimate lateral loads from Guo & Stolle (2005)

The ultimate displacement for lateral movement of pipe in sand is recommended as Eq. 2-9 by Honegger and Nyman (2004) which for $H/D=2$ results in $y_u=0.1D$ which is consistent with the ultimate displacement obtained from numerical analysis in the current study (Figure 5-5).

For dense sand a lower value of ultimate displacement has been suggested from other experimental studies (Trautmann 1983 and Audibert & Nyman 1977):

Eq. 5-3

$$y_u=0.02\sim 0.03(H+D/2)$$

This equation gives a range of $y_u=0.05\sim 0.075D$ for $H/D=2$ which is consistent with a value of ultimate displacement of $0.07D$ from the numerical analysis on the light pipe condition conducted in this study (Figure 5-6). Increasing the pipe weight or decreasing the pipe upward movement during lateral pipe/soil relative displacement increases the size of the passive wedge in front of the pipeline. This effect explains the slightly higher lateral displacements required during numerical analysis with heavy pipe (Figure 5-5) to reach the ultimate load.

Figure 5-7 shows the displacement field in front of the pipe for the two cases of lateral movement of heavy and light pipes with load-displacement curves shown in Figure 5-5 and Figure 5-6, respectively. Both displacement fields are relevant to a lateral pipe displacement of $0.3D$ where load-displacement curves reach a residual state. The difference between the size of the passive wedge in front of the pipe and the vertical component of movement of the pipe are noticeable. The heavy pipe causes initial

horizontal pipe motion which forces the soil material at the pipe invert level to go down (log spiral mechanism) due to dilation. Sheared material at the pipe invert level tends to dilate and forces the soil towards lower confining pressure space. The lighter pipe allows pipe to move up and the soil to displace horizontally which stops initial log spiral portion.

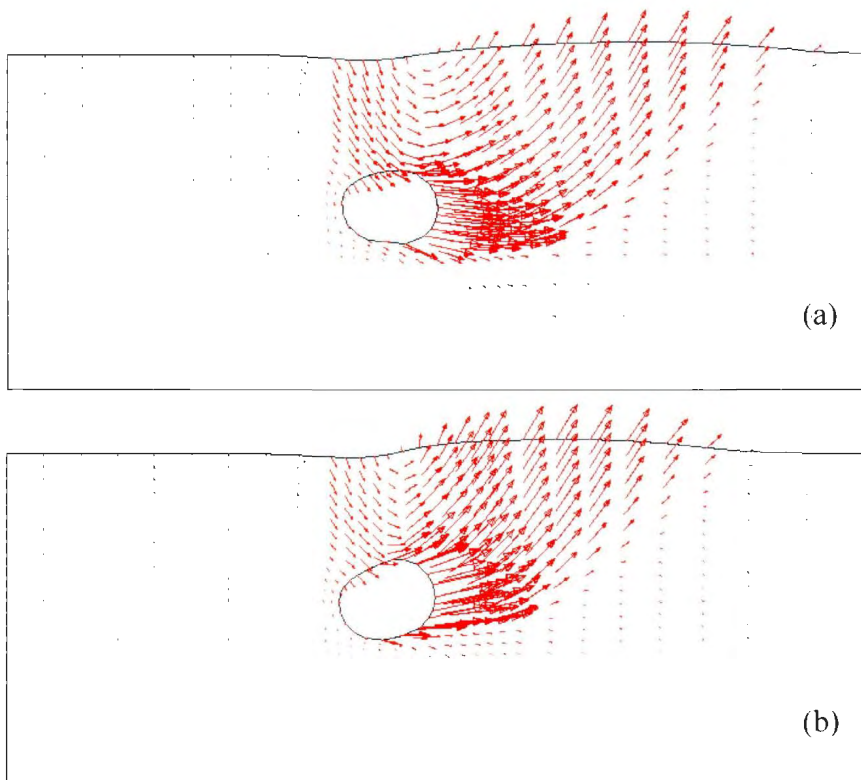


Figure 5-7: Soil displacement field in front of the pipe for (a) heavy and (b) light pipe after lateral displacement of $0.3D$.

5.5.2 Pure axial loading test

Figure 5-8 compares the numerical, theoretical and experimental data for axial pipe/soil interaction. Experimental data is discussed in Section 4.3 and the discrepancy between the experimental data and what is expected from theoretical methods is explained. The axial

interaction factor of about 2 from numerical analysis in the current study compares well with a value of 1.94 from Eq. 2-6. Coefficient of active earth pressure of 0.19 and pipe selfweight of 24.7 kN/m are considered in this calculation.

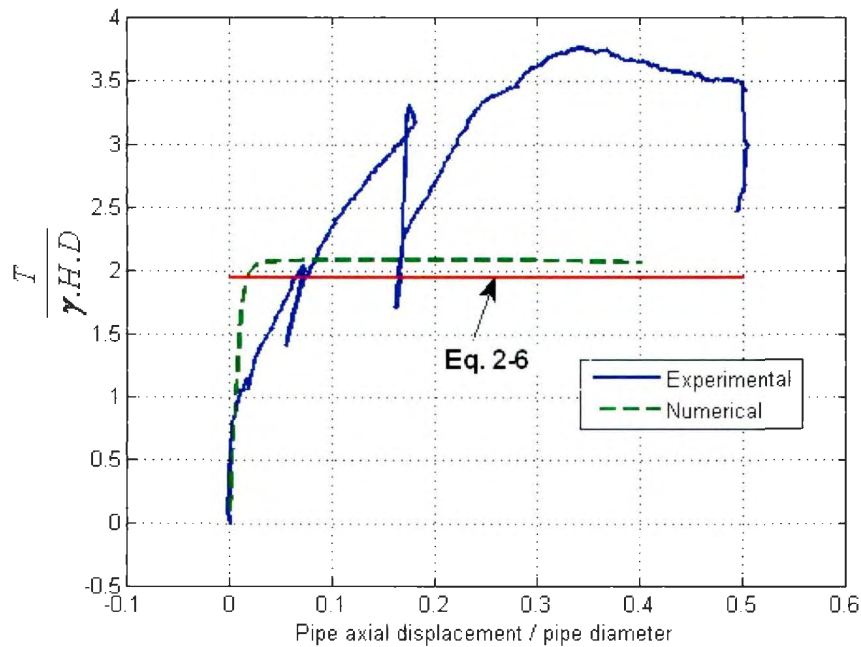


Figure 5-8: Numerical vs. experimental (Test #2) curves for axial loading test

5.5.3 Oblique loading tests

Oblique loading centrifuge tests were conducted for 40° and 70° angles of attack. Comparisons of numerical and experimental load-displacement curves for oblique 70° and 40° tests are presented in Figure 5-9 and Figure 5-10 respectively.

The numerical models have been able to predict the ultimate loads in axial and lateral directions well. Discrepancies between the physical modeling data and numerical simulations exist in the estimated ultimate displacements. This discrepancy can be

attributed to test bed construction disturbance during sand pluviation which is discussed in the sections on lateral loading in Chapter four (Section 4.2).

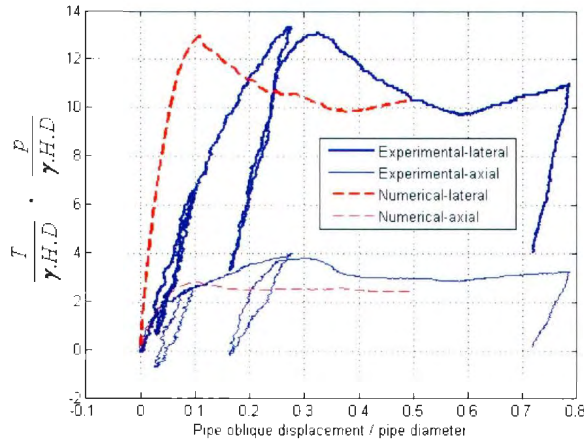


Figure 5-9: Numerical vs. experimental (Test #4) curves-Oblique 70° test

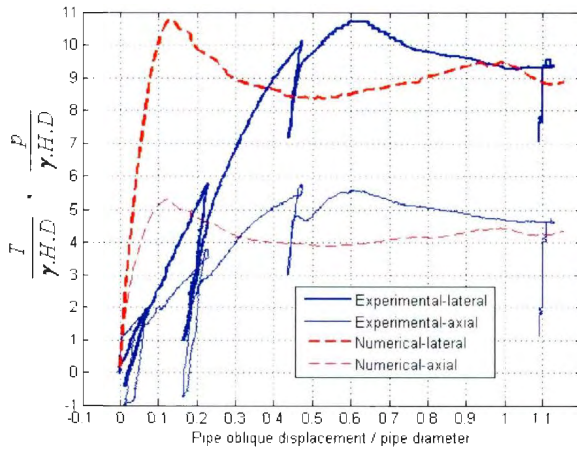
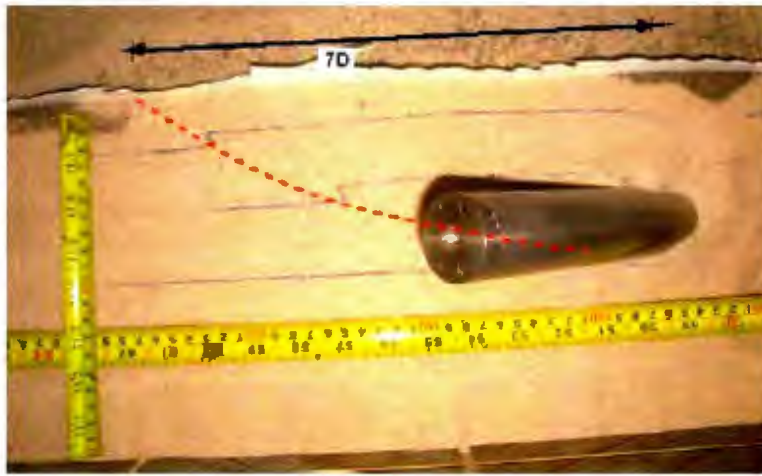


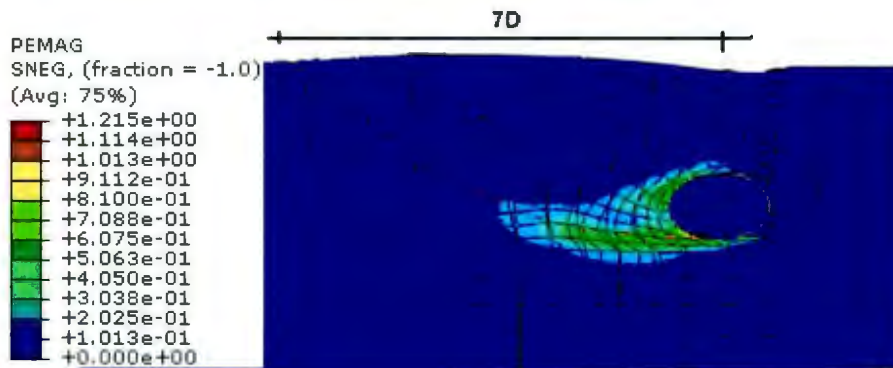
Figure 5-10: Numerical vs. experimental (Test #3) curves-Oblique 40° test

A comparison of the soil failure mechanisms observed at the end of the oblique 40° and 70° centrifuge tests and those predicted by numerical simulations are presented in Figure 5-11 and Figure 5-12. The deformation state shown in Figure 5-11.b corresponds to an oblique displacement of 0.6D where numerical model reaches a critical state similar to the

final stage of the physical modeling. Plastic strain magnitude (PEMAG), shown in the legend of the figures, is defined in Eq. 5-2. Both figures are presented in a plane parallel to the direction of pipe movement in the soil. The failure mechanism and surface heave from physical and numerical models are similar. The size of the passive wedge in front of the pipe are the same with a burial depth of two times pipe diameter ($2D$) and similar surface length of the passive wedge in front of the pipe shown in the figures.



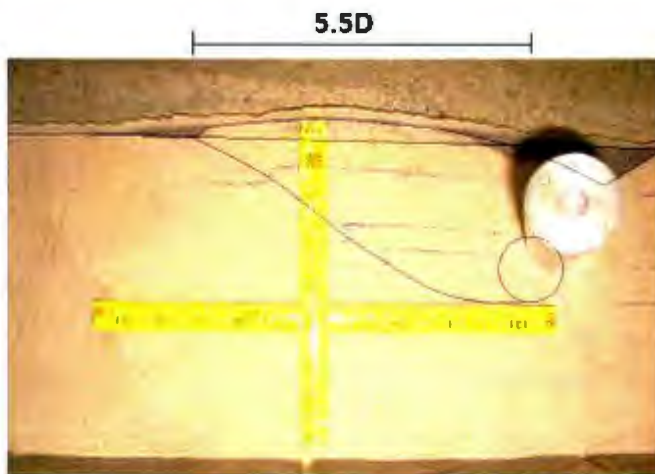
a) Observed at the end of physical modeling (oblique plane)



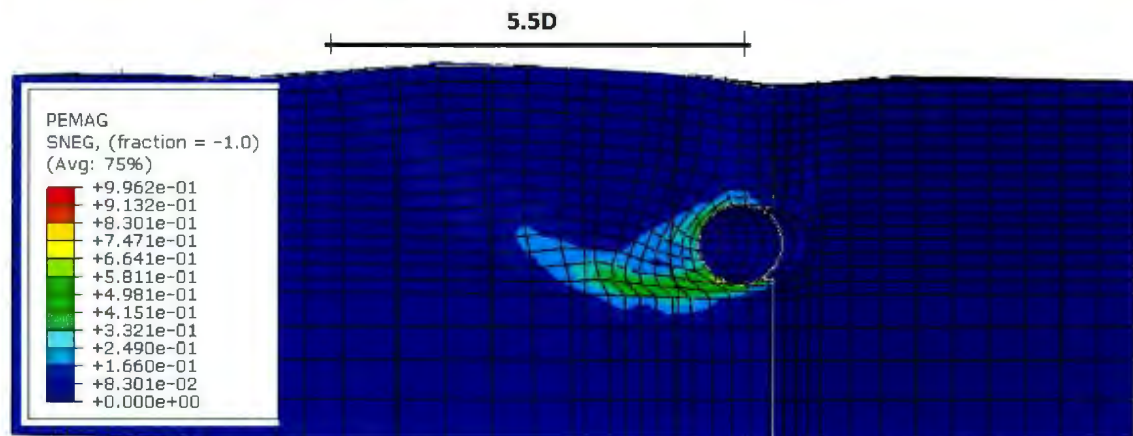
b) Calculated in numerical modeling (oblique plane)

Figure 5-11: Comparison of failure mechanisms during numerical and physical modeling for oblique 40° test (Test #3)

At the end of oblique 70° test and before starting the excavation, the pipe was moved vertically by mistake. However it did not affect the coloured sand layers or the soil surface configuration. The correct location of the pipe at the end of the test, soil surface configuration at the beginning and end of centrifuge test and the estimated shear band are highlighted in Figure 5-12.a.



a) Observed at the end of physical modeling (oblique plane)



b) Calculated in numerical modeling (oblique plane)

Figure 5-12: Comparison of failure mechanisms during numerical and physical modeling for oblique 70° test (Test #4)

Figure 5-13 shows the failure mechanism, after a lateral displacement of $0.3D$, during lateral pipe/soil interaction. A comparison of strain levels from three oblique angles shows the maximum plastic strain, which occurs at the pipe invert level in front of the pipe, increases by increasing the oblique angle from 40° to 90° . The size of the passive wedge in front of the pipe, in a direction perpendicular to the pipe axis, increases from $4.5D$ ($7D \sin 40^\circ$) for oblique 40° , to $5.2D$ ($5.5D \sin 70^\circ$) for oblique 70° , to $5.8D$ for lateral loading.

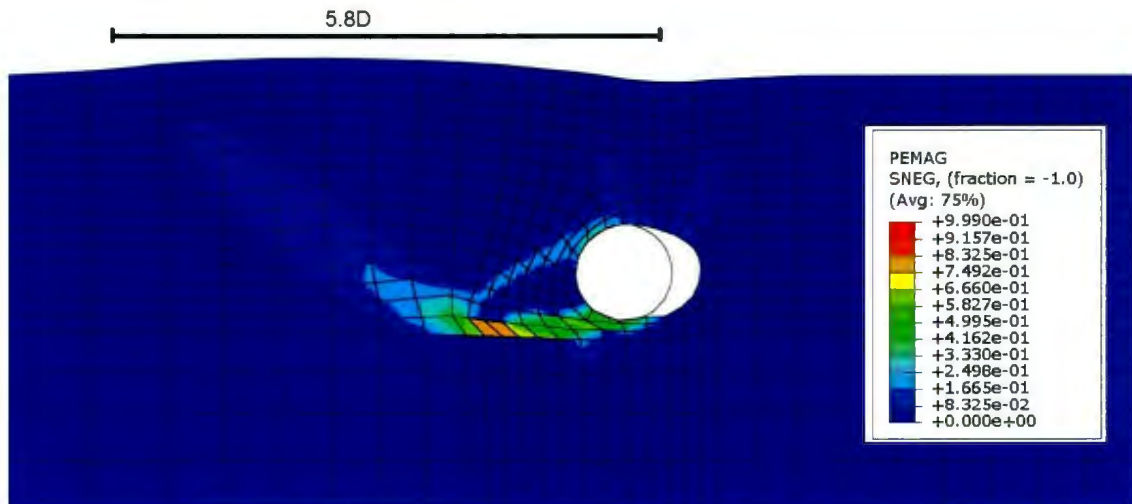


Figure 5-13: Failure mechanism from numerical modeling of lateral pipe/soil interaction, after a lateral displacement of $0.3D$.

5.6 Summary

- Numerical model development procedures, and comparisons with experimental data are presented and discussed in this Chapter,
- The finite element software package ABAQUS has been used for this analysis,
- Three-dimensional continuum pipe/soil model has been developed using eight

node continuum linear elements for soil, and four nodes linear shell elements for pipeline.

- The Mohr-Coulomb plasticity model implemented in ABAQUS has been used for soil material. A user defined subroutine was used to estimate the progressive mobilization of the soil shear strength parameters.
- The ultimate displacements from experimental and numerical analysis do not compare well. While the ultimate displacements from numerical analysis are consistent with design guidelines, the experimental displacements are too high which has been attributed to test bed construction disturbance.
- The effect of pipe selfweight on the ultimate loads is discussed. It is shown that the numerical model compares well with the experimental data and lateral bearing factors from Guo and Stolle (2005).
- The axial ultimate loads from numerical and experimental simulations do not compare well, which can be attributed to a small misalignment during experimental test.
- The numerical parametric study is discussed in the next Chapter.

6 Parametric studies on oblique pipe/soil interaction

6.1 Introduction

The numerical simulation described in Chapter five has been used to examine axial-lateral, axial-vertical and lateral-vertical pipe/soil interaction for various mechanical and geometrical parameters and different oblique angles in the following sections of this Chapter. Interaction curves are developed and compared with existing yield surfaces for different oblique planes.

6.2 Axial-lateral pipe/soil interaction

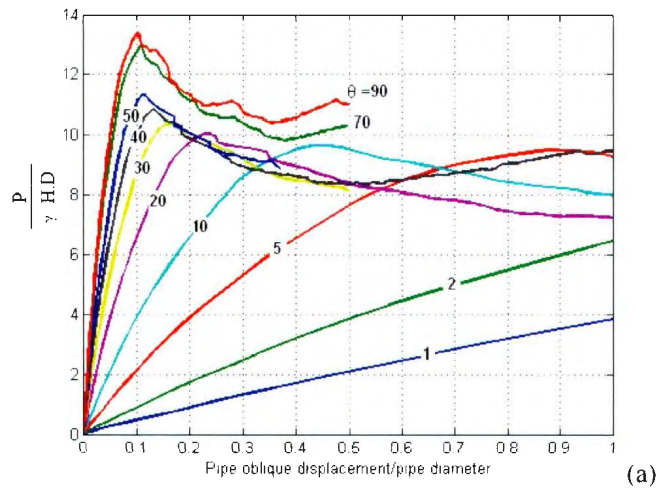
The finite element numerical model that was explained in previous Chapter is used to study the axial-lateral pipe/soil interaction in this section. Oblique interaction curves are developed for the same condition of centrifuge tests and then parametric studies are conducted to confirm that the resulted interaction curves are valid for the range of parameters examined in this thesis.

The experimental tests are extended for nine different oblique angles including 1, 2, 5, 10, 20, 30, 40, 50 and 70 degrees using numerical modeling. The lateral and axial loads against oblique displacements are presented in Figure 6-1.a and b. For oblique 1° and 2° the load-displacement curves are reported for a relative displacement of one pipe diameter which is less than the ultimate displacement. In this study loads and displacements corresponding to peak loads are used as ultimate loads and ultimate displacements. To

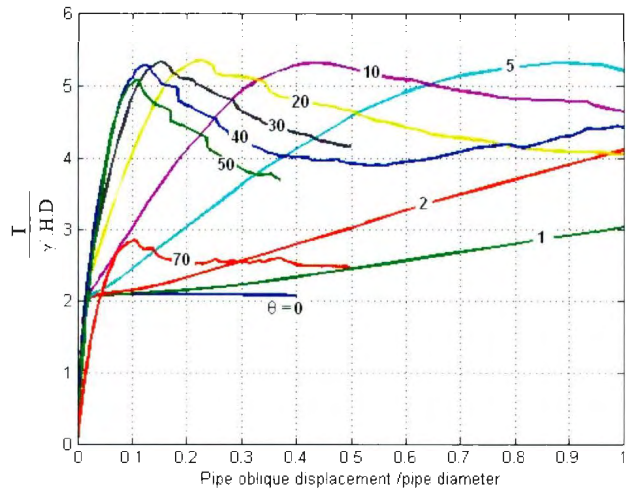
reach the peak axial and lateral loads on the pipe for small oblique angles, larger relative displacements (in terms of several pipe diameters) between pipe and soil are required, which is likely to occur during large ground deformation incidents. The corresponding axial and lateral interaction factors are presented in Figure 6-2.

By increasing the oblique angle (i.e. increasing the lateral component of displacement) the lateral load on the pipeline increases (Figure 6-1.a and Figure 6-2). The axial load increases with increasing oblique angle of attack due to increased axial frictional force related to the increased normal or lateral pressure on the pipe. For oblique angles larger than 40° the failure mechanism changes from axial slide on the pipe surface to shear in the soil mass. Increasing the oblique angle of attack to 90° (i.e. pure lateral loading) decreases the axial restraint on the pipe to zero.

A summary of experimental and numerical ultimate loads are presented in Figure 6-3. The interaction curve defined by Hsu et al. (2006) for dense sand is also shown in Figure 6-3 for comparison. The results indicate that for misalignment less than 40° , the axial force increases by a factor of 2.5. The higher axial resistance in the centrifuge test for pure axial (0°) loading was discussed in Chapter four and was attributed to possibly a small misalignment in the vertical plane or the effect of confined dilation.



(a)



(b)

Figure 6-1: Lateral (a) and axial (b) load vs. oblique displacement for different oblique angles

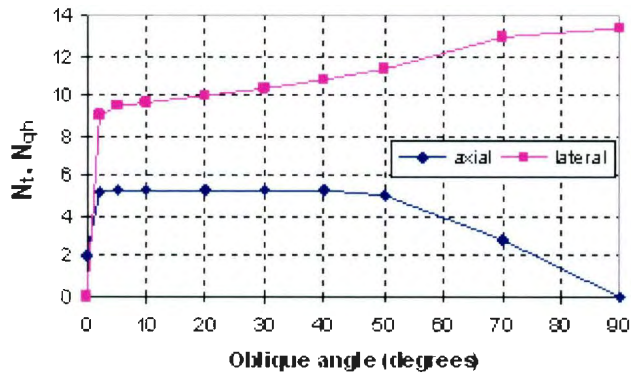


Figure 6-2: Variations of lateral and axial interaction factors with oblique angles

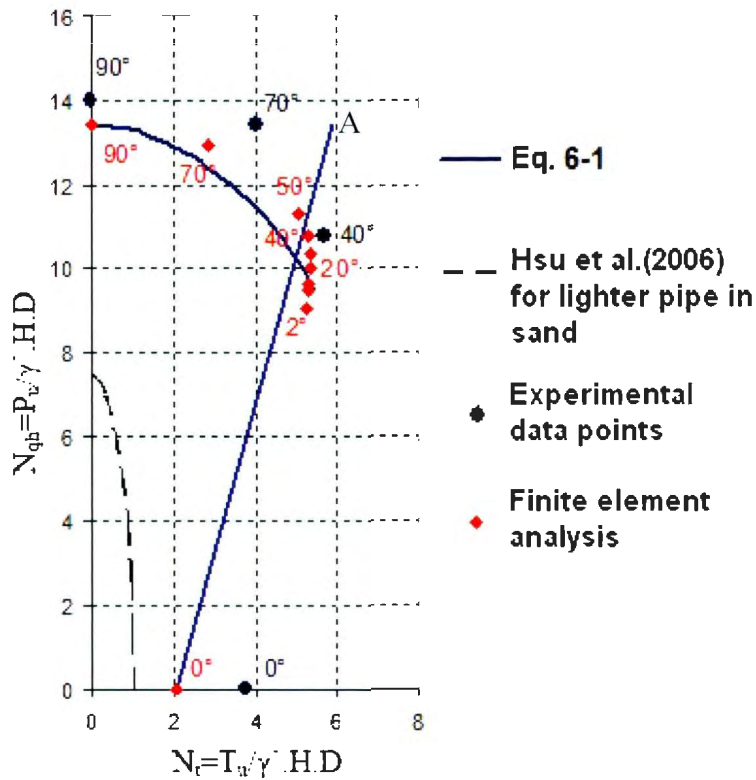


Figure 6-3: Axial-lateral pipe-soil interaction curves

The experimental and numerical data, from this study show similarity with the failure criterion proposed by Phillips et al. (2004b). The failure criterion consists of a linear part, associated with soil failure on the pipe circumference, and a nonlinear portion associated with failure through the soil mass. For this study, the transition between the linear and nonlinear components of the failure surface occurred at an oblique angle of approximately 40°.

Honegger et al. (2010) has referred to a similar series of centrifuge tests on sand with lower relative density and saturated clay that yielded similar interaction curve as this study and Phillips et al. (2004b). The equation of the curved part in Figure 6-3 is:

Eq. 6-1

$$N_{qh}^2 + 3N_t^2 = N_{qh(90)}^2$$

where $N_{qh(90)}$ is the ultimate lateral interaction factor during pure lateral pipe/soil relative movement. The linear part connects the point associated with the pure axial condition to a point (point A in Figure 6-2) with horizontal coordinate of $(\mu.N_{qh})$ and vertical coordinate of (N_{qh}) .

Figure 6-1 and Figure 6-2 show that applying a small amount of lateral displacement to an axially loaded pipe (even an oblique angle of 1°) will increase the axial soil restraints on the pipe considerably. This increase has not been considered in the current engineering guidelines. In the current engineering practice, it is assumed that the maximum axial load on the pipe occurs during pure axial loading, while Figure 6-1, Figure 6-2 and Figure 6-3 show for a wide range of oblique angles the axial soil restraint on the pipeline is more than for the pure axial condition. This can be particularly important where upheaval buckling occurs or in other pipe/soil interaction event where axial soil forces play a significant role in the physical mechanisms.

6.2.1 Ultimate displacements

While this study has concentrated on the ultimate loads, on the pipe, during oblique movements, proper estimation of ultimate displacements bears the same significance for defining reliable soil spring stiffness terms or material model parameters for macro-elements (e.g. Cocchetti et al. 2009). Figures 6-4.a and b show the normalized lateral

and axial loads as a function of the normalized lateral and axial displacements, respectively, for the same cases presented in Figure 6-1. The ratios of normalized ultimate loads to normalized ultimate displacements, for oblique angles shown in Figure 6-4, are summarized in Figure 6-5. These data provide a measure of soil spring stiffness.

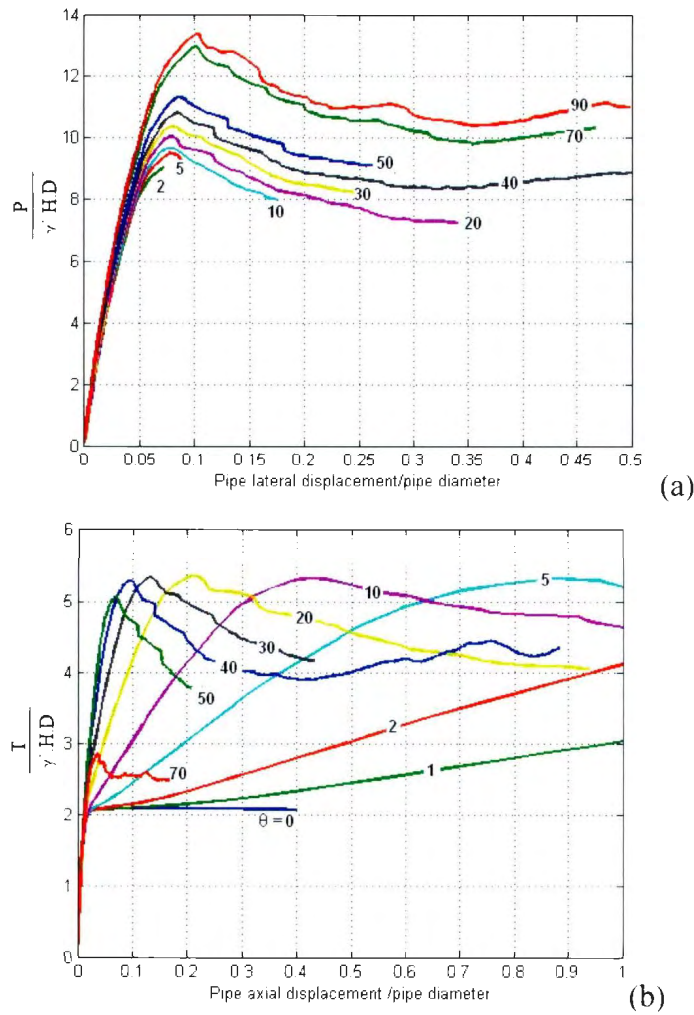


Figure 6-4: Lateral (a) and axial (b) loads vs. lateral and axial displacements respectively, for different oblique angles

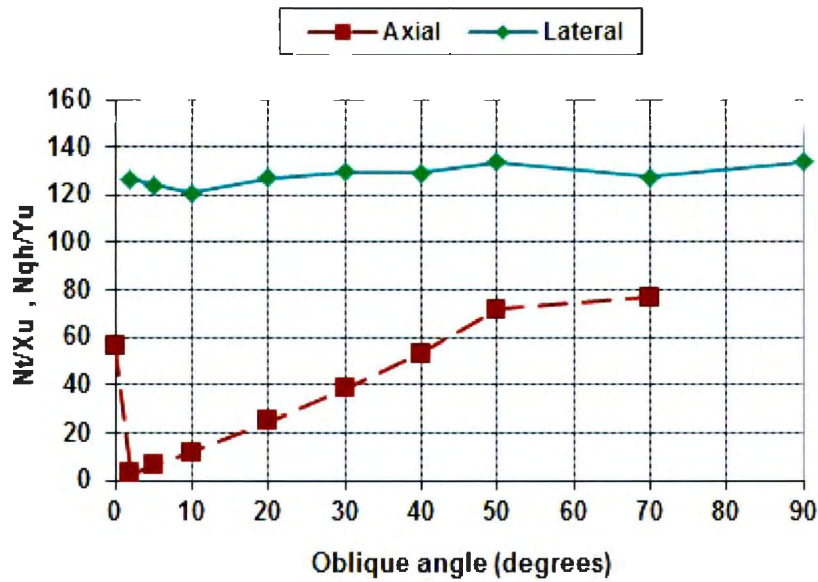


Figure 6-5: Ratio of normalized ultimate load over normalized ultimate displacement vs. oblique angles

In the lateral direction, the soil ultimate loads and displacements increase with increasing the oblique angles while the slope of the load-displacement curve remains almost constant (Figure 6-5). In the axial direction, excluding the case of pure axial loading, the soil ultimate displacement decreases by increasing the oblique angle. A more complex load-displacement relationship should be developed for axial direction. The bilinear relationship does not provide adequate estimates, particularly for small oblique angles.

6.2.2 Parametric studies

Parametric studies have been conducted to obtain a better understanding of the dependence of the interaction curve presented in Figure 6-3 on soil properties and important geometrical parameters such as burial depth ratio (H/D). A pipe with external diameter over thickness (D/t) ratio of 50, burial depth ratio (H/D) of 2, and pipe surface

friction factor of $f = \delta/\phi = 0.5$ was examined. Three peak friction angles of 35° , 40° and 45° were investigated. The hardening law, presented in Figure 5-4, was modified in accordance with the corresponding peak friction angles as shown in Figure 6-6. The procedures to obtain these curves are explained in Section 5.4. The high value of dilation angles are the artefact of extrapolation from the model calibrated against triaxial test (Figure 5-4).

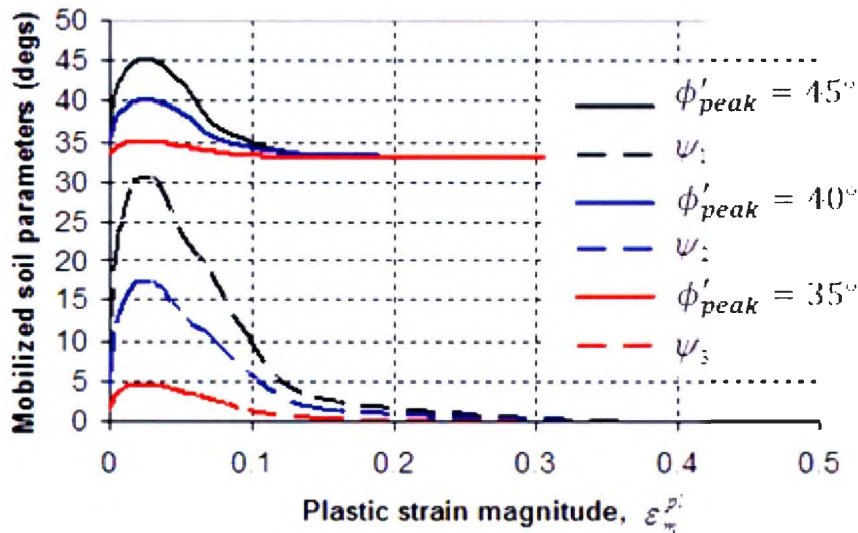


Figure 6-6: Mobilization of friction and dilation angles used for parametric studies. ψ_1 , ψ_2 and ψ_3 are dilation angles relevant to peak friction angles of 45° , 40° and 35° degrees respectively.

Figure 6-7 shows as the friction angle increases, the yield surface expands. The increase in the lateral interaction factor occurs because of higher shear strength in the soil media. The increase in the axial component of the interaction factor depends on the nature of mechanism occurring during pipe/soil relative movement. For the case of pure axial movement, where the dominant mechanism is sliding on the interface, the increase in the axial interaction factor is a function of the increase in the coefficient of friction on the

interface. For larger oblique angles (e.g. 70°) the increase in axial interaction factor is proportional to increase in lateral interaction factor i.e. the increase in normal pressure on the pipe surface. For small oblique angles (e.g. 10°) the increase in the axial interaction factor is affected by both increasing the lateral load and increasing the coefficient of friction on the interface.

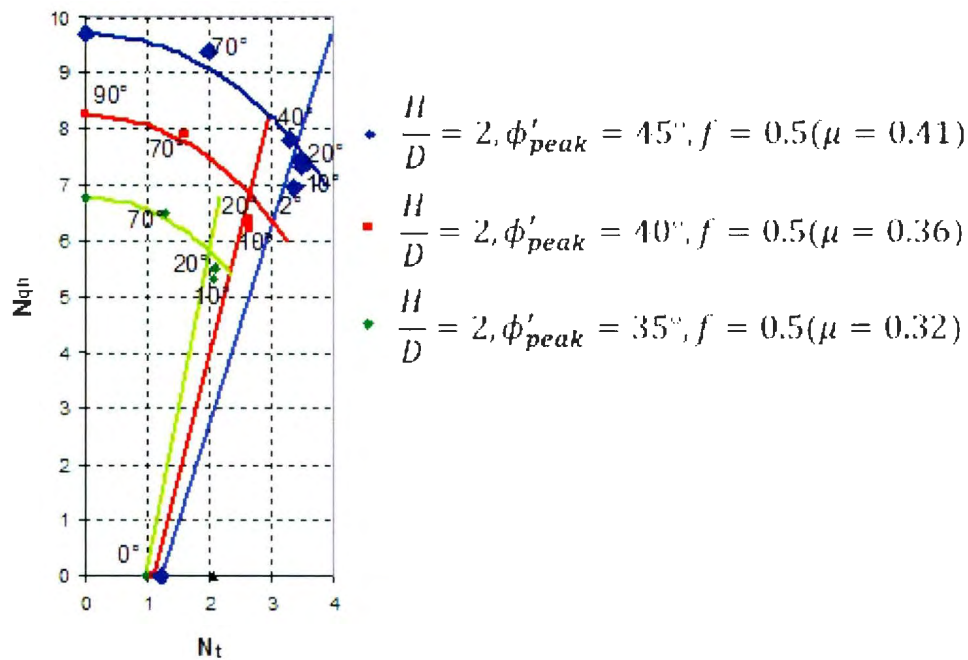


Figure 6-7: Effect of peak friction angle on axial-lateral pipe/soil interaction (solid lines are based on Eq. 6-1)

The effect of pipe external coating roughness on the axial-lateral interaction curves is shown in Figure 6-8. Two different friction factors of 0.5 and 0.8 are used to simulate pipelines with smooth (e.g. polyethylene) and rough (e.g. steel) external surfaces respectively. For constant soil parameters and geometrical conditions increasing the pipe surface friction factor from 0.5 to 0.8 (60% increase) increases the axial load on the

pipeline by almost the same percentage for oblique angles lower than 40° . For small oblique angles, increasing the axial component of the load on the pipeline decreases the lateral component of the load according to Eq. 6-1. The lateral interaction factor for pure lateral movement ($N_{qh(90)}$) slightly increases by increasing the roughness of the pipe external surface. For higher oblique angles, the small amount of increase in the axial component of the load on the pipeline is proportional to the increase in the lateral component of the load. These observations provide confirmation on the two failure mechanisms at lower and higher oblique angles.

Figure 6-9 presents the effect of burial depth on axial-lateral pipe/soil interaction. Increasing pipe burial depth causes an increase in the axial interaction factor due to higher lateral pressure (i.e. lateral interaction factor) during oblique movements. The axial interaction factor for pure axial movement of pipe ($\theta=0^\circ$) remains the same as the axial load is normalized by depth. Further increase in the axial and lateral interaction factors with burial depth ratio will be limited by a critical depth, where the lateral shear failure mechanism changes to a flow around mechanism.

For all cases presented in Figure 6-7, Figure 6-8 and Figure 6-9 the proposed interaction curves (Eq. 6-1) match the numerical data points well.

Structural modeling examples in Appendix B, investigate the effect of considering the axial-lateral pipe/soil interaction on the pipeline strain response for practical cases.

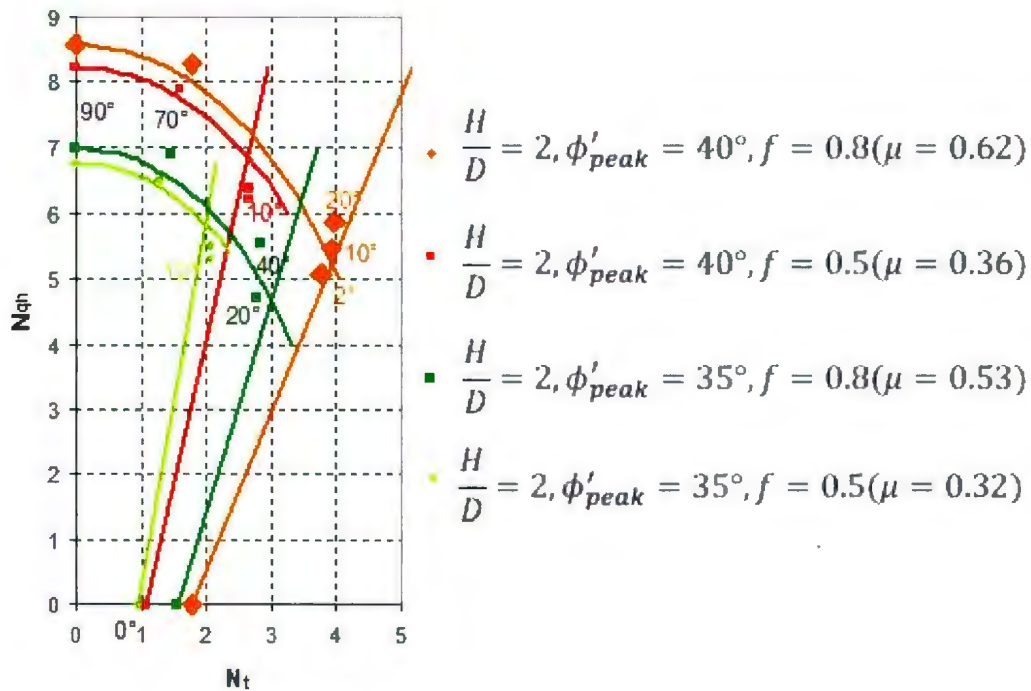


Figure 6-8: Effect of interface friction factor on axial-lateral pipe/soil interaction (solid lines are based on Eq. 6-1)

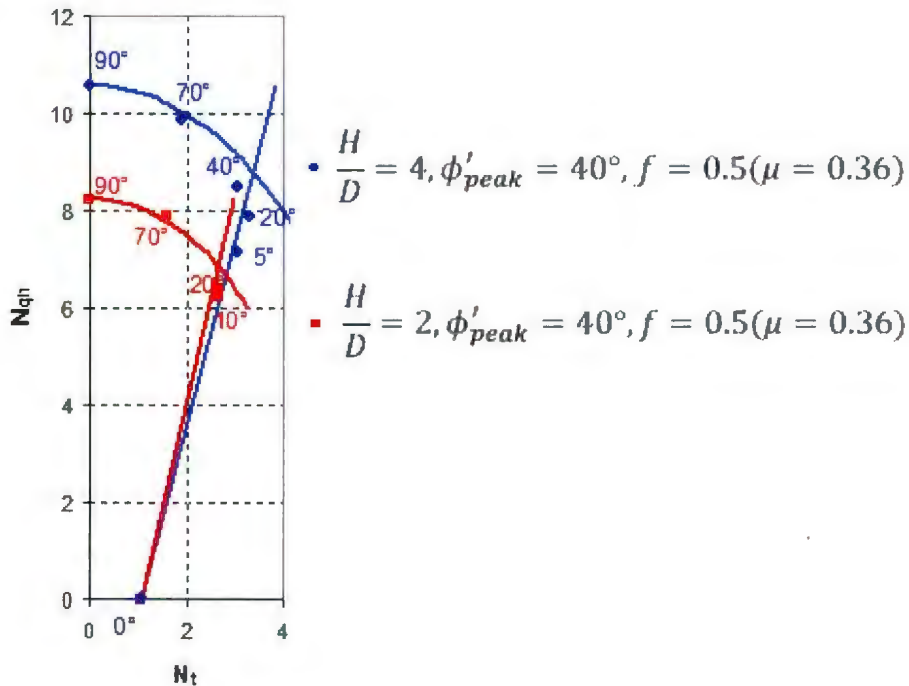


Figure 6-9: Effect of burial depth on axial-lateral pipe/soil interaction curve (solid lines are based on Eq. 6-1)

6.3 6.3 Axial-vertical (upward) pipe/soil interaction

As it was noted in Chapter two, no previous study could be found on axial-vertical pipe/soil interaction. The same numerical model that was developed and used for axial-lateral pipe soil interaction is used to investigate the pipe/soil interaction in the axial-vertical plane. This section is focused on vertical upward pipe/soil interaction. At the end of this Chapter a limited number of vertical downward analyses and some comments on the current state of practice are included.

Figure 6-10 compares the load-displacement curves for vertical upward movement of pipe with different burial depths, friction angles and pipe surface friction factors.

The ultimate vertical loads which are chosen as peak loads from Figure 6-10 compare well with rigorous finite element limit analysis by Merifield and Sloan (2006) for horizontal anchor plates (Figure 2-20). It is well known that the vertical soil restraint on the pipeline increases by increasing the burial depth. As it is discussed in Chapter 2, previous studies (e.g. Yimsiri et al 2004) have shown the deep mechanism occurs at burial depth ratio of more than 21 for the range of soil shear strength parameters in this study. Therefore in the current study with a range of burial depth ratios less than 7 ($H/D \leq 7$) deep mechanism was not observed. Vanden Berghe et al. (2005) have shown a flow around or circulation mechanism can occur at lower depths in very loose sand.

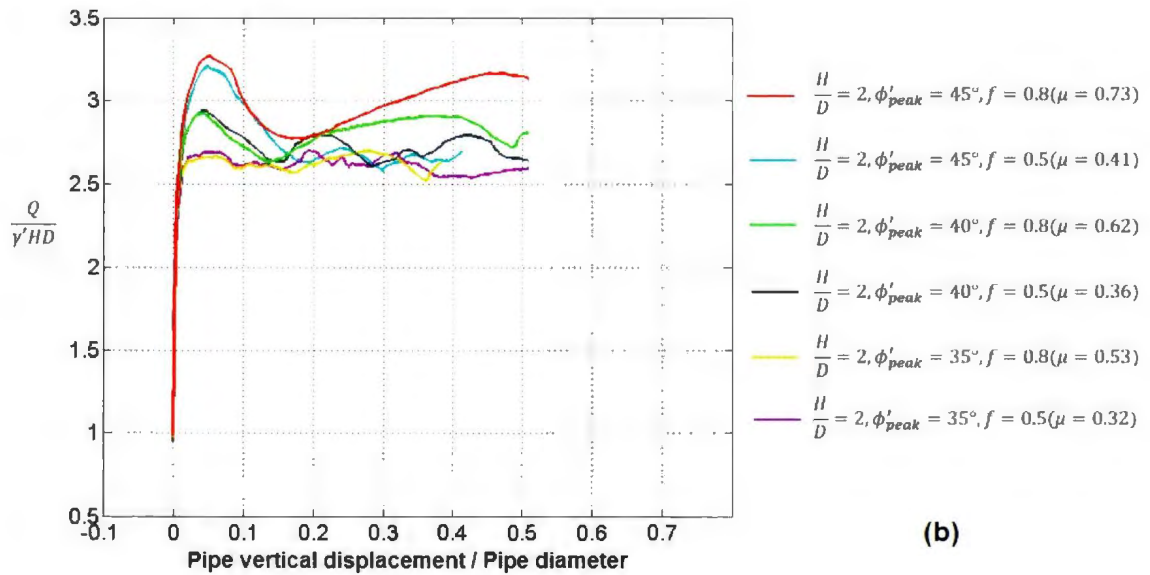
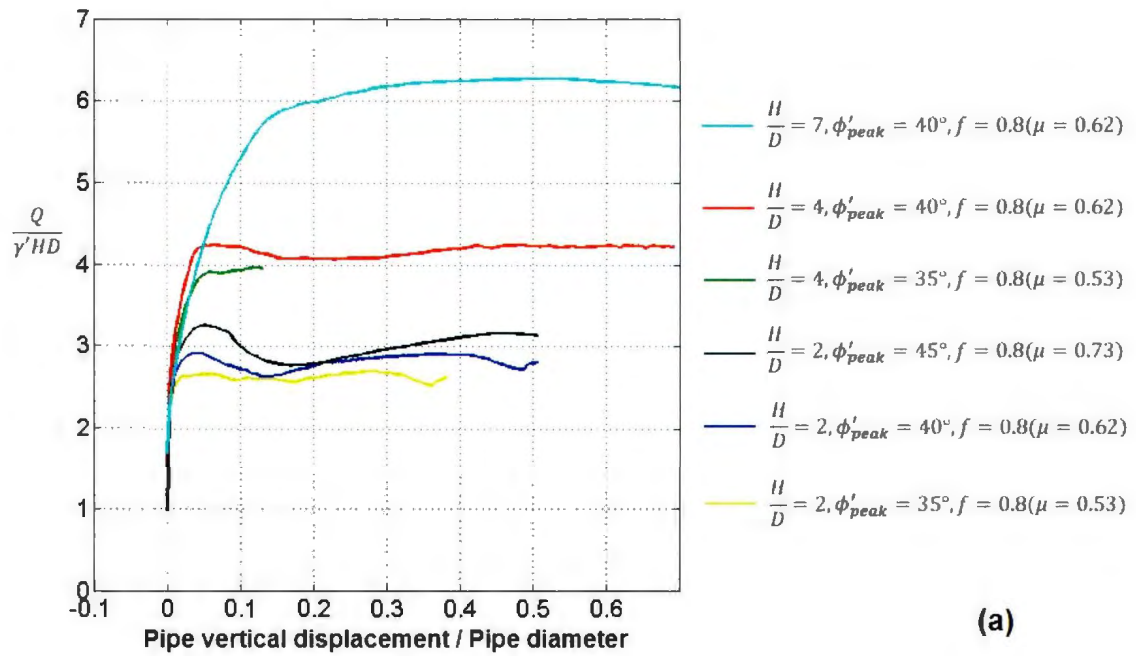


Figure 6-10: Vertical uplift load-displacement curves, (a) effect of burial depth ratio and friction angle, (b) effect of friction factor.

Increasing the soil peak friction angle increases the vertical soil restraint on the pipeline. Figure 6-10b shows pipe surface roughness has no or little effect on the ultimate vertical load on the pipeline which is consistent with previous studies e.g. Rowe and Davis (1982b) and Merifield and Sloan (2006), however pipe surface roughness affects the load on the pipeline at large displacements ($>0.2 D$). For smooth pipelines load-displacement curves for different friction angles converge at large displacements. When the pipeline surface is rough the load on the pipeline increases again at large displacements depending on the soil friction angle which may be an artefact of numerical analysis due to distortion in soil elements.

A comparison of displacement fields in the soil during upward movement of pipe are presented in Figure 6-11 and Figure 6-12 for a pipe displacement (d) of $0.2D$ and $0.15D$. Figures are shown at a displacement where the load-displacement curves reach a constant volume state (d is the pipe vertical displacement). The displacement fields include a rigid column of soil immediately above the pipe that moves upward, and a plastic zone of lateral and upward movement at the two sides of the rigid column of soil which is consistent with what is shown for horizontal anchor plates by Merifield and Sloan (2006). The size of this curved plastic zone is affected by soil friction angle and dilatancy, as is expected based on e.g. Rowe (1978) and Cheuk et al. (2008) among others.

Numerical axial-vertical pipe/soil interaction analyses are conducted for various parameters. Unit weight of soil is assumed constant equal to 16 kN/m^3 for all cases. To determine the pipe selfweight, a steel pipe with diameter over thickness ratio of $D/t \approx 50$ is assumed. Pipe selfweight makes a small fraction of the vertical interaction factor. For

example for a burial depth ratio of $H/D=2$, $D=0.5$ m and pipe selfweight $W_p=118$ kg/m, the contribution of pipe selfweight to the vertical interaction factor is $W_p/\gamma.H.D = 0.145$ which is about 6% of the total vertical interaction factor. As it is shown by Cheuk et al. (2008), vertical resistance mainly comprises of geostatic vertical stress and shearing resistance.

Axial and vertical load-displacement curves for different oblique angles for the case of a pipe buried at a burial depth of $H/D=4$, in a sand with $\phi_{peak}=40^\circ$ and pipe surface friction factor $f=0.8$ ($\mu=0.62$), are presented in Figure 6-13.

The definition of oblique angle in axial-vertical plane is similar to axial-lateral plane (Figure 2-22); 0° for pure axial and 90° for vertical upward movements.

As it is shown in Figure 6-13 , an interaction effect similar to what was observed during axial-lateral pipe/soil interaction is happening during axial-vertical relative movement between pipeline and soil. The ultimate axial load on the pipeline increases by about 50% respect to pure axial movement for small oblique angles. This increase is lower than what was observed during axial-lateral pipe/soil interaction which can be attributed to the fact that vertical soil restraint on the pipe is lower than lateral restraint, therefore the increase in normal load on the pipe surface during axial-vertical pipe/soil interaction is less.

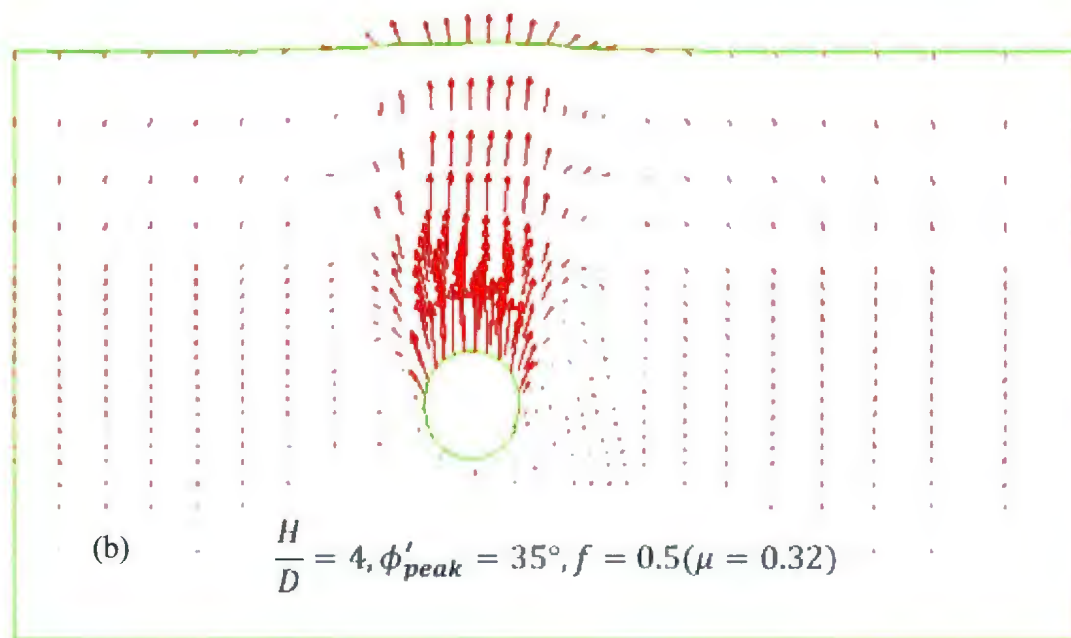
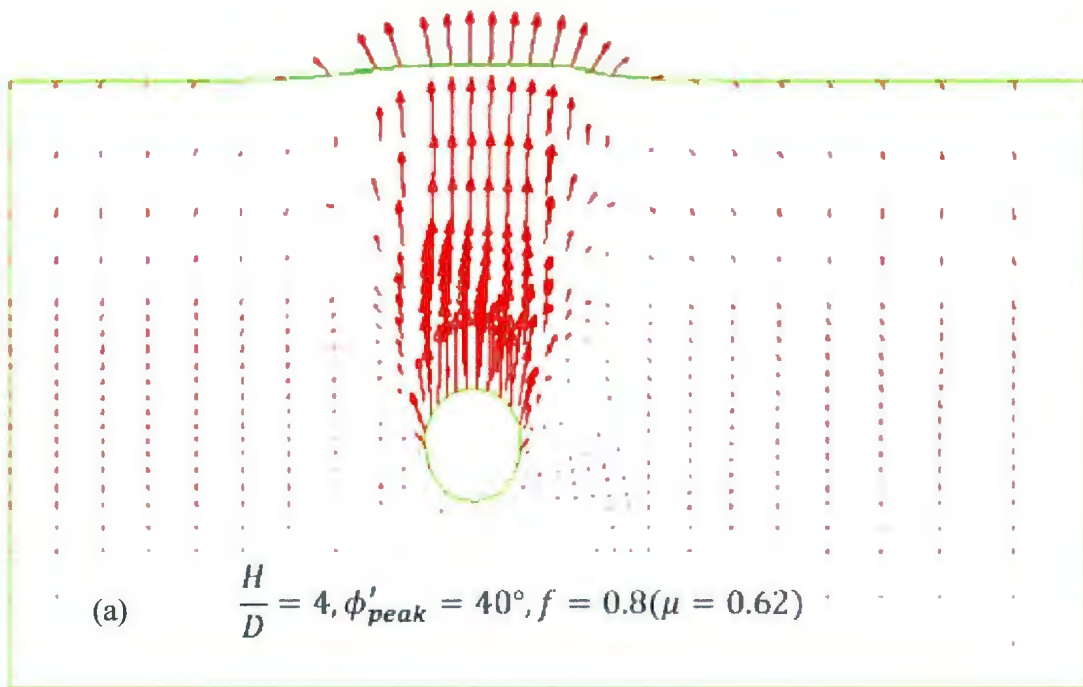


Figure 6-11: Comparison of displacement field in soil for $H/D=4, d=0.2D$.

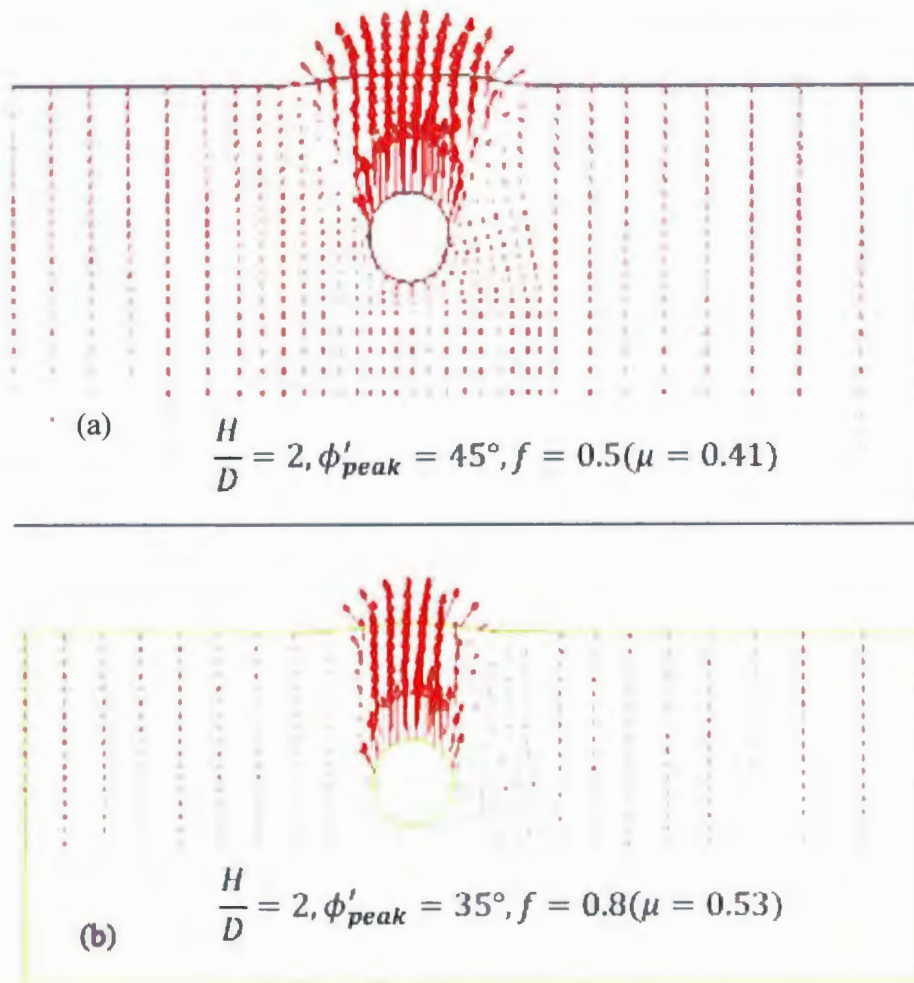


Figure 6-12: Comparison of displacement field in soil for $H/D=2, d=0.15D$.

For small oblique angles (2° and 5° in Figure 6-13.a), at early stages of loading, the axial load on the pipeline decreases and then increases again at larger relative displacements.

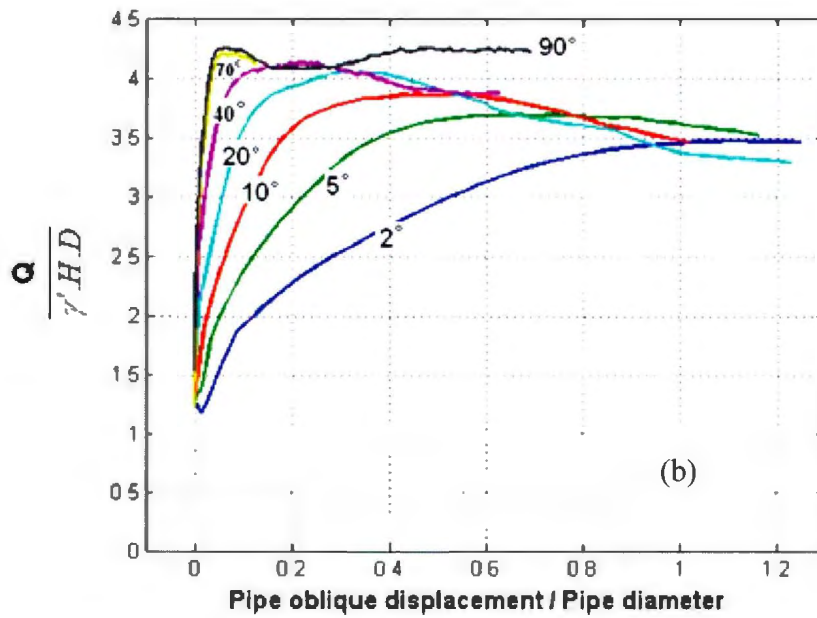
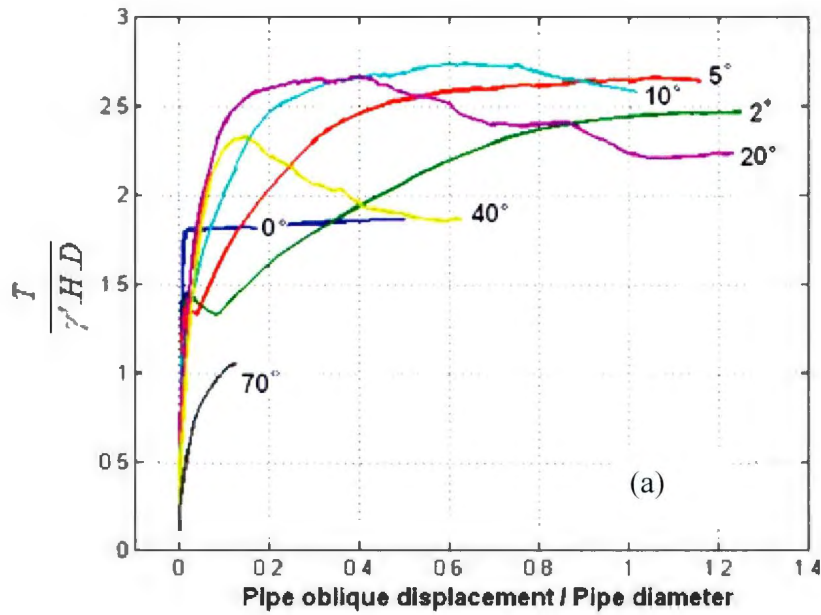


Figure 6-13: Axial (a) and vertical (b) load-displacement curves for different oblique angles; $H/D=4$, $\phi_{\text{peak}}=40^\circ$, $f=0.8$ ($\mu=0.62$).

Figure 6-14 shows how the axial load on the pipe circumference changes during various increments of oblique 2° axial-vertical movement. In Figure 6-14.b, T_n is the axial load

applied to each node on the pipe circumference. The axial load on the pipe is increasing from increment 1 to increment 7 as the axial resistance on the pipe surface is being mobilized by a small displacement. Pipe displacement relevant to each increment can be found in Figure 6-14.a and Table 6-1. From increment 7 to 13 the axial load on the pipe decreases because of the gap occurring at the bottom of the pipe as a result of upward movement of the pipe. For the rest of oblique displacement increments, the peripheral area of the pipe in contact with soil remains constant and almost half of the circumference is involved in pipe/soil interaction. The axial load on the pipe increases by increasing the vertical component of the load (Figure 6-14.a) and as a result the normal pressure on the pipe surface.

Axial and vertical interaction factors for different parameters are compared in Figure 6-15, Figure 6-16 and Figure 6-17. Similar to axial-lateral pipe/soil interaction a two part interaction curve seems to fit to all data sets well. The equations are different from what was proposed for axial-lateral pipe/soil interaction and consist of a linear part that connects the point $(N_{l(0)}, 0)$ and $(\mu \cdot (N_{qv(90)} + 0.7), N_{qv(90)})$, and a curve part with the following equation:

Eq. 6-2

$$N_{qv}^2 + 0.3N_l^2 = N_{qv(90)}^2$$

where $N_{qv(90)}$ is interaction factor for pure vertical loading condition.

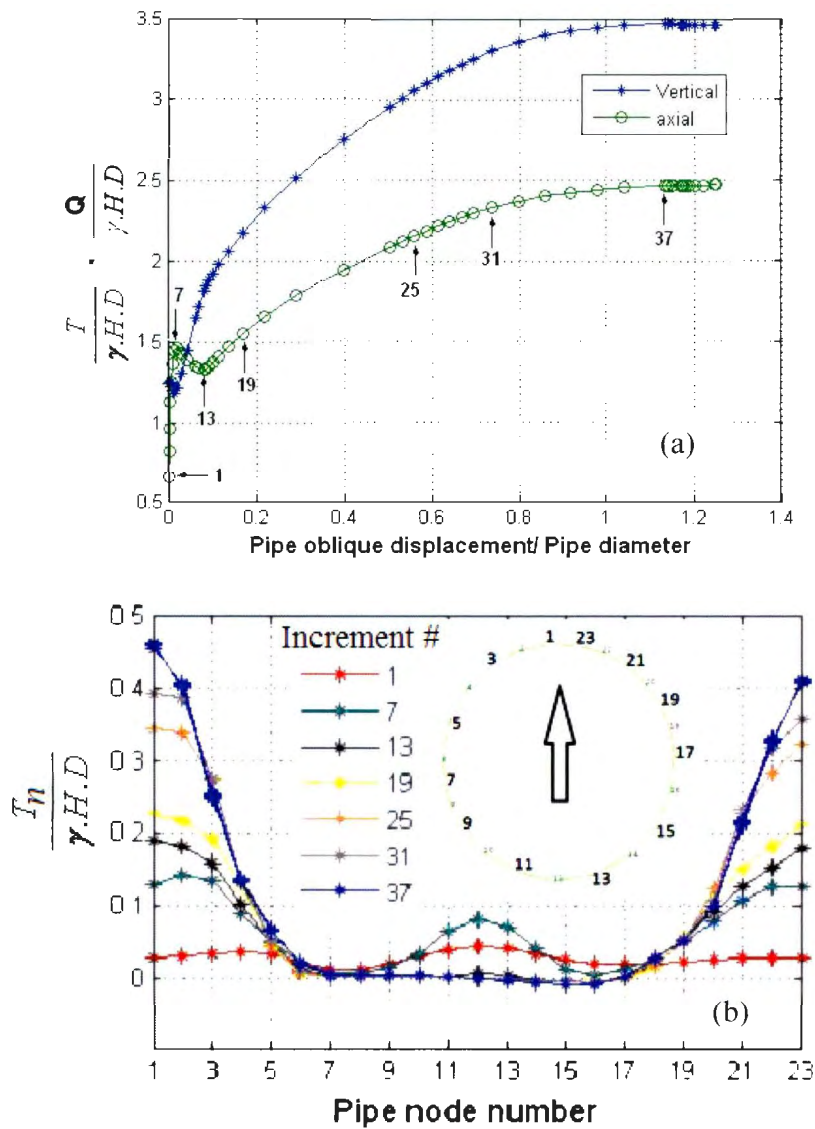


Figure 6-14: (a) Axial-vertical load-displacement curves for oblique 2°, and (b) normalized axial loads applied at different nodes of pipe at specified increments shown in (a)

Table 6-1: Displacement levels at different increments shown in Figure 6-14 (D=400 mm).

Increment #	1	7	13	19	25	31	37
Axial displacement (×D)	0.0031	0.014	0.081	0.169	0.56	0.74	1.13
Vertical displacement (×D)	0.0001	0.0005	0.0028	0.006	0.0196	0.026	0.04

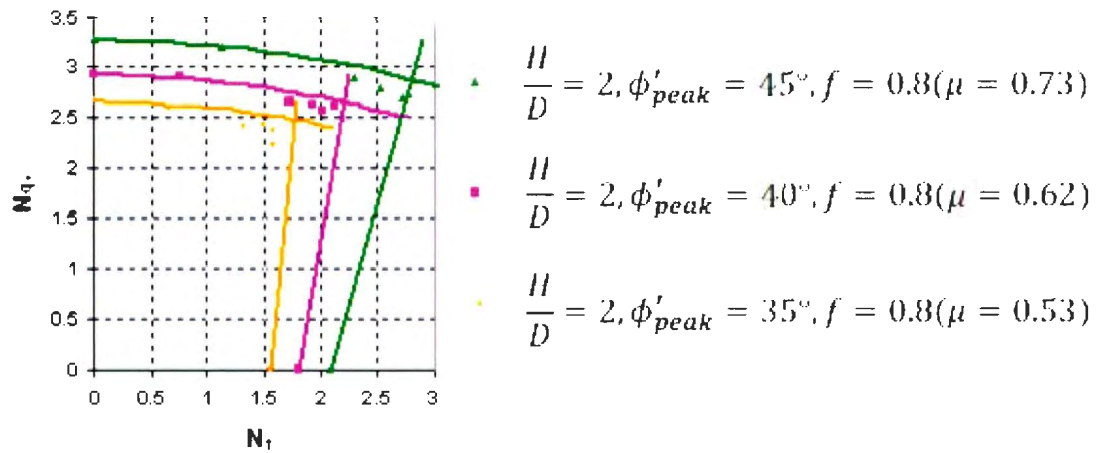


Figure 6-15: Effect of friction angle on axial-vertical pipe/soil interaction (solid lines based on Eq.6-2)

Figure 6-15 shows the effect of soil friction angle on axial and vertical components of load on the pipeline. By increasing the friction angle both the axial and vertical components of load increase accordingly.

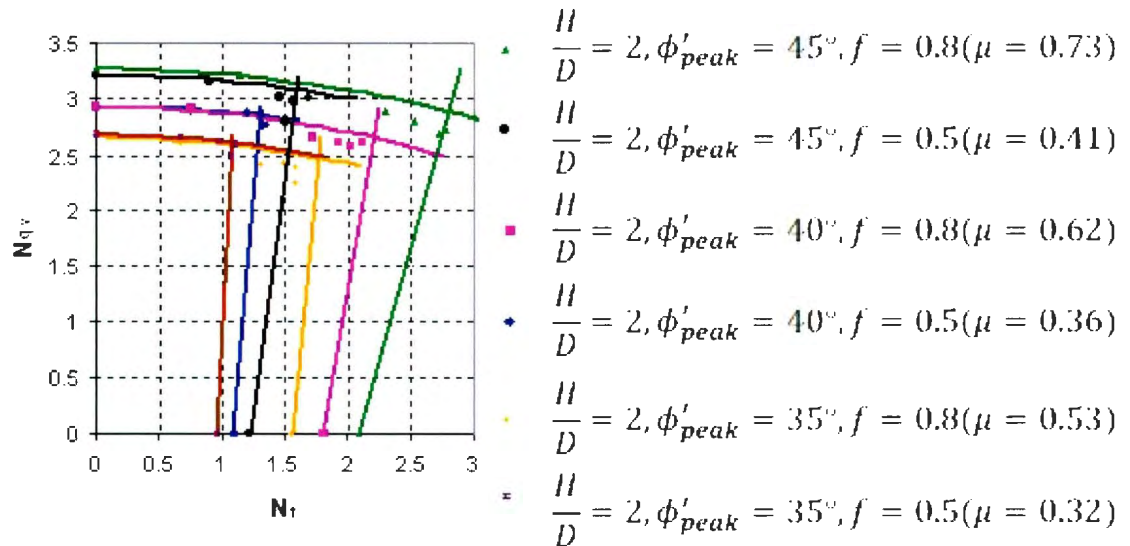


Figure 6-16: Effect of interface friction factor on axial-vertical pipe/soil interaction (solid lines based on Eq.6-2)

Figure 6-16 presents the effect of pipe surface friction factor. By increasing the pipe surface roughness the axial load on the pipeline increases for oblique angles less than or equal to 40° while the lateral component of the load decreases according to Eq. 6-2. For higher oblique angles the surface roughness has little or no effect on the soil restraint on the pipe.

The effect of burial depth ratio is shown in Figure 6-17. By increasing the burial depth the vertical load on the pipe increases which results in larger normal stress on the pipe surface and increases the axial load on the pipeline.

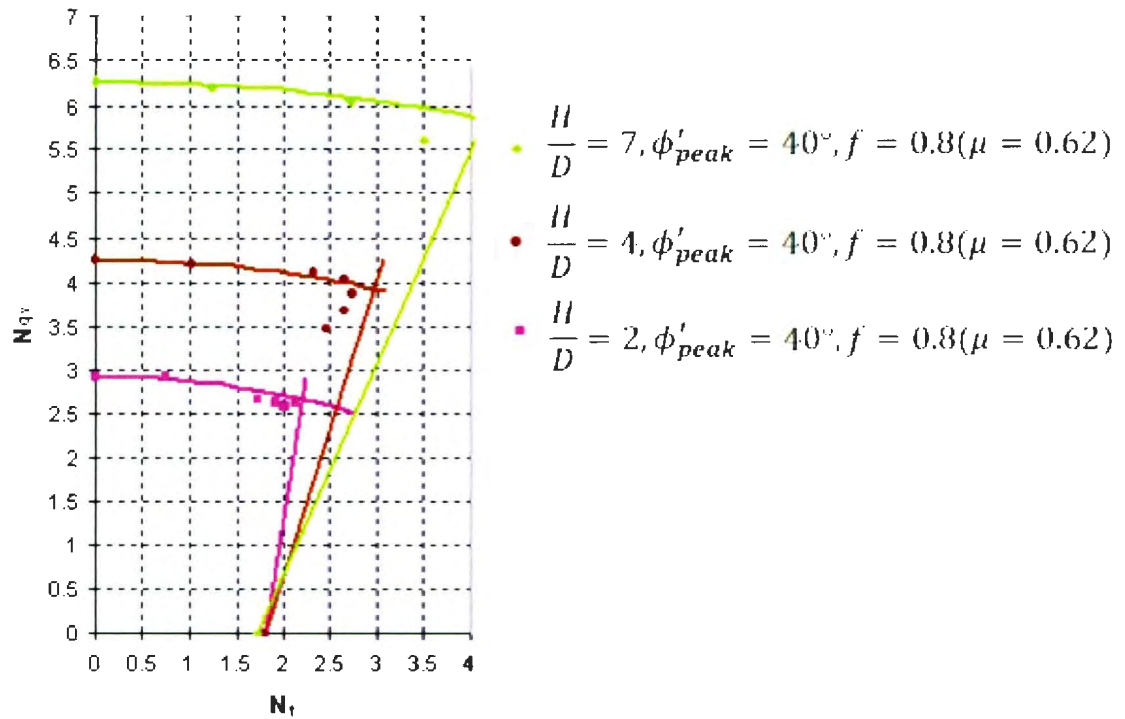


Figure 6-17: Effect of burial depth on axial-verticle pipe/soil interaction (solid lines based on Eq.6-2)

6.4 6.4 Lateral-vertical pipe/soil interaction

The same numerical model that was developed in previous Chapters of this thesis and used for parametric studies in previous sections is used for lateral-vertical pipe/soil interaction. Pipe/soil interaction during pure lateral and pure vertical upward relative displacements are discussed in previous sections of this Chapter. In this section some analysis are conducted for oblique lateral-vertical upward pipe/soil interaction and the results are compared to available interaction curves in the literature.

Load/displacement curves for three different cases are presented in Figure 6-18, Figure 6-19 and Figure 6-20. The oblique angles in lateral-vertical plane are defined from horizontal surface i.e. pure lateral= 0° and vertical upward= 90° .

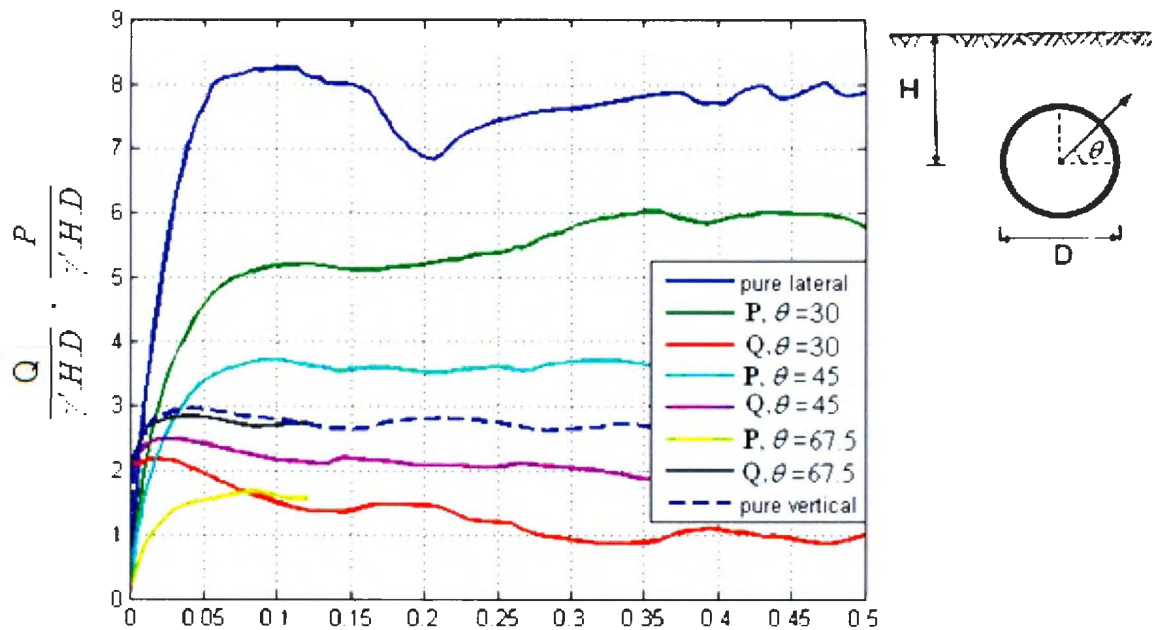


Figure 6-18: Lateral-vertical load-displacement curves for $H/D=2$, $\phi=40^\circ$, $f=0.5$.

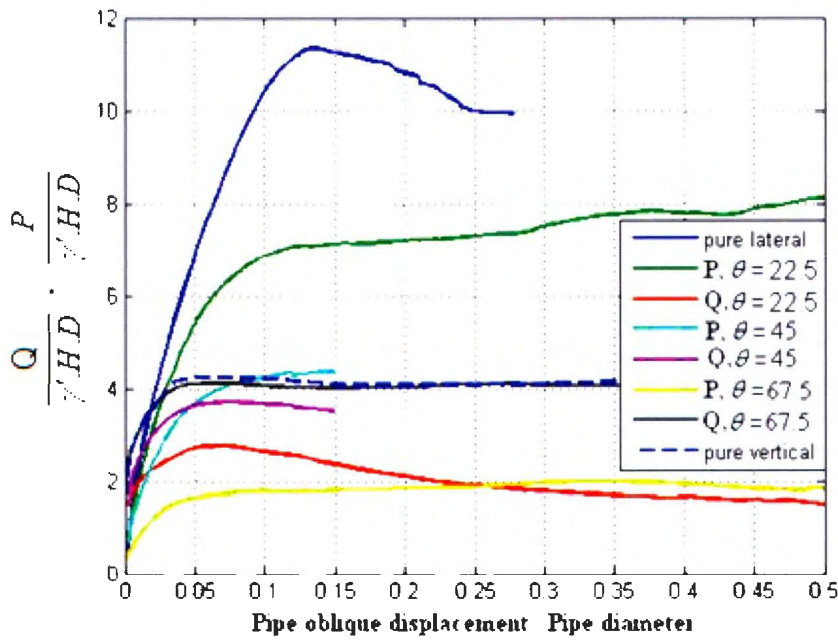


Figure 6-19: Lateral-vertical load-displacement curves for $H/D=4$, $\phi=40^\circ$, $f=0.8$

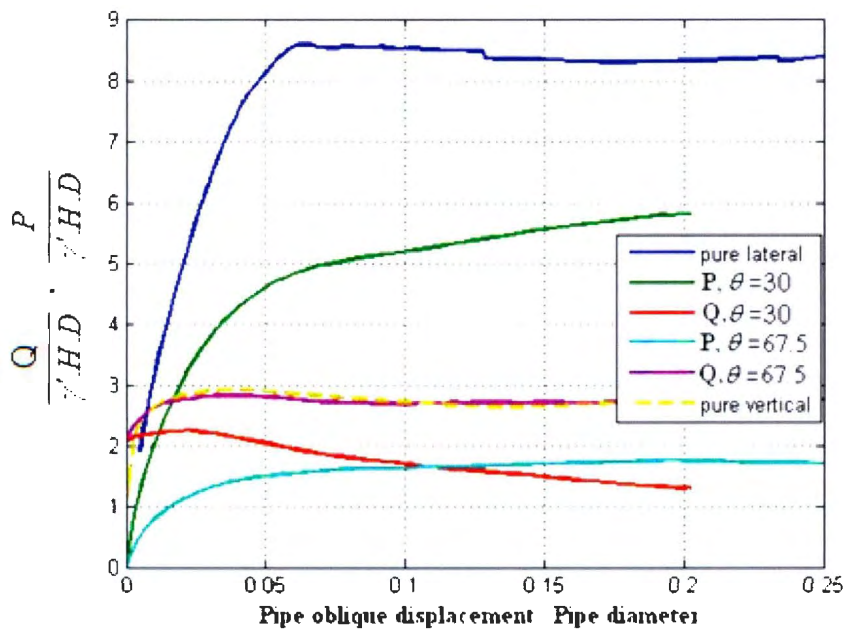


Figure 6-20: Lateral-vertical load-displacement curves for $H/D=2$, $\phi=40^\circ$, $f=0.8$

It can be observed from load-displacement curves that the effect of oblique movement is more significant for lateral component of the load on the pipeline as the range of difference in vertical load is much less than lateral load. For instance an obliquity equal to or less than 22.5° with respect to vertical direction has almost no effect on vertical component of load on the pipe.

Interaction factors presented in Figure 6-21 are normalized by pure lateral and pure vertical upward interaction factors. The yield surface is part of a circle:

Eq. 6-3

$$\left(\frac{N_{qh}}{N_{qh(0)}}\right)^2 + \left(\frac{N_{qv}}{N_{qv(90)}}\right)^2 = 1$$

Guo (2005) presented a similar yield surface for lateral-vertical upward pipe/soil interaction in clay. Figure 6-21 shows numerical data points are scattered around this yield surface.

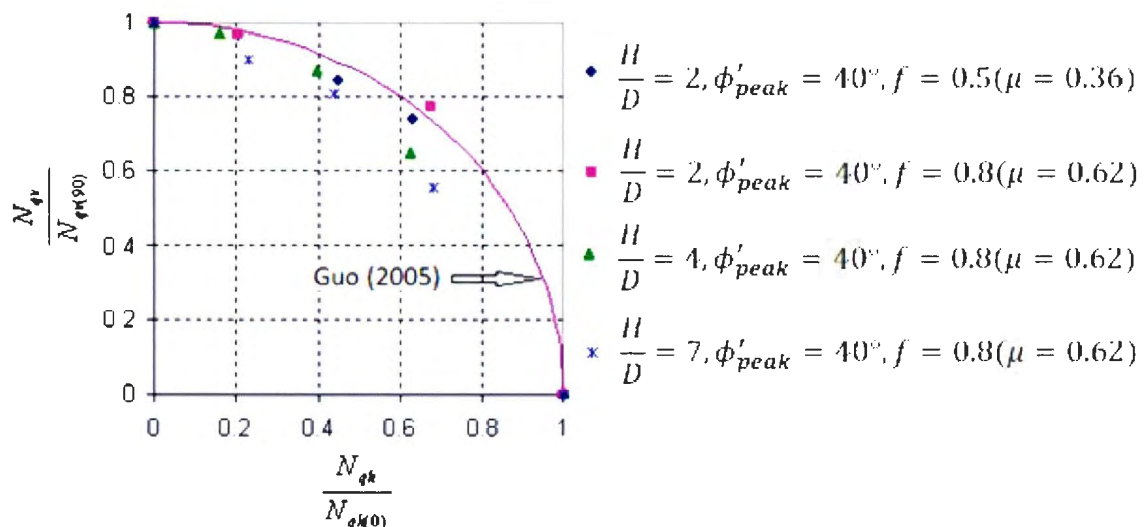


Figure 6-21: Summary of normalized interaction factors for lateral-vertical upward pipe/soil interaction.

Figure 6-22 compares the continuum finite element results with Nyman (1984) theoretical interaction curve. Numerical data points show very good agreement with Nyman's interaction curve. A few data points related to $H/D=2$ are a bit away from the interaction curve which is probably because of Nyman's assumption that the direction of pipe movement in the soil coincides with the direction of resultant load on the pipeline. Figure 6-23 shows this assumption is correct for deeply buried pipes while it is not correct for the case of oblique movement of shallow buried pipes. Hsu (1996) via experimental data and Van den Berghe et al. (2005) through numerical analysis reported good agreement with Nyman's interaction curve.

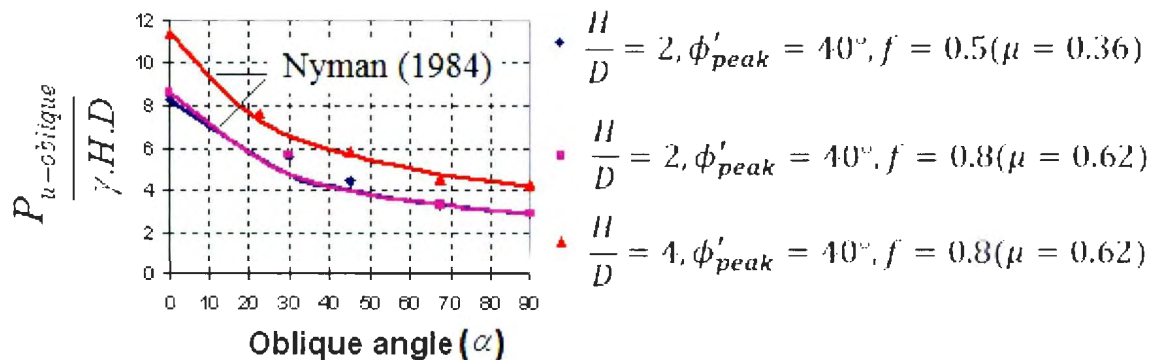


Figure 6-22: Comparison of FE data points with Nyman's interaction curve

There are other studies that investigated using a plasticity model approach for analysing lateral-vertical pipe/soil interaction. Yield surfaces proposed by some recent studies are discussed here.

Zhang et al. (2002) presented Eq. 6-4 for shallow or partly buried pipelines in sand:

Eq. 6-4

$$H - \mu(V_{\max} - V) \cdot \left(\frac{V}{V_{\max}} - \frac{V_{\min}}{V_{\max}} \right) = 0$$

where V and H are vertical and horizontal loads on pipeline and V_{\max} and V_{\min} are vertical downward and upward loads on the pipe respectively.

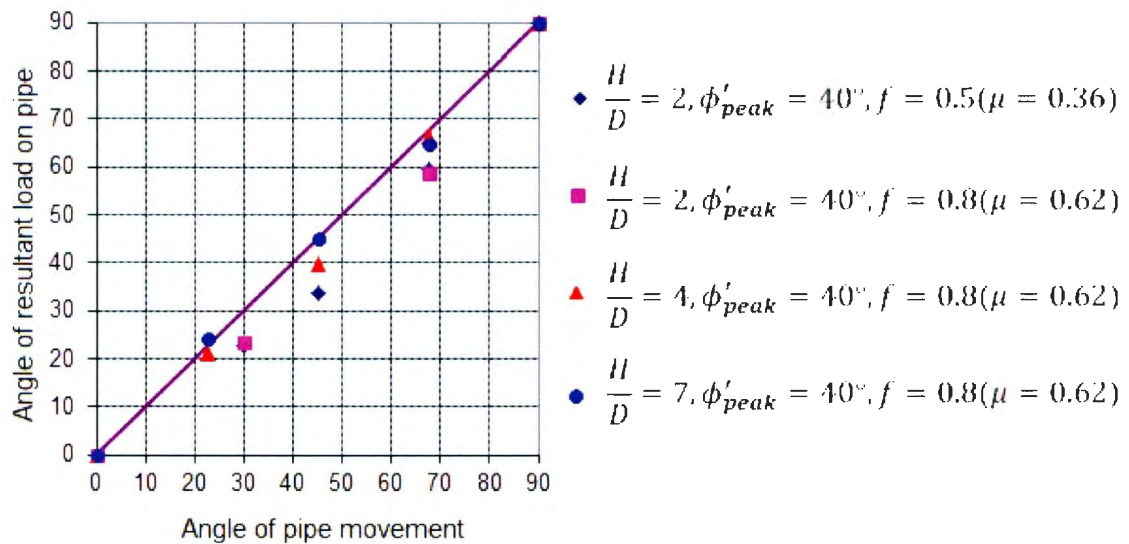


Figure 6-23: Direction of oblique load vs. oblique movement during lateral-vertical upward pipe/soil interaction

Cocchetti et al. (2009a) suggested a 3D failure criteria for pipelines buried in sand which does not account for the axial-lateral and axial-vertical pipe/soil interaction that was discussed in the previous sections of this Chapter. The proposed failure criteria in lateral-vertical plane can be shown as:

Eq. 6-5

$$\left(\frac{H}{H_0}\right)^2 - \left(\frac{V_0 - V}{V_0}\right)^{2*0.95} \cdot \left(\frac{V - V_t}{V_t}\right)^{2*0.6} = 0$$

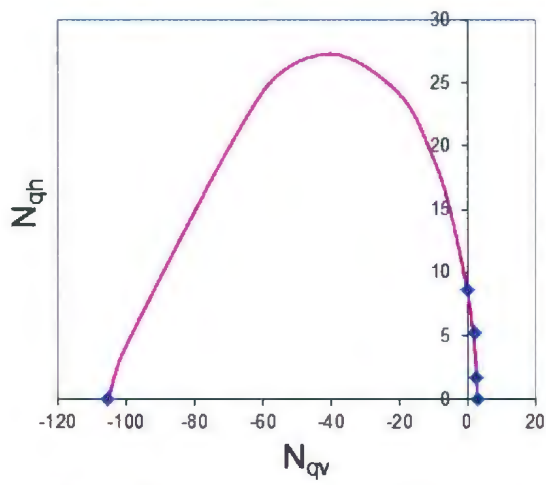
where H_0 is the soil restraint on the pipe during pure lateral movement and V_0 and V_t are vertical downward and upward soil restraints on the pipe respectively.

Hodder & Cassidy (2010) presented the following equation for shallow or partly buried pipelines in clay:

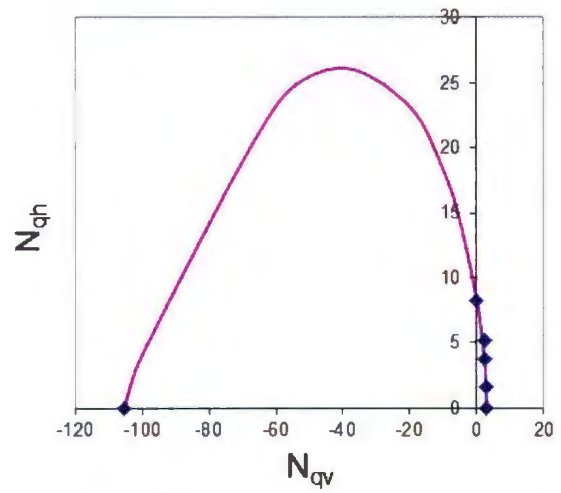
Eq. 6-6

$$\left(\frac{H}{H_0}\right) - \left(\frac{2V_0}{V_0 - V_t}\right)^{1.5} \cdot \left(\frac{V - V_t}{V_0}\right)^{0.75} \cdot \left(\frac{V_0 - V}{V_0}\right)^{0.75} = 0$$

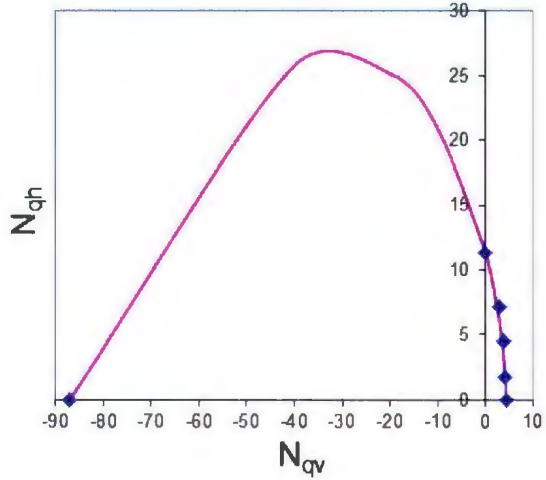
Cocchetti et al. (2009a) failure criteria for lateral-vertical pipe/soil interaction in sand (Eq. 6-5) is compared to numerical finite element data from current study in Figure 6-24.a, b, c & d. Numerical data show good match with the yield surface (Eq. 6-5) suggested by Cocchetti et al. (2009) and this equation can be adopted for lateral-vertical (upward/downward) pipe/soil interaction for buried pipelines. Combining this equation with axial-lateral and axial-vertical interaction curves gives a 3D yield surface for pipe/soil interaction analysis. Pure vertical downward data points are calculated using Eq. 2-13.



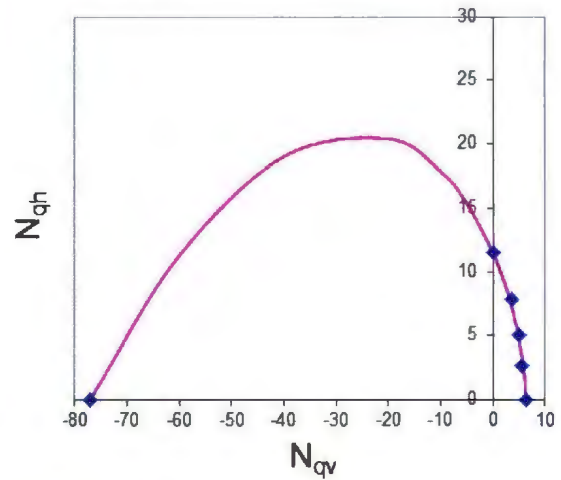
(a) • $\frac{H}{D} = 2, \phi'_{peak} = 40^\circ, f = 0.8 (\mu = 0.62)$



(b) • $\frac{H}{D} = 2, \phi'_{peak} = 40^\circ, f = 0.5 (\mu = 0.36)$



(c) • $\frac{H}{D} = 4, \phi'_{peak} = 40^\circ, f = 0.8 (\mu = 0.62)$



(d) • $\frac{H}{D} = 7, \phi'_{peak} = 40^\circ, f = 0.8 (\mu = 0.62)$

Figure 6-24: Comparison of Cocchetti et al. (2009a) yield surface (solid lines) with numerical data points from current study for lateral-vertical pipe/soil interaction (vertical upward +, vertical downward -).

6.5 6.5 Vertical downward pipe/soil interaction

Although this study is mainly focused on axial-lateral-vertical upward space, some numerical analyses are conducted to investigate the pipe/soil interaction in vertical downward direction.

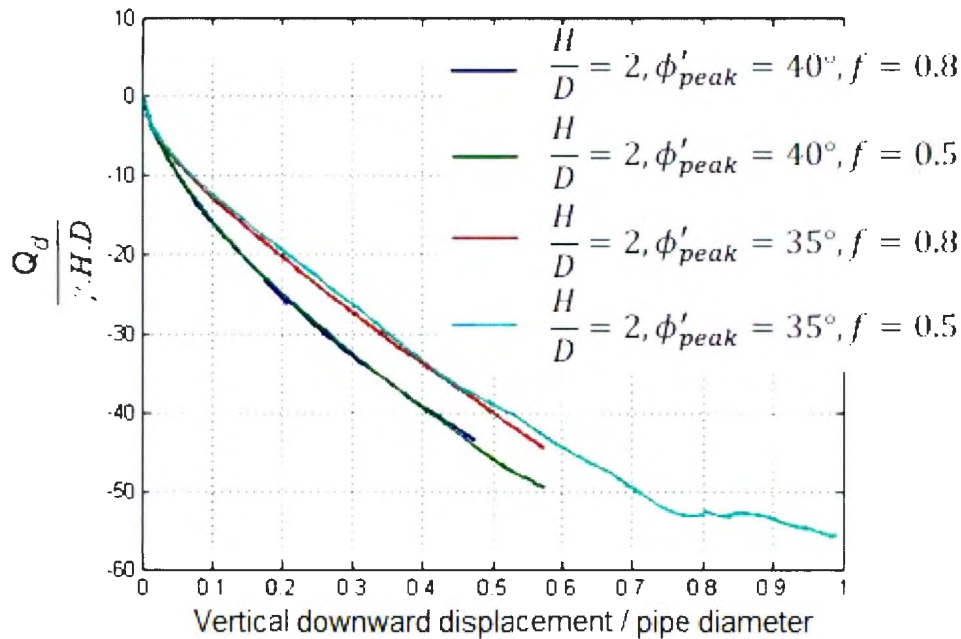


Figure 6-25: Comparison of load-displacement curves during downward movement of pipe.

Figure 6-25 shows four load-displacement curves for pure downward movement of pipe in four different cases of soil shear strength and pipe surface coating conditions. For three out of four cases in Figure 6-25 the numerical model could not reach the ultimate displacement because of convergence problem during large deformations. The ultimate displacements are in the range of 1D, which is obviously much higher than what is proposed in the guidelines (about 0.1 D) as discussed in Chapter two. This observation is

consistent with the numerical results of Calvetti et al. (2004). Calvetti et al. (2004) numerical model has been developed using Distinct Element Method (DEM) and compared well with small scale experimental modeling. A vertical downward ultimate displacement in the range of 1.5D has been observed.

A series of large scale tests conducted by C-CORE shows ultimate displacements in the range of 2D for vertical downward movement of pipes in sand.

The ultimate loads in Figure 6-25 are consistent with what is proposed by guidelines (Eq.2-13) based on theory of bearing capacity for a cylindrical foundation. For a case of $H/D=2$, $\phi'_{\text{peak}}=35^\circ$, having $\gamma=16 \text{ kN/m}^3$, $N_q=35$, $N_\gamma=45$, $c=4 \text{ kPa}$ and $N_c=45$ results in a vertical downward bearing capacity of $N_{vd}=57$, which is consistent with Figure 6-25.

It can be concluded from above observations that although using similar relations for bearing capacity of a shallow foundation and downward movement of pipeline is valid, using the same range for ultimate displacements can be erroneous. More studies, particularly experimental studies, are required to investigate the vertical downward pipe/soil interaction.

Figure 6-26 shows the load-displacement curves for lateral-vertical downward movement of pipeline buried at a burial depth ratio of $H/D=2$ in a soil with $\phi'=40^\circ$. Oblique angles are measured from horizontal line and clockwise rotation is shown with negative sign. The load-displacement curves confirm the increase in lateral interaction factor by increasing the downward component of pipe movement, which is consistent with what is reported by other researchers (e.g. Cocchetti et al. 2009a).

This coupling is an important effect that has not been considered in the current engineering guidelines.

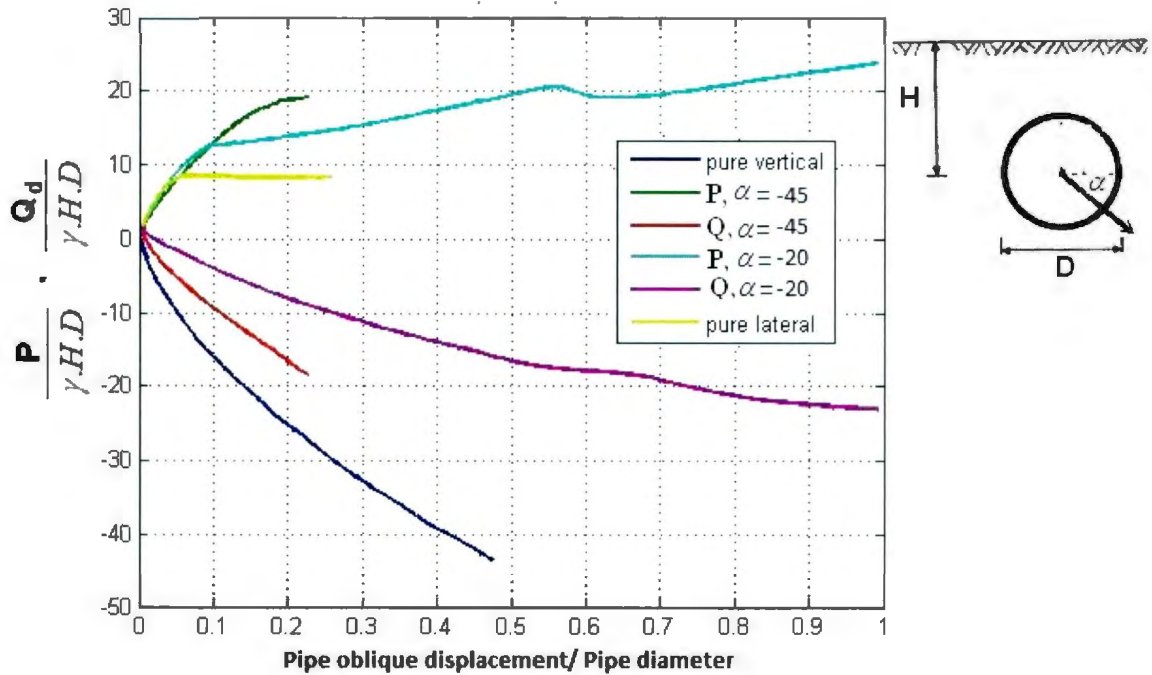


Figure 6-26: Lateral-vertical downward pipe/soil interaction curves for $H/D=2$, $\phi'=40^\circ$, $f=0.8$.

6.6 Summary

- The numerical model developed in Chapter 5, has been used for parametric studies in this Chapter.
- Axial-lateral, axial-vertical and lateral-vertical pipe/soil interaction were examined by means of parametric studies and interaction curves are compared with existing yield surfaces in the literature.
- The parameters considered for parametric studies are oblique angle, burial

depth ratio, effective friction angle and the pipe surface friction factor.

- The conclusions are summarized in Chapter 7.

Closing remarks

The structural (beam-spring) model is a practical approach used in the pipeline industry particularly when long lengths of pipelines are involved. The interaction curves, such as curves presented in this study, can be used to define the coupling effects for axial, lateral and vertical loading within a beam-spring engineering model simulating pipeline/soil interaction events. Depending on the angle of movement, the ultimate soil restraints in axial, lateral and vertical directions can be determined from interaction curves (or semi-empirical equations). These ultimate values can be used to define the coupled load- displacement relationships for soil springs.

Examples for application of interaction curves to improve the soil spring behaviour in structural modeling of pipe-soil interaction are presented in Appendix B.

7 Conclusions

- In this study centrifuge and numerical modeling studies have shown that soil load coupling mechanisms during pipe-soil interaction events can be significant.

7.1 Axial-lateral pipe/soil interaction

- The predicted ultimate loads from numerical simulations were consistent with the experimental data. Using heavy pipes during experimental modeling resulted in larger ultimate loads on pipe. The effect of pipe self-weight on ultimate loads on pipeline is shown using numerical modeling and explained. There was discrepancy between ultimate displacements observed from centrifuge tests and those from numerical modeling. The ultimate displacements from the centrifuge tests were influenced by test bed preparation; whereas, the ultimate displacements predicted by numerical modeling were consistent with existing industry practice guidelines and literature.
- For oblique axial-lateral pipeline/soil interaction events, the results from this study support and enhance a two-part failure criterion proposed by Phillips et al. (2004b). The failure surface defines soil failure mechanism on the pipeline circumference for lower oblique angles (for axial-lateral oblique angle definition see Figure 2-22), generally less than 40°, and shear failure mechanisms through the soil at higher oblique angles of attack.

- The axial restraint can increase by a factor of 2.5, during axial-lateral pipe/soil interaction, for oblique angles less than 40° . The lateral soil restraint can be reduced by a factor of 0.75 for small oblique loading angles.
- Parametric studies were conducted to investigate the effect of soil friction angle, pipe/soil interface friction factor and pipe burial depth on axial-lateral, axial-vertical and lateral-vertical pipeline/soil interaction events.
- For axial-lateral pipe/soil interaction, it was shown that increasing soil friction angle and burial depth, increases the lateral and axial interaction factors for all oblique angles proportionally. Increasing the pipe external surface friction factor did not affect the axial and lateral interaction factors for higher oblique angles. For lower oblique angles (in general less than 40°), the axial interaction factors increased proportionally with surface friction factor and decreased with lateral interaction factor. The proposed failure criterion fitted numerical data from various sets of parameters well.
- The ultimate axial and lateral displacements and their effects on soil spring stiffness are discussed. It is shown that while lateral stiffness remains almost constant for different oblique angles, for the axial stiffness a more complex relationship is required to define the soil spring stiffness.

7.2 Axial-vertical pipe/soil interaction

- For axial-vertical pipe/soil interaction, a two-part failure criterion based on the same concept as the axial-lateral failure surface is proposed.

- The ultimate axial load is shown to increase by about 50% during axial-vertical movement while the vertical component of the load on the pipeline decreases slightly for small oblique angles.
- Parametric studies are conducted to investigate the effect of soil friction angle, pipe/soil interface friction factor and pipe burial depth on axial-vertical pipeline/soil interaction. The proposed failure criterion fits numerical data from various sets of parameters.

7.3 Lateral-vertical pipe/soil interaction

- Numerical analyses are conducted to investigate lateral-vertical (upward) pipe/soil interaction. The numerical simulations were consistent with failure criteria proposed by Nyman (1984) and Cocchetti et al. (2009a). Cocchetti et al. (2009a) criteria show a significant interaction between ultimate lateral and vertical loads on the pipeline during lateral-vertical downward pipe/soil interaction which is not accounted for in the current guidelines.

7.4 General conclusions

- These observations raise questions on the adequacy of current structural-based pipeline/soil interaction models to predict behavior and assess pipeline integrity for specific design conditions. Therefore investigating the effects of this coupling on the soil deformation and failure mechanism is important. Developing an improved pipe/soil structural system that is able to consider the interaction between the soil restraints on a pipe moving in different

directions with respect to the surrounding soil is important for estimating the ground effect on the pipeline. An example of improved structural modeling, considering the axial-lateral pipe/soil interaction, is presented in Appendix B. The effects of this improvement on pipe's internal strains assessment are discussed.

- The outcomes of this study are expected to improve the current guidelines and state of practice in designing energy pipelines by improving understanding of soil loads and resistances on pipelines. Better understanding the soil behavior reduces the design uncertainties and pipelines vulnerability against the incidents caused by ground movements and results in more economic designs for cases where soil provides resistance against pipeline deformation or structural instabilities such as pipe buckling.

8 Recommendations

Based on discussions and observations in the previous sections, the following recommendations are made for further research/engineering works:

8.1 Practical recommendations

- Incorporating an equation similar to what is proposed by Guo and Stolle (2005) (Figure 2-6) in the guidelines to consider the scale effect for lateral and vertical pipe/soil interaction effects.
- Incorporating an equation similar to what is proposed by Philips et al. (2004a) for lateral pipe/soil interaction in clay in the guidelines, to consider the effects of both burial depth ratio and overburden ratio.
- Incorporating more updated solutions such as Merifield et al. (2001) and Merifield and Sloan (2006) for vertical upward pipe/soil interaction in the engineering guidelines.
- Improving numerical tools such as macro-elements proposed by Cocchetti et al. (2009a) or the method used in Appendix B of this thesis to facilitate implementing the pipe/soil interaction curves in engineering applications.

8.2 Future directions of research

- Investigating the effect of pipe selfweight or vertical restraint on pipe/soil interaction.
- Investigating ultimate load and displacement during vertical downward pipe/soil

interaction using experimental and numerical methods.

- Investigating axial-lateral and axial-vertical pipe/soil interaction in cohesive materials.
- Developing three-dimensional failure criteria such as suggested by Cocchetti et al. (2009a) for pipe/soil interaction in granular and cohesive materials.

References

- American Lifeline Alliance (2001). Guidelines for the design of buried steel pipe. American Lifeline Alliance (ALA), Federal Emergency Management Agency (FEMA), Washington, D.C.
- ASCE (1984). Guidelines for the seismic design of oil and gas pipeline systems. American Society of Civil Engineers, Committee on gas and liquid fuel lifelines, Technical Council on Lifeline Earthquake Engineering, ASCE, New York.
- Aubeny, C. P., Han, S. W. and Murff, J. D. (2003). Inclined Load Capacity of Suction Caissons. *International Journal for Numerical and Analytical Methods in Geomechanics*, 27(14): 1235-1254, doi:10.1002/nag.319.
- Audibert, J. M. E. and Nyman, K. J. (1977). Soil restraint against horizontal motion of pipes. *Journal of Geotechnical Engineering Division, ASCE*, 103(10), 1119-1142.
- Bolton, M. D. (1986). The strength and dilatancy of sands. *Geotechnique* 36, No. 1, pp. 65-78.
- Calvetti, F., Prisco, C., and Nova, R. (2004). Experimental and numerical analysis of soil-pipe interaction. *Journal of Geotechnical and Geoenvironmental Engineering*, 130 (12).
- Cheuk, C. Y., White, D. J., Bolton, M. D. (2008). Uplift mechanisms of pipes buried in sand. *Journal of Geotechnical and Geoenvironmental Engineering, ASCE*, 134(2).

- Cocchetti, G., Prisco, C., Galli, A. and Nova, R. (2009a). Soil-pipeline interaction along unstable slopes: a coupled three-dimensional approach. Part 1: Theoretical formulation. *Canadian Geotechnical Journal*, 46 (11): 1289-1304.
- Cocchetti, G., Prisco, C., and Galli, A. (2009b). Soil-pipeline interaction along unstable slopes: a coupled three-dimensional approach. Part 2: Numerical analysis. *Canadian Geotechnical Journal*, 46 (11): 1305-1321.
- Das, B. M. (1985). Resistance of shallow inclined anchors in clay. Uplift behavior of anchor foundations in soil. S.P. Clemence, ed., ASCE, New York.
- Dickin, E. A. (1988). Stress-displacement of buried plates and pipes. In *Proceedings of the International Conference on Geotechnical Centrifuge Modeling (Centrifuge 88)*, Paris, France, 25-27 April 1988, Edited by J.F.Corte'. A.A.Balkema, Rotterdam, the Netherlands, pp.205-214.
- Dickin, E. A. (1994). Uplift resistance of buried pipelines in sand. *Soils and Foundations*, 34(2), pp.41-48.
- European Gas Pipeline Incident Data Group (2005). *Gas Pipeline Incidents*. EGIG, Groningen, the Netherlands. 6th EGIG Report 1970-2004, No. EGIG 05-R-0002.
- Finch, M. (1999). Upheaval buckling and floatation of rigid pipelines: The influence of recent geotechnical research on the current state of the art. *Offshore Technology Conference*, OTC 10713.
- Finch, M., Fisher, R., Palmer, A. and Baumgard, A. (2000). An integrated approach to pipeline burial in the 21st century. *Proceedings of Deep Offshore Technology 2000*.

- Guo, P. (2005). Numerical modeling of pipe-soil interaction under oblique loading. *Journal of Geotechnical and Geoenvironmental Engineering*, ASCE, 131(2), pp. 260-268.
- Guo, P. and Stolle, D. F. (2005). Lateral pipe-soil interaction in sand with reference to scale effect. *Journal of Geotechnical and Geoenvironmental Engineering*, ASCE, 131(3): 338-349.
- Hansen, J. B. (1961). The ultimate resistance of rigid piles against transversal forces. Danish Geotechnical Institute, Copenhagen, Denmark, Bulletin 12, pp. 5-9.
- Hibbitt D., Karlsson B., and Sorensen P. (2005). ABAQUS User's Manual. Version 6.5 [computer program]. ABAQUS Inc., Providence, R.I.
- Hodder, M. S. and Cassidy, M. J. (2010). A plasticity model for predicting the vertical and lateral behavior of pipelines in clay soils. *Geotechnique*, 60, No. 4, pp. 247-263.
- Honegger, D. G. (1999). Field measurements of axial soil friction forces on buried pipelines. *Proceedings of the Fifth U.S. Conference on Lifeline Earthquake Engineering*, Technical Council on Lifeline Earthquake Engineering, Monograph No.16, American Society of Civil Engineers.
- Honegger, D. G., Hart, J. D., Phillips, R., Popelar, C. and Gailning, R. W. (2010). Recent PRCI guidelines for pipelines exposed to landslide and ground subsidence hazards. *Proceedings of IPC2010, International Pipeline Conference*, Calgary.

- Honegger, D. G. and Nyman, J. (2004). Guidelines for the seismic design and assessment of natural gas and liquid hydrocarbon pipelines. Pipeline Research Council International, Inc., No.L51927.
- Horvath, J. S. (2002). Soil-structure interaction research project; basic SSI concepts and applications overview. Report No. CGT-2002-2, Manhattan Coll., Bronx, NY.
- Hsu, T. W. (1996). Soil restraint against oblique motion of pipelines in sand. *Canadian Geotechnical Journal*, pp. 180-188.
- Hsu, T. W., Chen, Y. J. and Wu, C. Y. (2001). Soil friction resistance of oblique pipelines in loose sand. *Journal of Transportation Engineering, ASCE*, 127(1), pp. 82-87.
- Hsu, T. W., Chen, Y. J. and Hung, W. Y. (2006). Soil restraint to oblique movement of buried pipes in dense sand. *Journal of Transportation Engineering, ASCE*, 132(2), pp. 175-181.
- Jacky, J. (1944). The coefficient of earth pressure at rest. *Journal of the society of Hungarian Architects and Engineers, Budapest, Hungary*, pp. 355-358.
- Jardine, R. J., and Overy, R. F. (1996). Axial capacity of offshore piles driven in dense sand. *Proceedings Offshore International Conference, Houston, Texas, USA.*, pp. 161-180.
- Karimian, S. A. (2006). Response of buried steel pipelines subjected to longitudinal and transverse ground movement. Ph.D. Thesis, The University of British Columbia.

- Kennedy, R. P., Chow, A. W., and Williamson, R. A. (1977). Fault movement effects on buried oil pipelines. *Journal of the Transportation Engineering Division, ASCE*, vol. 103, pp. 617-633.
- Kenny, S., Bruce, J., King, T., McKenna, R., Nobahar, A. and Phillips, R. (2004). Probabilistic design methodology to mitigate ice gouge hazards for offshore pipelines. *International Pipeline Conference, IPC 2004*.
- Krstelj, I. (1996). Behavior of laterally loaded pipes in dry and saturated sand (Centrifuge testing). Ph.D. Thesis, Princeton university.
- Kulhawy, F. H. C., Trautmann, C. H., Beech, J. F., O'Rourke, T. D., and McGuire, W. (1983). Transmission line structure foundations for uplift-compression loading. Report No. EL-2870, Electric Power Research Institute.
- Mackenzie, T. R. (1955). Strength of deadman anchors in clay. MSc. Thesis, Princeton University, USA.
- Martin, C. M. and Houlsby, G. T. (2000). Combined Loading of Spudcan Foundation on Clay: Laboratory Tests. *Geotechnique* 50, No. 4, pp. 325-338.
- Merifield, R. S. and Sloan, S. W. (2006). The ultimate pullout capacity of anchors in frictional soils. *Canadian Geotechnical Journal*, 43, pp. 852-868.
- Merifield, R. S., Sloan, S. W. and Yu, H. S. (2001). Stability of plate anchors in undrained clay. *Geotechnique* 51, No.2, pp. 141-153.
- Meyerhof, G. G. (1955). Influence of roughness of base and ground water conditions on the ultimate bearing capacity of foundations. *Geotechnique*, Vol. 5, pp. 227-242.

- Meyerhof, G. G. (1973). Uplift resistance of inclined anchors and piles. Proceedings 8th International Conference on Soil Mechanics and Foundation Engineering, Vol. 2, Moscow, USSR, pp. 167-172.
- Murray, E. J. and Geddes, J. D. (1989). Resistance of passive inclined anchors in cohesionless medium. *Geotechnique* 39, No. 3, pp. 417-431.
- Neely, W. J., Stuart, J. G. and Graham, J. (1973). Failure load of vertical anchor plates in sand. *Journal of the Soil Mechanics and Foundations Division, ASCE*, 99(9), pp. 669-685.
- Ng, P. C. F. (1994). Behavior of buried pipelines subjected to external loading. Ph.D. Thesis. University of Sheffield, England.
- Ng, C. W. W., and Springman, S. M. (1994). Uplift resistance of buried pipelines in granular materials. *Centrifuge 94*, Leung, Lee and Tan, eds., pp. 753-758.
- Nobahar, A., Kenny, S. and Phillips, R. (2007). Buried pipelines subject to subgouge deformations. *International Journal of Geomechanics*, 7(3).
- Nobahar, A., Popescu, R., and Konuk, I. (2000). Estimating progressive mobilization of soil strength. Proceedings 53rd Canadian Geotechnical Conference, Montreal, Que., 15-18 Oct. 2000. Edited by D. Leboeuf. Bi Tech Publishers Ltd., Richmond, B.C.
- Nyman, K.J. (1984). Soil response against oblique motion of pipes. *Journal of Transportation Engineering*, 110(2), pp. 190-202.
- O'Rourke, T.D. (1989). Seismic design considerations for buried pipelines. *Annals of the New York academy of sciences*, ISSN 0077-8923, Vol. 558, pp. 324-346.

- O'Rourke, T.D., Turner, J.E., Jeon, S-S., Stewart, H.E, Wang, Y. and Shi, P. (2005). Soil-structure interaction under extreme loading conditions. The 13th Spencer J. Buchanan Lecture.
- Ovesen, N. K. (1964). Anchor slab calculation methods and model tests. Danish Geotechnical Institute, Copenhagen, Denmark, Bulletin 16, 40p.
- Palmer, A. C., White, D. J., Baumgard, A. J., Bolton, M. D., Barefoot, A. J., Finch, M, Powell, T., Faranski, A. S., and Baldry, J. A. S. (2003). Uplift resistance of buried pipelines: comparison between centrifuge modeling and full-scale tests. *Geotechnique* 53, No. 10, pp. 877-883.
- Paulin, M. J., Phillips, R. and Boivin, R. (1995). Centrifuge modeling of lateral pipeline/soil interaction-Phase II. Proceedings of the 14th International Conference on Offshore Mechanics and Arctic Engineering (OMAE 95), Copenhagen, Denmark, Volume 5, pp.107-123.
- Paulin, M. J. (1998). An investigation into pipelines subjected to lateral soil loading. Ph.D. Thesis, Memorial University of Newfoundland, St.John's, Canada.
- Paulin, M. J., Phillips, R., Clark, J. I., Trigg, A. and Konuk, I. (1998). A full scale investigation into pipeline/soil interaction. Proceedings of 1998 International Pipeline Conference, ASME, Calgary, AB, June 1998, Vol.2, pp. 779-787.
- Phillips, R., Nobahar, A. and Zhou, J. (2004a). Trench effects in pipe-soil interaction. Proceedings of international pipeline conference (IPC2004), Calgary, Canada, 4-8 Oct. 2004. American Society of Mechanical Engineers (ASME).

- Phillips, R., Nobahar, A. and Zhou, J. (2004b). Combined axial and lateral pipe-soil interaction relationships. Proceedings of international pipeline conference (IPC2004), Calgary, Canada 4-8 Oct. 2004. American Society of Mechanical Engineers (ASME).
- Popescu, R., Phillips, R., Konuk, I., Guo, P., and Nobahar, A. (2002). Pipe-soil interaction: Large-scale tests and numerical modeling. Proceedings of the International Conference on Physical Modeling in Geotechnics, ICPMG'02, St. John's, N.L., 10-12 July 2002. Edited by R. Phillips, P.Guo, and R. Popescu. A.A. Balkema Publishers, Rotterdam, the Netherlands, pp. 917-922.
- Popescu, R., Phillips, R., Konuk, I. and Deacu, D. (1999). Numerical and physical analysis of pipe-soil interaction. Proceedings 52nd Canadian Geotechnical Conference, Regina, Sask., pp. 437-444.
- Reese, L. C., and Casbarian, A. O. P. (1968). Pipe soil interaction for a buried offshore pipeline. 43rd Annual meeting of the Society of Petroleum Engineers of AIME, SPE 2343, Houston, Texas.
- Rizkalla, M., Poorooshab, F. and Clark, J. I. (1992). Centrifuge modeling of lateral pipeline/soil interaction. Proceedings of 11th Offshore Mechanics and Arctic Engineering Symposium, 13p.
- Rizkalla, M., Trigg, A. and Simmonds, G. (1996). Recent advances in modeling of longitudinal pipeline/soil interaction for cohesive soils. Proceedings of the 15th

- International Conference on Offshore Mechanics and Arctic Engineering, vol. V, pp. 325-332.
- Rowe, R. K. (1978). Soil structure interaction analysis and its application to the prediction of anchor behaviour. Ph.D. thesis, University of Sydney, Sydney, Australia.
- Rowe, R. K., and Davis, E. H. (1982a). The behavior of anchor plates in clay. *Geotechnique*, 32(1), pp. 9-23.
- Rowe, R. K., and Davis, E. H. (1982b). The behavior of anchor plates in sand. *Geotechnique*, 32(1), pp. 25-41.
- Scarpelli, G., Sakellariadi, E. and Furlani, G. (1999). Longitudinal pipeline-soil interaction: Results from field full scale and laboratory testing. In *Geotechnical engineering for transportation infrastructure*, Barends et al. (eds), Balkema, Rotterdam, ISBN 90 5809 047 7, pp. 511-519.
- Schaminee, P. E., Zorn, N. F., and Schotman, G. J. M. (1990). Soil response for pipeline upheaval buckling analyses: full scale laboratory tests and modeling. Proceedings of the 22nd annual Offshore Technology Conference (OTC 6486), Houston, Texas. pp. 563-572.
- Sherif, M. A., Fang, Y. S. and Sherif, R. I. (1984). K_u and K_0 behind rotating and non-yielding walls. *ASCE Journal of Geotechnical Engineering*, 110, pp. 41-56.
- Sladen, J. A. (1992). The adhesion factor: Application and limitations. *Canadian Geotechnical Journal*, 29, pp. 326-333.

- Stroud, M. A. (1971). Sand under low stress levels in simple shear apparatus. PhD thesis, Cambridge University, Cambridge, UK.
- Taylor, R. N. (1995). Geotechnical centrifuge technology. Blackie academic & professional, London, 296p.
- Taiebat, H. A. and Carter, J. P. (2000). Numerical studies of the bearing capacity of shallow foundations on cohesive soil subjected to combined loading. *Geotechnique* 50, No. 4, pp. 409-418.
- Trautmann, C. H. (1983). Behavior of pipe in dry sand under lateral and uplift loading. Ph.D. thesis, Cornell University, Ithaca, New York.
- Trautmann, C. H. and O'Rourke, T. D. (1985). Lateral force-displacement response of buried pipe. *Journal of Geotechnical Engineering, ASCE*, 111(9), pp. 1077-1092.
- Vanden Berghe, J. F., Cathie, D., and Ballard, J. C. (2005). Pipeline uplift mechanisms using finite element analysis. *Proceedings of the 16th International Conference on Soil Mechanics and Geotechnical Engineering*, Osaka, Japan.
- Vesic, A. S. (1971). Breakout resistance of objects embedded in ocean bottom. *Journal of Soil Mechanics and Foundation Division, ASCE* 97, No.9, pp. 1183-1205.
- Wantland, G. P., O'Neil, M. B., Coelogyne, E. H. and Reese, L. C. (1982). Pipeline lateral stability in soft clay. *Journal of Petroleum Technology*, 34(1), pp. 217-220.
- Wijewickreme, D., Karimian, A., Honegger, D.G. (2005). Effectiveness of some methods of reducing axial soil loads on buried pipelines subjected to ground movements. *Proceedings of the 58th Canadian Geotechnical Conference*, Saskatoon.

- Wijewickreme, D., Karimian, H. and Honegger, D. (2009). Response of buried steel pipelines subjected to relative axial soil movement. *Canadian Geotechnical Journal*, 46, pp. 735-752.
- Winkler, E. (1867). *Die Lehre Von Elastizitat und Festigkeit (Teachings on Elasticity and Stiffness)*. Prague, Czechoslovakia, 182p.
- Yimsiri, S., Soga, K., Yoshizaki, K., Dasari, G. R. and O'Rourke, T. D. (2004) Lateral and upward soil-pipeline interactions in sand for deep embedment conditions. *Journal of Geotechnical and Geoenvironmental Engineering*, 130(8), pp. 830-842.
- Zhang, J., Stewart, D. P. and Randolph, M. F. (2002). Modeling of shallowly embedded offshore pipelines in calcareous sand. *Journal of Geotechnical and Geoenvironmental Engineering*. ASCE, Vol. 128, No.5, pp. 363-371.

Appendix A: Parametric Study of Lateral-Vertical Pipeline/Soil Interaction in Clay



Parametric Study of Lateral-Vertical Pipeline/Soil Interaction in Clay

N.Daiyan¹, S.Kenny², R.Phillips³ and R.Popescu⁴

¹ Graduate Student, Memorial University of Newfoundland, St. John's, NL, Canada

² Assistant Professor, Memorial University of Newfoundland, St. John's, NL, Canada, Corresponding author

³ Principal Consultant, C-CORE, St. John's, NL, Canada

⁴ Consulting Engineer, URS Corporation, Princeton, NJ, USA

Abstract: This paper presents the ultimate soil resistance to oblique (lateral-vertical) relative movement of rigid pipes in undrained saturated clay. A parametric study is performed using continuum finite element method with the software package ABAQUS to investigate the effect of important parameters like the pipe diameter, burial depth, undrained shear strength of clay, soil weight and angles of movement. Equations are proposed to evaluate the pure lateral and pure vertical (uplift) restraints of soil on the pipeline; then equations are suggested to calculate the lateral and vertical components of the soil restraint on the pipeline during oblique lateral-vertical (upward) relative pipe/soil movement. These equations can be used to provide alternative soil-spring formulations that account for coupled soil deformation mechanisms during oblique pipeline/soil interaction events.

1. Introduction

Energy pipelines are one of the most efficient ways to transmit large volumes of oil and gas from their sources to target markets or processing facilities over short or long distances. Pipelines are vital infrastructure and both their integrity and safety are important to continue to supply oil/gas to consumers. Energy pipelines are usually buried. One issue considered in the design, construction and maintenance of buried pipelines is accounting for any geohazards resulting from large permanent ground deformations (PGD) such as fault movements due to earthquakes, landslides and large settlements. Pipelines pass through different types of lands with a variety of geotechnical, topographic and environmental conditions and in some parts of their length they may be subjected to such large ground deformation. This type of loading can cause excessive deformation or failure of pipelines that may result in environmental pollution, economic loss and even loss of life. An understanding of the load displacement behavior of soil due to relative pipe/soil movements is important to assess the pipeline's response.

Current engineering practice for pipe/soil interaction include idealized structural models that evaluate pipeline mechanical response using specialized beam elements and soil behavior using discrete springs with load-displacement relationships provided for principal directions (i.e. longitudinal, lateral horizontal, vertical upward and vertical downward). Soil springs in conventional engineering practice are independent and do not consider the shear transfer between principal directions during oblique or 3D pipe/soil interaction.

This study is part of a research program to develop 3D failure surfaces to be used to define alternative soil springs in conventional design approach. A parametric study of oblique pipeline/soil interaction helps pipeline designers to have a better understanding of a general three-dimensional pipe/soil interaction event. This paper concentrates on evaluating soil's ultimate restraint in oblique lateral-vertical direction on rigid pipelines. The response surface methodology is used to analyze results from the numerical investigations to develop equations defining the lateral and vertical components of the soil resistance on the pipeline during oblique lateral-vertical upward pipe/soil relative movement.

1.1. Lateral pipe/soil interaction

Transverse horizontal restraint represents the load on the pipe by surrounding soil due to any horizontal lateral pipe/soil relative displacement.

Most early studies on lateral pipe/soil interaction in clay are based on experimental studies of vertical anchor plates moving horizontally in the soil (e.g. Mackenzie 1955). Also they include some analogy between the response of retaining walls and shallow pipelines, or similarities between laterally loaded piles or deep strip footings and deeply buried pipes (e.g. Hansen 1961). Several experiments on lateral pipe/soil interaction have been reported such as Wantland et al. (1982), Rizkalla et al. (1992), Paulin et al. (1998), and Paulin (1998).

Based on experimental investigations by Wantland et al. (1982) and numerical studies by Rowe and Davis (1982) and comparing with the theoretical model suggested by Audibert

et al. (1977), PRCI guidelines (Honegger and Nyman (2004)) for the seismic design of pipeline systems consider the soil restraint on pipeline buried in clay under undrained loading as:

$$p_u = c_u N_{ch} D \quad (\text{Eq.1})$$

Where:

p_u : Maximum lateral soil restraint

c_u : Undrained shear strength

N_{ch} : Bearing capacity factor for vertical strip footings, horizontally loaded, after Hansen (1961) (Hansen's bearing capacity factor values are shown in Fig.3 of this paper)

D: Pipe diameter

Phillips et al. (2004) suggested that the lateral interaction factor in clay can be represented as follows to include the soil weight term and be capped for deep burial mechanism:

$$N_{ch} = \min \left(N_{ch}^* + \beta \frac{\gamma H}{c_u}, N_{ch}^{\max} \right) \quad (\text{Eq.2})$$

Where:

γ : Soil unit weight

H: Burial depth to the center of pipe

N_{ch}^* : Interaction factor associated with soil strength

$\beta \frac{\gamma H}{c_u}$: Factor to account for the soil weight which is related to the vertical stress level

N_{ch}^{\max} : Upper limit of the lateral interaction factor associated with deep burial mechanism

Rowe and Davis (1982) indicated that β is a function of $\frac{\gamma H}{c_u}$ and H/D and presented different curves over a range of H/D ratios which cap at different $\frac{\gamma H}{c_u}$. Merrifield et al. (2001) calculated upper and lower bound solutions for lateral and vertical capacity of anchor plates in clay using FE analysis based on limit analysis method and proposed different curves for various H/D ratios with $\beta=1$ where all curves cap at a constant value of $\beta \frac{\gamma H}{c_u}$.

1.2. Vertical pipe/soil interaction

Vesic (1971) calculated the vertical uplift capacity of circular and strip anchor plates based on cavity expansion model. Circular slip surfaces and plane strain conditions were assumed in his analysis and the ultimate resistance (q_0) was suggested as:

$$q_0 = c F_c + \gamma' H F_q \quad (\text{Eq.3})$$

Where;

F_c, F_q are cavity expansion factors which depend on shape and depth of cavity and friction angle of soil (ϕ). Cavity factors are calculated for buried horizontal cylinders (like pipes) as well as circular and strip anchor plates for H/D from 0.5 to 5.

Rowe and Davis (1982) performed elasto-plastic finite element (FE) analysis of uplift loading of strip anchors with H/D ranging from 1 to 8. For undrained behavior of an anchor plate in saturated clay Rowe and Davis (1982) showed a significant difference between soil fully bonded to the back of the anchor and immediate break away conditions. It was also indicated that the anchor uplift capacity in clay increases up to a H/D of about three and after that it remains almost constant.

1.3. Lateral/vertical pipe/soil interaction

Nyman (1982) performed an implicit limit equilibrium analysis on buried pipes based on Meyerhof (1973) limit equilibrium model for inclined anchor plates. Nyman considered a passive wedge with planar failure surfaces which is acceptable for shallow burial depths.

The ultimate soil restraint in the oblique direction was defined as:

$$p_{u-oblique} = i q_u \quad (\text{Eq. 4})$$

Where:

$$i = 1 + \left(\frac{0.25\alpha}{90^\circ - 0.75\alpha} \right) (i_u - 1) \quad (\text{Eq.5})$$

$i_u = p_u / q_u$: ratio of ultimate horizontal restraint to ultimate vertical restraint

α : angle of oblique movement measured from vertical direction

Experimental results by Das (1985) from small scale tests on anchor plates in clay and by Hsu (1996) from large scale tests on pipes in loose sand indicate good agreement with equation 4.

Guo (2005) developed an associative hardening elastoplasticity model for lateral-vertical

pipe/soil interaction in clay. The yield surface was presented as $(\frac{p}{p_u})^2 + (\frac{q}{q_u})^2 = 1$,

where p and q are lateral and vertical components of ultimate oblique load on the pipeline. Guo (2005) indicated good agreement between his numerical model's predictions and Nyman's analytical results.

2. Numerical model

Several numerical investigations (e.g. Rowe and Davis (1982), Popescu et al.(1999), Phillips et al.(2004), Guo (2005) and Ng (1994)) have indicated that continuum finite element modeling provides a reliable tool to solve soil/structure interaction problems by addressing nonlinearities from soil or pipe/soil contact behavior. In numerical continuum modeling pipe and soil are usually discretized using finite elements which are connected using contact elements or surfaces.

In this study 3D finite element analyses are conducted using ABAQUS/Standard finite element code. ABAQUS is a commercial finite element software that provides a variety of elements and constitutive models for soils, pipes and required contact surfaces for pipe/soil interfaces.

The continuum model includes a rigid pipeline surrounded by soil elements (Fig.1). The pipe/soil interface is modeled using the contact surface procedure implemented in ABAQUS. Each part of the model is explained separately in the following sections.

Eight node linear brick elements with reduced integration (C3D8R) are used to model soil in this study for 3D pipe/soil interaction model. The linear brick elements (C3D8R) were used by Phillips et al. (2004) to investigate the pipe/soil interaction using a 3D model in ABAQUS/Standard.

Von-Mises plasticity implemented in ABAQUS/Standard is used to model the behavior of undrained saturated clay in this study. Popescu and Konuk (2001), Guo (2005) and Phillips et al. (2004) used this elastic perfectly plastic model for pipe/soil interaction in clay in 2D and 3D analysis. This model can simulate fairly well the undrained behavior of clay where a single phase material is sufficient.

In this study the main concern is estimating the load-deformation behavior of soil as a function of the relative displacement between pipe and soil in a specified oblique direction. Therefore rigid pipe is used in the numerical modeling for simplification. To ensure the rigidity of the pipe a large value for modulus of elasticity of pipe is used in FE model.

S4R5 shell elements are used to model the pipe in 3D. These elements are 4 node, doubly curved thin shell elements with 5 degrees of freedom per node.

The interface between pipe and soil is simulated using the contact surface approach implemented in ABAQUS/Standard. This approach allows for separation and sliding of finite amplitude and arbitrary rotation of contact surfaces. A coefficient of friction (μ) equal to 0.25 is specified between pipe and soil which is an average value for oil/gas pipelines with smooth coatings. Since surface roughness is of little significance in lateral-

vertical pipe/soil interaction (e.g. Rowe and Davis (1982)), it is not considered to be a variable in this study.

Loads are applied in two steps including a geostatic step to obtain initial stress equilibrium in the soil medium and a rigid pipe movement up to a distance equal to pipe diameter in the specified oblique angle movement direction.

To define the ultimate load on the pipeline from load-displacement curve different methods are adopted in literature. Four methods are summarized in Fig.2. The ultimate load p_1 is defined as the point of intersection of the tangent to the upper part of the curve and the vertical axis. Neely et al. (1973) used this method to investigate vertical anchor plates in soil. Wantland et al. (1982) determined the failure load as the load value of the point of intersection of the tangents to the two straight line portions of the curve (p_2 in Fig.2). Rowe and Davis (1982) proposed a failure load which corresponds to an apparent stiffness of one quarter of the elastic stiffness which is called k_4 method (p_4 in Fig.2). Terzaghi's definition for local shear failure has been used in this study as the load at which the load-displacement curve passes into a steep straight tangent (p_3 in Fig.2). This definition results in larger soil restraints on pipelines compared to the first two methods and very close restraints to k_4 method.

In vertical pipe/soil interaction, for some cases a clearly defined peak exists in the load-deformation curve which is selected as the ultimate load.

To avoid interference from the boundary conditions, the total soil load on pipe at each displacement increment is calculated over the middle third of the pipe length; where the load distribution is almost uniform.

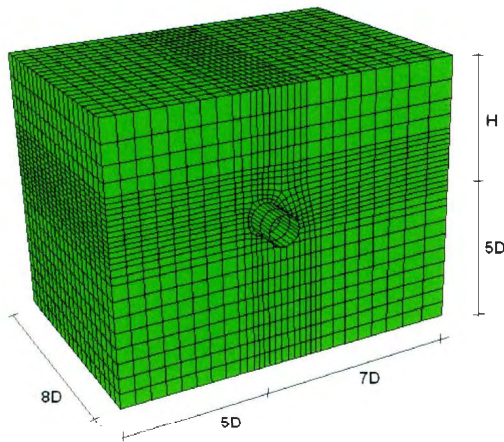


Fig.1: Typical finite element mesh

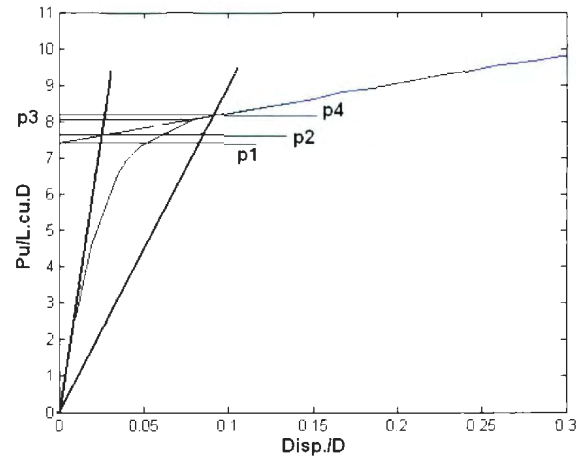


Fig.2: Four different methods of defining ultimate load

3. Parametric investigation

One important geometrical parameter in estimating the soil restraint is the ratio of burial depth to pipe diameter (H/D). Several studies (e.g. Rowe and Davis (1982) and Paulin (1998)) have indicated that over the range of H/D from 1 to 7 a shallow failure mechanism will change to a local failure mechanism for both lateral and vertical (uplift) pipe movements in clay. This H/D range is examined in this study.

Pipe diameters are considered in the range of 0.4 to 1 m which is a practical range for oil and gas pipelines. In lateral-vertical pipe/soil interaction, the angle of attack (α) is

measured from vertical direction i.e. it is zero for pure vertical and 90 degrees for pure lateral direction.

The undrained shear strength (c_u) of clay affects the bearing capacity of the soil. The range of c_u in this study includes soft clay ($c_u=5$ kPa) to stiff clay ($c_u=95$ kPa). Furthermore Rowe and Davis (1982) indicated that break away condition of lateral or vertical anchors depends on the ratio of overburden pressure to undrained shear strength of clay ($\frac{\gamma H}{c_u}$) which is in the range of 0.5 to 6.5 in this study and covers most practical conditions.

4. Results and discussion

Response surface methodology (RSM) is used in this study to define how these factors interact with each other and the significance of the effect of each factor on the response as well as to obtain a simplified equivalent response surface to predict responses for a given level of factors. Analyses are conducted using Design Expert v.6 software (www.statease.com).

4.1. Lateral pipe/soil interaction

Assessing the results of finite element analysis using RSM method of two non-dimensional factors H/D and $\frac{\gamma H}{c_u}$, on the non-dimensional lateral interaction factor results in the following equation:

$$N_{ch} = N_{ch}^* + \beta_h \frac{\gamma H}{c_u} \quad (\text{Eq.6})$$

Where;

$$N_{ch}^* = 0.20 * \frac{H}{D} * (10.5 - \frac{H}{D}) + 2 \quad \text{for } H/D < 5 \quad (\text{Eq.7})$$

$$N_{ch}^* = 7.5 \quad \text{for } H/D \geq 5$$

$$\beta_h = 0.97 + 0.07 * \frac{H}{D} - 0.052 * \frac{\gamma H}{c_u} \quad (\text{Eq.8})$$

Equations 6 to 8 are valid for $1 \leq \frac{H}{D} \leq 7$ and $0.5 \leq \frac{\gamma H}{c_u} \leq 6.5$.

Fig.3 compares the weightless term of the interaction factor (N_{ch}^*) with Rowe and Davis (1982) upper and lower bound solutions that are based on no break away and immediately break away assumptions respectively. Also it is compared to Hansen's analytical and Phillips et al. (2004) numerical solutions. The interaction factor increases up to an embedment ratio of 5 and then remains constant.

Fig.4 shows changes in the contribution of the overburden ratio in interaction factor in Eq.6, with $\frac{H}{D}$ and $\frac{\gamma H}{c_u}$. The slope of each line at each point is β_h that determines the amount of the soil weight that contributes to the lateral soil restraint on the pipeline. Coefficient β_h may be related to the geometry of the failure surfaces or the size of the passive wedge in front of the pipeline.

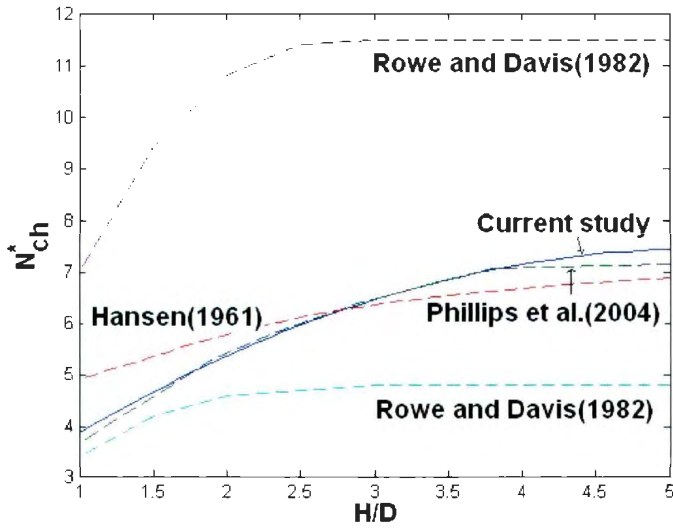


Fig.3: Comparison of lateral interaction factor for a weightless soil with some existing solutions

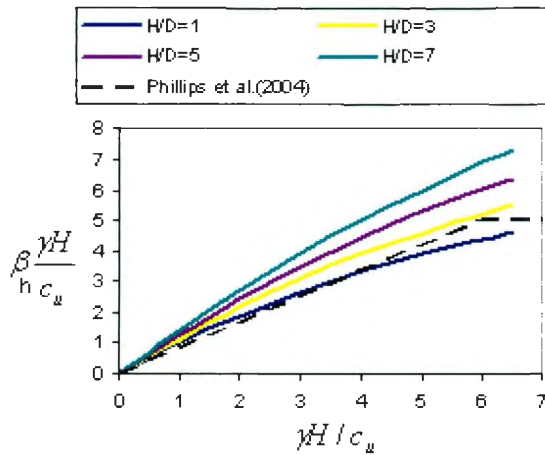


Fig.4: Variations of the weight term of the lateral interaction factor with $\frac{H}{D}$ and $\frac{\gamma H}{c_u}$

4.2. Vertical pipe/soil interaction

Similar analysis on vertical pipe/soil interaction yields the following equations for the vertical interaction factor:

$$N_{cv} = N_{cv}^* + \beta_v \frac{\gamma H}{c_u} \quad (\text{Eq.9})$$

Where:

$$N_{cv}^* = 0.25 * \frac{H}{D} * (11.2 - \frac{H}{D}) - 0.94 \quad \text{for } H/D < 5.5 \quad (\text{Eq.10})$$

$$N_{cv}^* = 6.9 \quad \text{for } H/D \geq 5.5$$

$$\beta_v = 1.034 + 0.039 * \frac{H}{D} - 0.06 * \frac{\gamma H}{c_u} \quad (\text{Eq.11})$$

Equations 9 to 11 are valid for $1 \leq \frac{H}{D} \leq 7$ and $0.5 \leq \frac{\gamma H}{c_u} \leq 6.5$.

The resulted weightless term of the interaction factor (N_{cv}^*) is compared with Rowe and Davis (1982) upper and lower bound solutions and Vesic's cavity expansion solution in Fig.5. As it is indicated in the figure the interaction factor increases up to an embedment ratio of 5.5 and for larger H/D it remains constant. Fig.6 plots the weight term of the interaction factor (Eq.9). Coefficient β_v changes from 1 to 1.25 at small $\frac{\gamma H}{c_u}$ to 0.65 to 0.9 at large $\frac{\gamma H}{c_u}$.

As Merifield et al. (2001) indicated the critical embedment depth (where the failure mechanism changes from a surface failure to a fully flow around mechanism) is a complex function of overburden ratio and embedment ratio. Figs.7 and 8 indicate both the lateral and vertical interaction factors (which are plotted based on equations 6 and 9) increase by overburden ratio but the rate of increase decreases up to a limiting point

where the shallow behavior changes to deep mechanism. In other words in a constant embedment depth the soil failure mechanism can be shallow or deep depending on the value of $\frac{\gamma H}{c_u}$. The effect of $\frac{\gamma H}{c_u}$ on changing the failure mechanism from local shear failure to a flow around mechanism for an oblique loading case can be observed in Fig.9. The limiting value for overburden ratio could not be captured in this study as it seems to be more than 6.5 that is the maximum value for $\frac{\gamma H}{c_u}$ in this study.

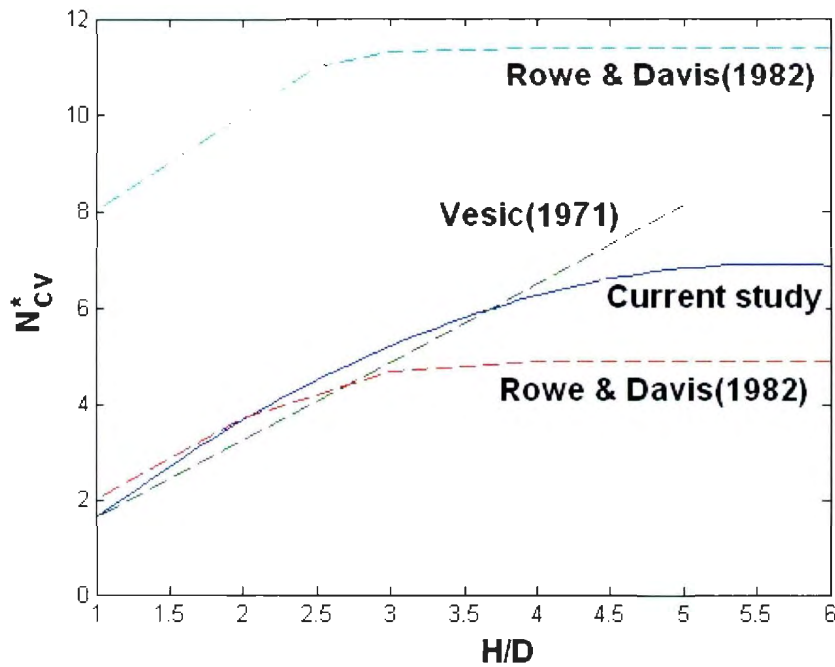


Fig.5: Comparison of vertical interaction factor for a weightless soil with some existing solutions

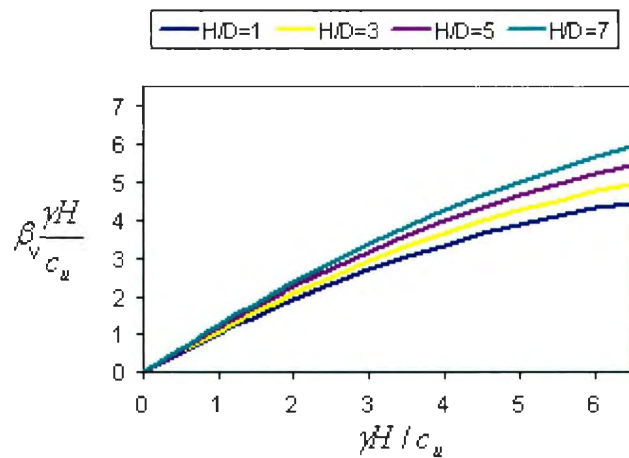


Fig.6: Variations of the weight term of the vertical interaction factor with $\frac{H}{D}$ and $\frac{\gamma H}{c_u}$

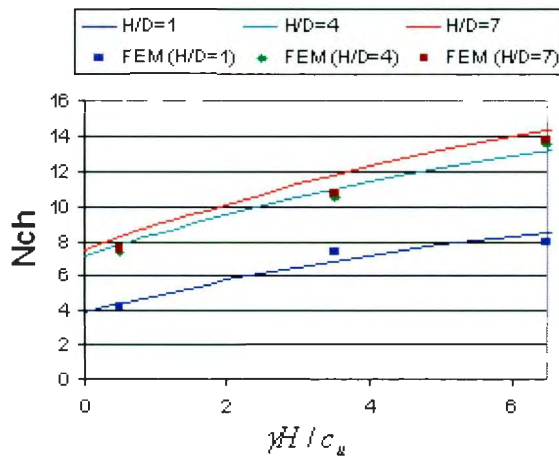


Fig.7: Effect of overburden ratio on lateral vertical interaction factor

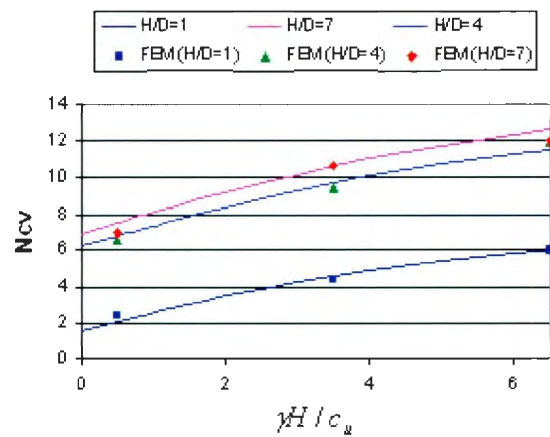
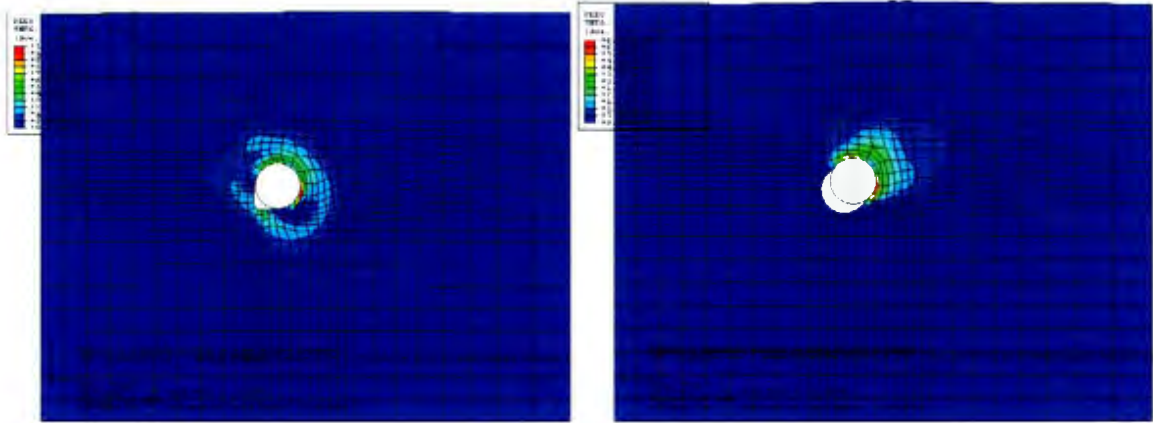


Fig.8: Effect of overburden ratio on interaction factor



a) $H/D=4$, $\gamma H/c_u=6.5$, $\text{angle}=45$

b) $H/D=4$, $\gamma H/c_u=0.5$, $\text{angle}=45$

Fig.9: Effect of $\frac{\gamma H}{c_u}$ on changing the failure mechanism for oblique pipe/soil interaction

(Disp./D=0.2)

4.3. Oblique pipe/soil interaction

Similar RSM analyses are conducted for oblique pipe/soil interaction. The factors are $\frac{H}{D}$

, $\frac{\gamma H}{c_u}$ and k (oblique angle(α)/90). The responses are p/p_u and q/q_u ratios between lateral

(p) and vertical (q) components of oblique load and soil loads when the pipeline moves laterally (p_u) or vertically (q_u). Ratios of oblique load components to the pure ultimate loads in lateral and vertical directions are calculated as:

$$\frac{P}{p_u} = k (1.576 - 0.576 k) \quad (\text{Eq.12})$$

$$\frac{q}{q_u} = 1 - k (0.244 + 0.756 k) \quad (\text{Eq.13})$$

As it is reflected in equations 12 and 13, effects of $\frac{H}{D}$ and $\frac{\gamma H}{c_u}$ are not significant when normalized loads p/p_u and q/q_u are used as responses. Equations 12 and 13 are plotted and compared to other methods in Fig.10. Results of current study are located generally between Nyman (1982) and Guo (2005) solutions and are very close to the range of the experimental results by Das (1985) and Meyerhof and Hanna (1978)'s solution for inclined loaded foundations. In Fig.10 Nyman (1982), Meyerhof and Hanna (1978) and Das (1985) results are shown by an assumption of $p_u/q_u=1.5$.

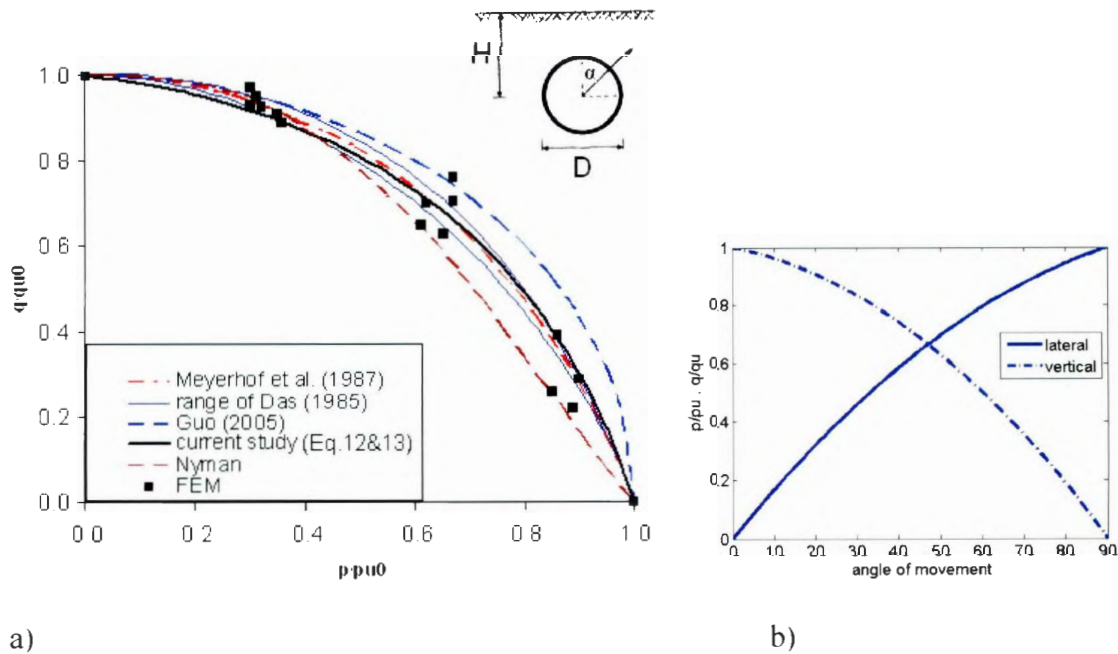


Fig.10: Normalized lateral and vertical components of ultimate oblique load on the pipeline. a) comparison to other studies, b) from equations 12 and 13.

Unlike Nyman (1982) and most of other researchers who assume that the direction of oblique load on the pipeline coincides with the direction of pipe movement in the soil which is not always true for this case, there is no need for such assumption in this study as the lateral and vertical components are calculated separately.

5. Conclusions

This paper investigated the ultimate loads on pipelines during oblique lateral-vertical pipe/soil relative displacements. Numerical analysis using finite element and von-Mises plasticity for soil was conducted and response surface methodology was used to process the numerical analysis results and produce replacement models for the soil/pipeline interaction forces.

Expressions for the lateral and vertical components of the oblique load on the pipeline are proposed as a function of the angle of movement and the pure lateral and vertical restraints on the pipeline. Relevant equations are suggested to find the pure lateral and vertical restraints on the pipeline using pipe/soil geometrical and mechanical properties. Dependence of the lateral, vertical and oblique load to the embedment ratio and overburden ratio is indicated. This study is a work in progress and updated results will be published later.

6. References

Audibert, J.M.E., and Nyman, K.J. (1977). Soil restraint against horizontal motion of pipes. *Journal of the geotechnical engineering division, ASCE*. 103(10), 1119-1142.

- Das, B.M. (1985). Resistance of shallow inclined anchors in clay. Uplift behavior of anchor foundations in soil. S.P. Clemence, ed., ASCE, NewYork
- Guo, P. (2005). Numerical modeling of pipe-soil interaction under oblique loading. Journal of Geotechnical and geoenvironmental engineering, ASCE, 131(2), PP. 260-268.
- Hansen, J.B. (1961). The ultimate resistance of rigid piles against transversal forces. Bulletin 12, Danish geotechnical institute, Copenhagen, Denmark, pp.5-9.
- Honegger, D.G., Nyman, J. (2004). Guidelines for the seismic design and assessment of natural gas and liquid hydrocarbon. Pipeline Research Council International.
- Hsu, T.W. (1996). Soil restraint against oblique motion of pipelines in sand. Canadian geotechnical journal, pp. 180-188.
- Mackenzie, T.R. (1955). Strength of deadman anchors in clay. MSc. Thesis, Princeton University, USA.
- Merifield, R.S., Sloan, S.W. and Yu, H.S. (2001). Stability of plate anchors in undrained clay. Geotechnique 51, No.2, 141-153.
- Meyerhof, G.G. (1973). Uplift resistance of inclined anchors and piles. Proceedings 8th international conference on soil mechanics and foundation engineering, Vol.2, Moscow, USSR, pp.167-172.
- Meyerhof, G.G., and Hanna, A.M. (1978). Ultimate bearing capacity of foundation on layered soil under inclined load. Can. Geotech. J., 15(4), 565-572.
- Neely, W.J., Stuart, J.G. and Graham, J. (1973). Failure load of vertical anchor plates in sand. Journal of the soil mechanics and foundations division, ASCE, 99(9), 669-685.

- Ng, P.C.F. (1994). Behavior of buried pipelines subjected to external loading. Ph.D. Thesis. University of Sheffield, England.
- Nyman, K.J. (1982). Soil response against the horizontal-vertical motion of pipes. Preprint 82-534. Presented at ASCE National Convention, New Orleans.
- Paulin, M.J. (1998). An investigation into pipelines subjected to lateral soil loading. Ph.D. Thesis, Memorial University of Newfoundland, St.John`s, Canada.
- Paulin, M.J., Phillips, R., Clark, J.I., Trigg, A. and Konuk, I. (1998). A full scale investigation into pipeline/soil interaction. Proceedings of 1998 International Pipeline Conference, ASME, Calgary, AB, June 1998, Vol.2, pp.779-787.
- Phillips, R., Nobahar, A. and Zhou, J. (2004). Trench effects in pipe-soil interaction. Proceedings of IPC2004, International pipeline Conference, Calgary, Canada.
- Popescu, R., Konuk, I. (2001). 3D finite element analysis of rigid pipe interaction with clay. Proceedings 10th international conference on computer methods and advances in geomechanics, Tucson, AZ, vol.2, pp.971-976.
- Popescu, R., Phillips, R., Konuk, I. and Deacu, D. (1999). Numerical and physical analysis of pipe-soil interaction, Proceedings 52th Canadian geotechnical conference, Regina, Sask., pp.437-444.
- Rizkalla, M., Poorooshab, F. and Clark, J.I. (1992). Centrifuge modeling of lateral pipeline/soil interaction. Proceedings of 11th offshore mechanics and arctic engineering symposium, 13p.
- Rowe, R.K., and Davis, E.H. (1982). The behavior of anchor plates in clay. Gotechnique, 32(1), 9-23.

Vesic, A.S. (1971). Breakout resistance of objects embedded in ocean bottom. *J. Soil Mech. Found. Div. ASCE* 97, No.9, 1183-1205.

Wantland, G.P., O'Neil, M.B., Coelogyne, E.H. and Reese, L.C. (1982). Pipeline lateral stability in soft clay. *Journal of petroleum technology*, 34(1), 217-220.

Appendix B: Examples of Structural Modeling of Pipeline/Soil Interaction Considering the Effect of Axial-Lateral Pipe/Soil Interaction

8.3 B.1 Introduction

This section presents some examples to show the effect of considering the axial-lateral pipe/soil interaction on the level of strains in the pipeline. The analyses are conducted using finite element structural modeling with ABAQUS/Standard software package. The pipeline was discretized using 3-node quadratic PIPE32 elements. These elements consider a constant hoop stress under internal and external pressures. The elasto-plastic stress-strain relationship in pipeline is considered using Ramberg-Osgood formulation and von-Mises failure criteria.

The soil response is defined using three perpendicular springs as recommended by guidelines (discussed in Chapter 2). Linear, 2-node, 3-D truss elements, T3D2, are used to define the soil springs. The reason to use truss elements instead of spring elements is the need to update the elements' stiffness at each increment based on interdependence of loads in axial and lateral soil springs. The dependency of loads in axial and lateral soil springs (i.e. truss elements) is implemented using a FORTRAN subroutine.

Two examples of pipelines buried in sand subjected to large soil displacements are presented. The soil displacements are applied at the supporting end of the truss elements (Figure B-1). For each example the analysis are conducted for two cases of conventional independent soil springs and dependent soil springs in axial and lateral directions according to interaction curves presented in Chapter 6 (Figure 6-3). Comparisons are made to show the effect of considering the axial-lateral pipe/soil interaction (as described in this thesis) on the pipeline strains.

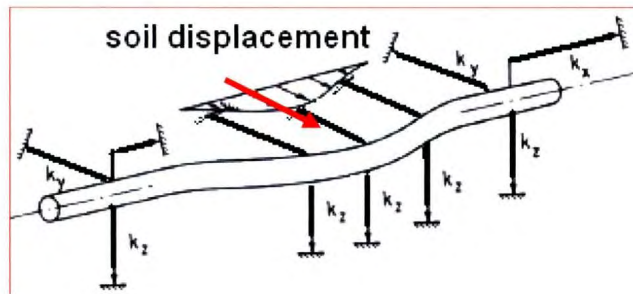


Figure B-1: Schematic configuration of soil springs and soil displacement applied to the pipe.

In both examples a length of 172 m of a pipeline is considered (Figure B-2). The pipeline is subjected to 5 m lateral and 1.2 m vertical soil displacements at 60 m of its length. Pipes' diameters, thicknesses and internal pressures for the two cases are shown in Table B-1.

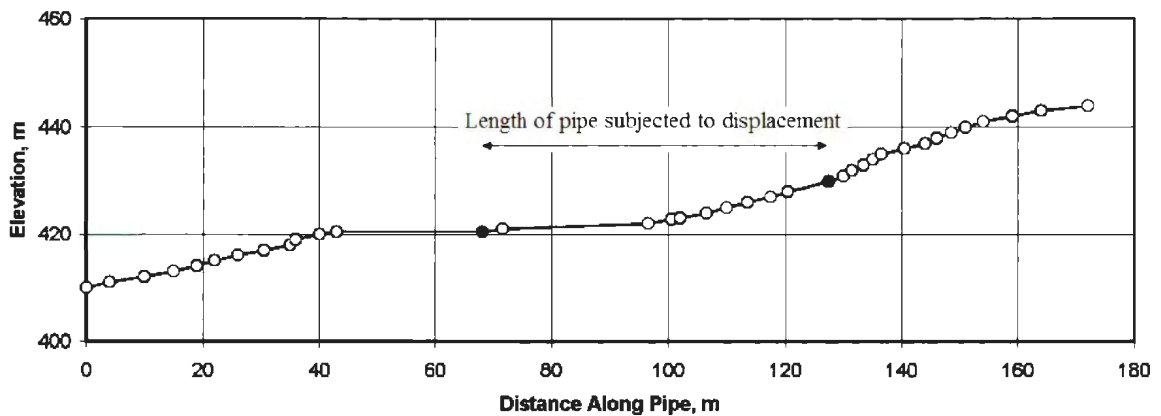


Figure B-2: General configuration of the pipeline discussed in examples 1 and 2.

Table B-1: Pipe geometry and internal pressures for two examples

	Pipe outer diameter (m)	Thickness (mm)	Internal pressure (MPa)
NG line	0.81	17.5	9.9
NGL line	0.355	6.35	10.4

The pipe material for both cases is of grade X70 with 414 MPa yield stress. The ultimate loads and displacements for each direction are calculated based on guidelines recommendations (Honegger and Nyman 2004) and are presented in Table B-2.

For each example the analyses are conducted for two cases of without and with considering the axial-lateral interaction.

Table B-2: Summary of equivalent prototype test parameters

Direction	Ultimate load (kN/m)		Ultimate displacement (m)	
	NG line	NGL line	NG line	NGL line
Axial	33	22	0.005	0.005
Lateral	185	167	0.084	0.098
Vertical upward	39	68	0.026	0.034
Vertical downward	619	360	0.102	0.051

8.4 B.2 Example 1: NG line

Figure B-3 shows the axial-lateral interaction curve using the equations discussed in Chapter 6 and geometrical and mechanical properties summarized in Tables B-1 and B-2. Relative displacements in both positive and negative directions are considered.

The soil reaction forces on pipeline and the pipe/soil relative displacements, without considering the axial-lateral pipe/soil interaction are presented in Figures B-4 and B-5. The axial strain in the pipeline calculated for this case is shown in Figure B-6. Same quantities are shown in Figures B-7, B-8 and B-9 with considering the interaction effect between axial and lateral soil reactions on pipe.

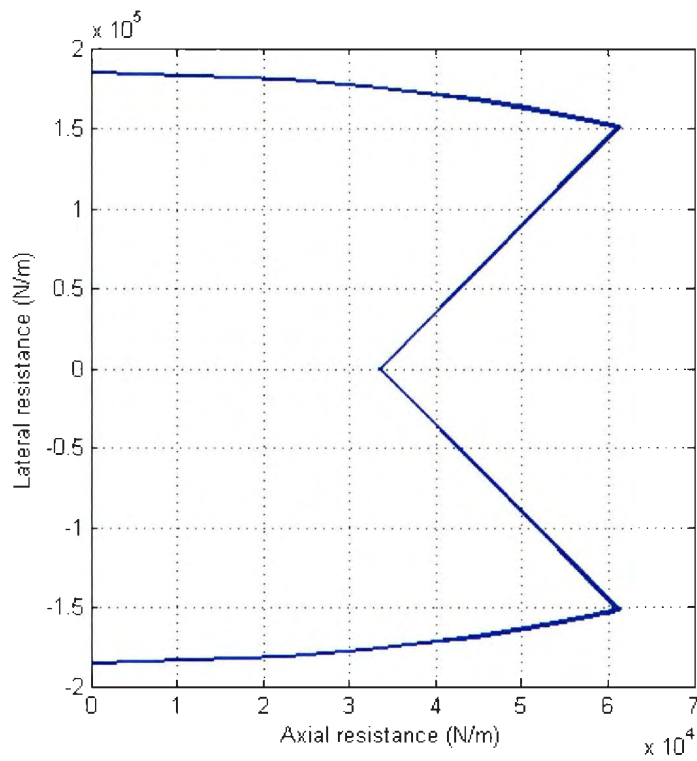


Figure B-3: Axial-lateral interaction curve for soil restraint on NG pipeline.

NG- No Interaction

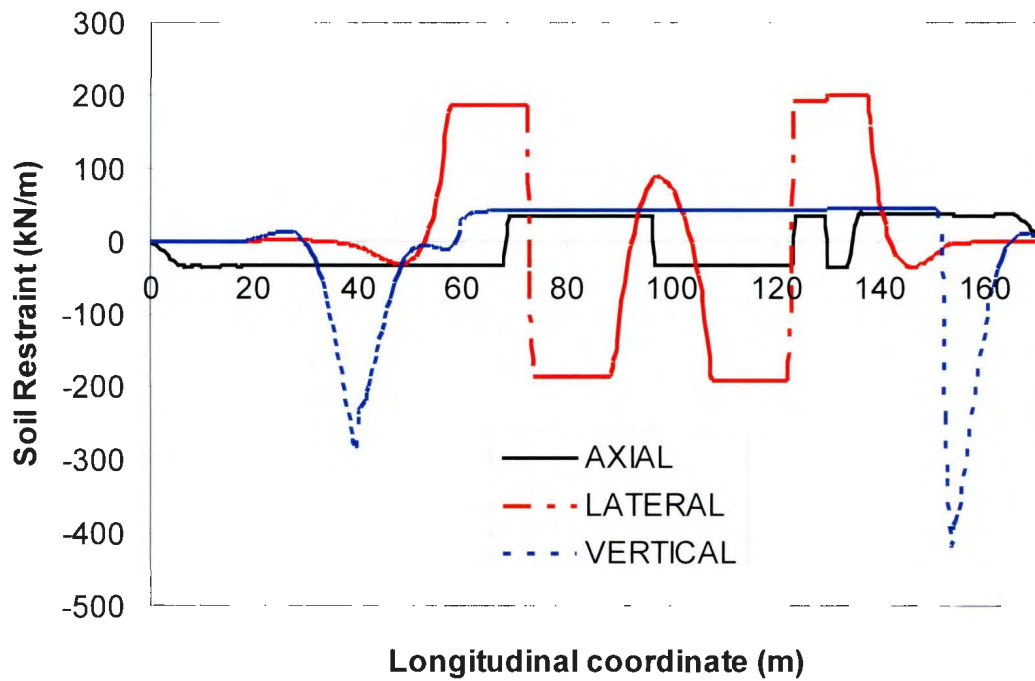


Figure B-4: Soil reaction forces on pipeline when no interaction is considered.

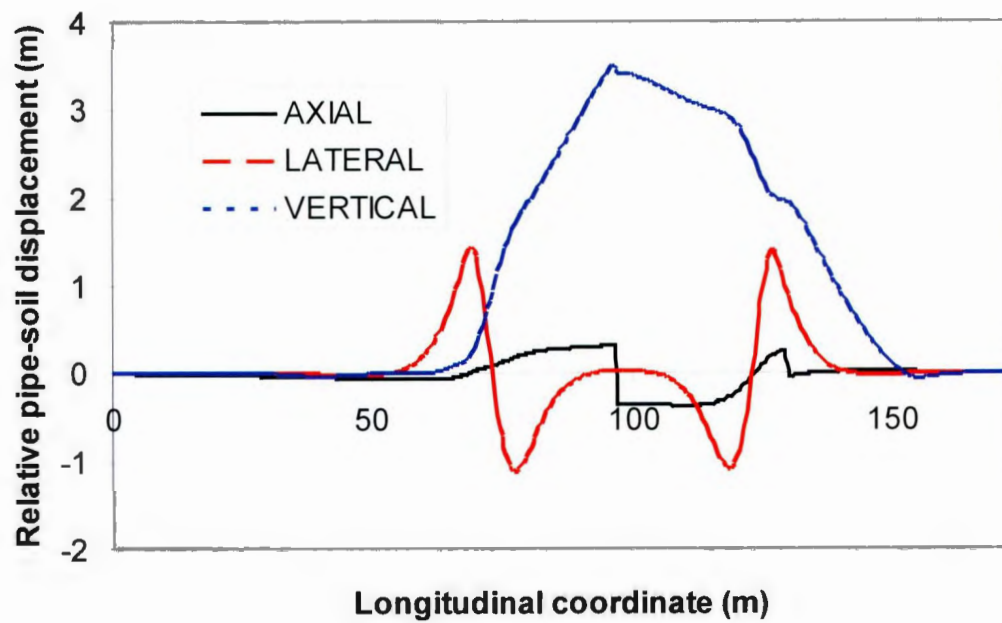


Figure B-5: Relative pipe/soil displacement when no interaction is considered.

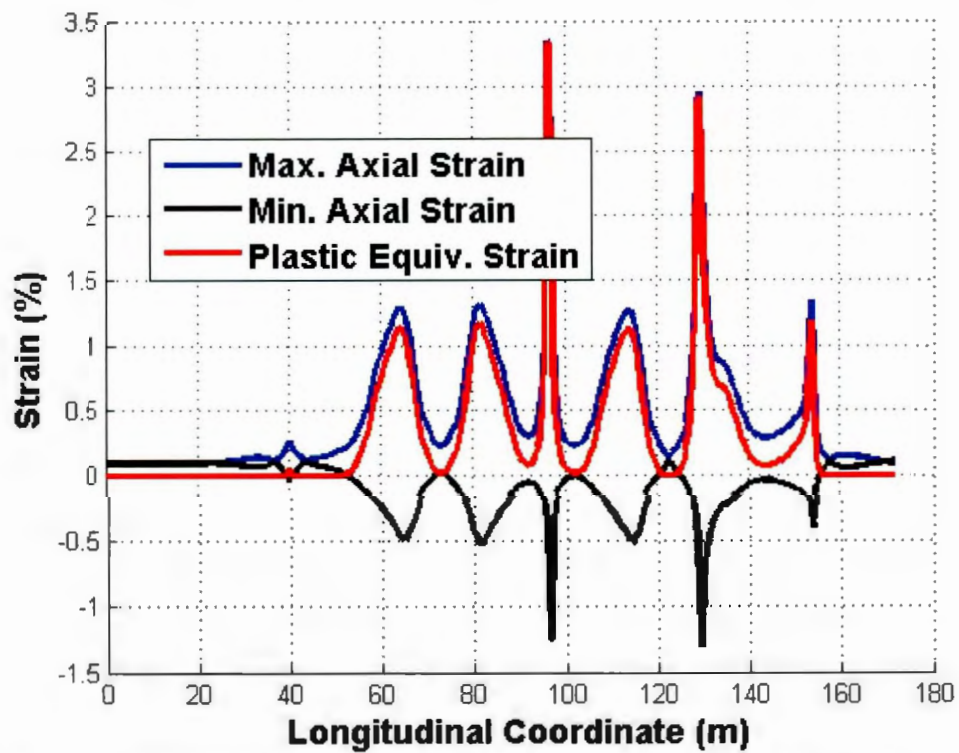


Figure B-6: Maximum, minimum axial strain and equivalent plastic strain in the pipe section when no interaction is considered.

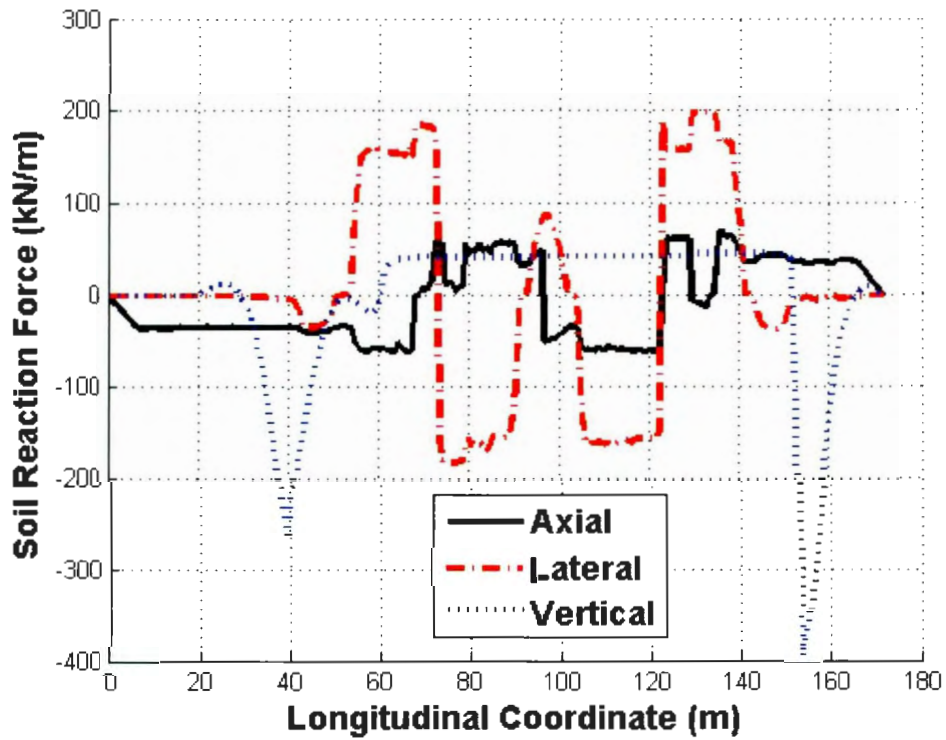


Figure B-7: Soil reaction forces on pipeline when interaction is considered.

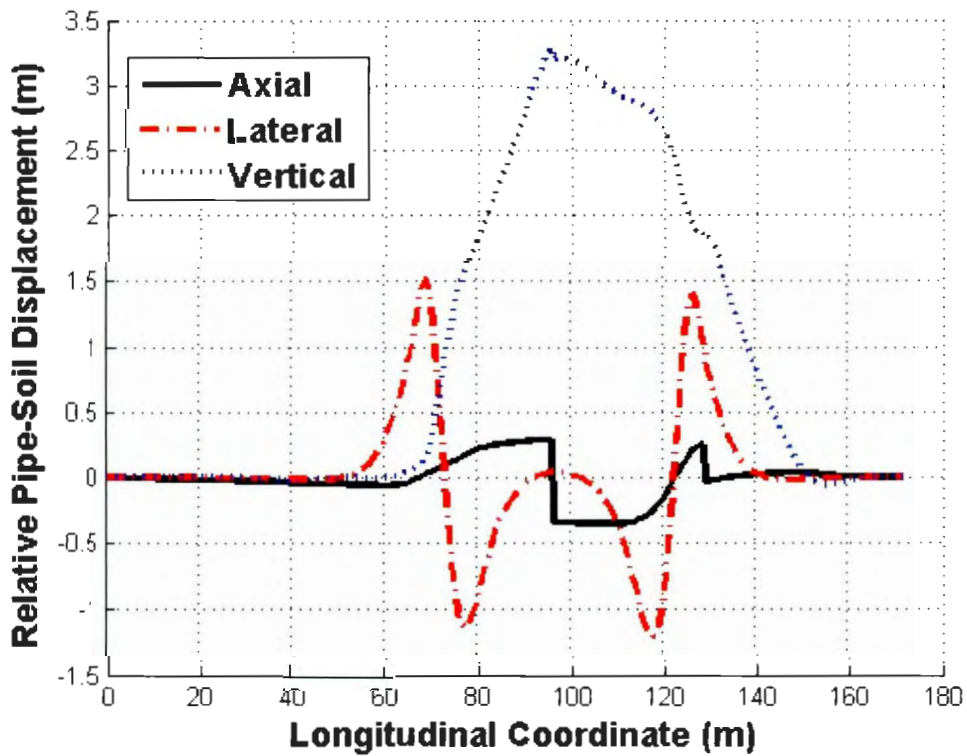


Figure B-8: Relative pipe/soil displacement when interaction is considered.

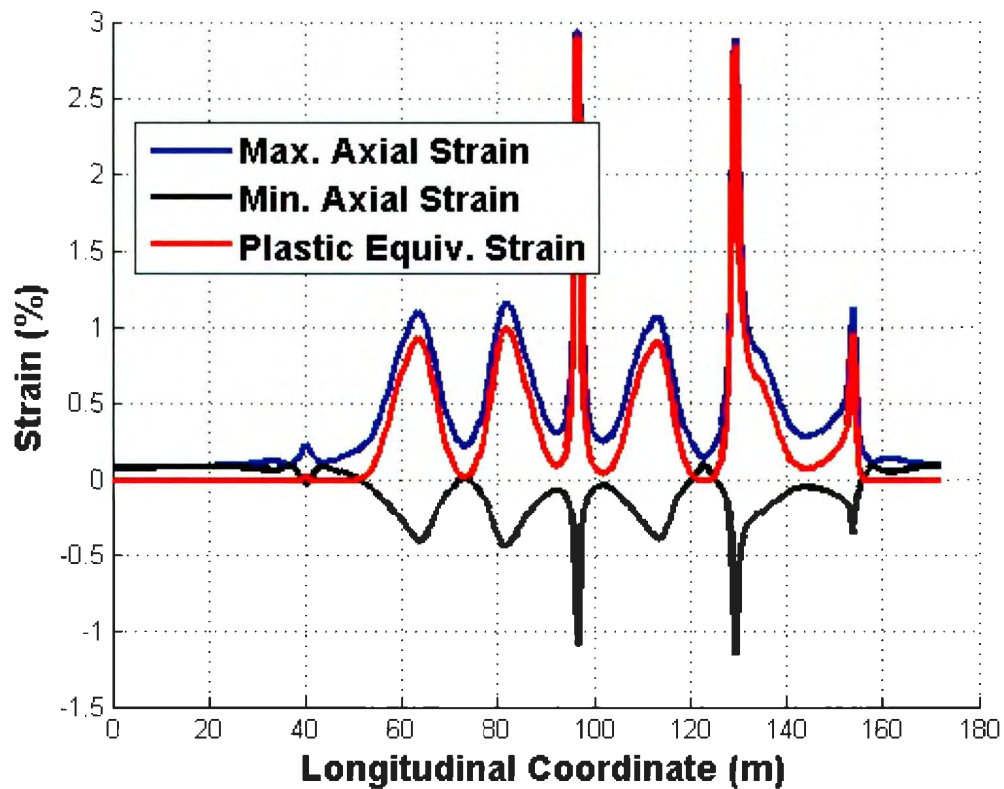


Figure B-9: Maximum, minimum axial strain and equivalent plastic strain in the pipe section when interaction is considered.

The maximum axial strains for the two cases, with and without interaction, occur at the same places of the length of the pipeline. These are the points with maximum change in elongation in the loaded part of the pipeline. The maximum strain in the pipeline decreases by about 12% by considering the interaction effect. This reduction can be attributed to the increase in the soil axial restraint on the pipeline by considering the interaction effect and also the reduction in the lateral restraint.

8.5 B.3 Example 2: NGL line

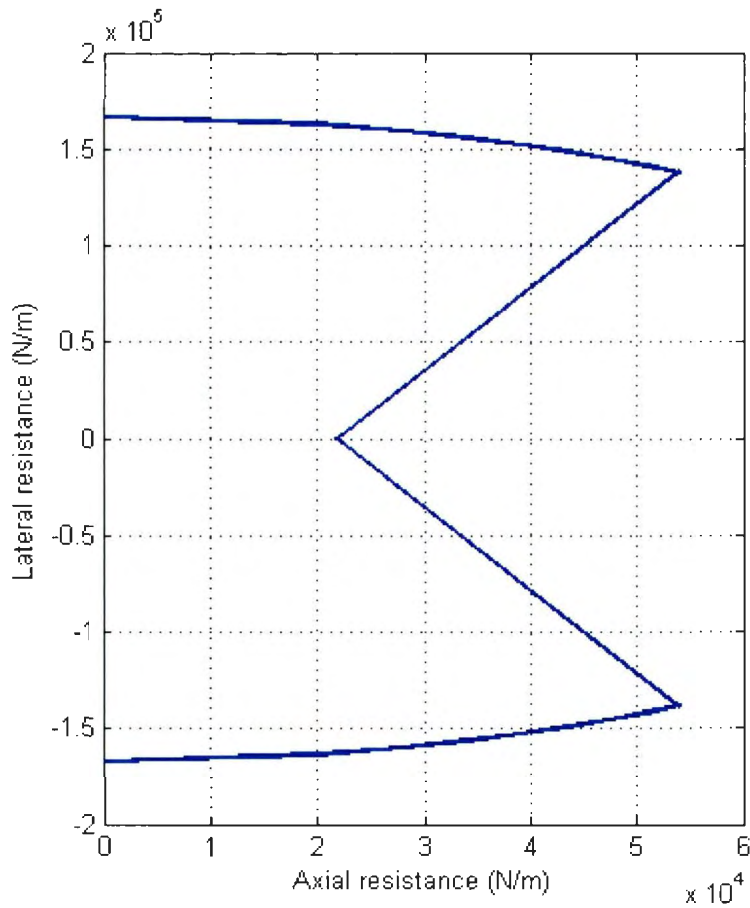


Figure B-10: Axial-lateral interaction curve for NGL line.

A similar problem to section B-2, with a more flexible pipeline NGL, is considered in this section. The soil reaction forces on pipeline, pipe/soil relative displacements and the maximum axial strain at each section in the pipeline, without and with considering the axial-lateral pipe/soil interaction effect, are presented in Figures B-11, B-12, B-13, B-14, B-15 and B-16 respectively. The axial-lateral interaction curve is shown in Figure B-10.

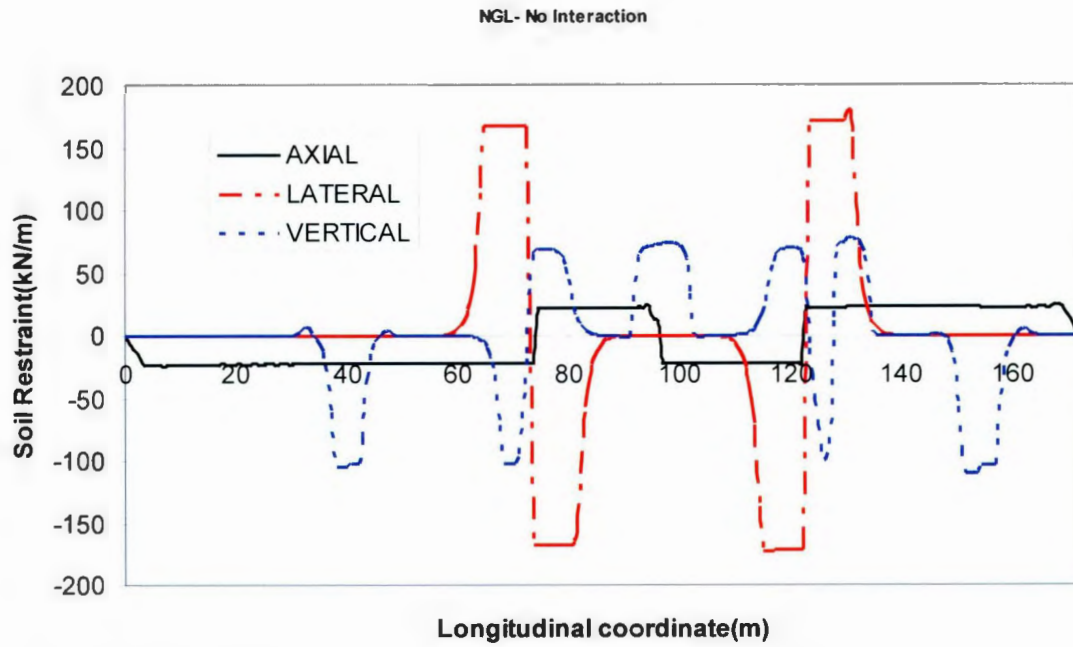


Figure B-11: Soil reaction forces on pipeline when no interaction is considered.

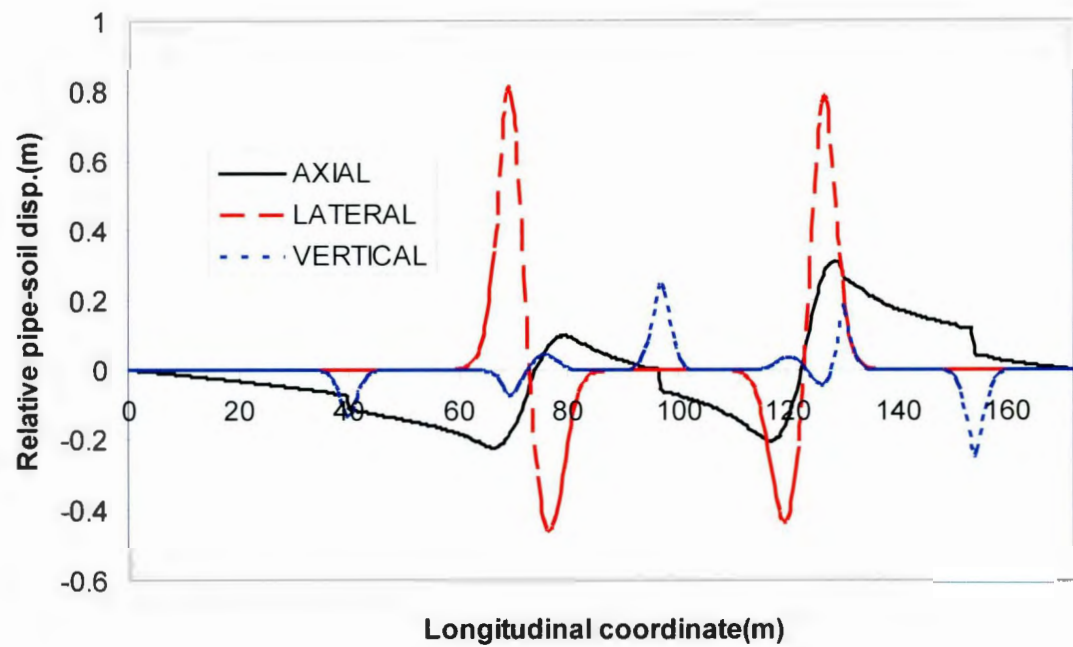


Figure B-12: Relative pipe/soil displacement when no interaction is considered.

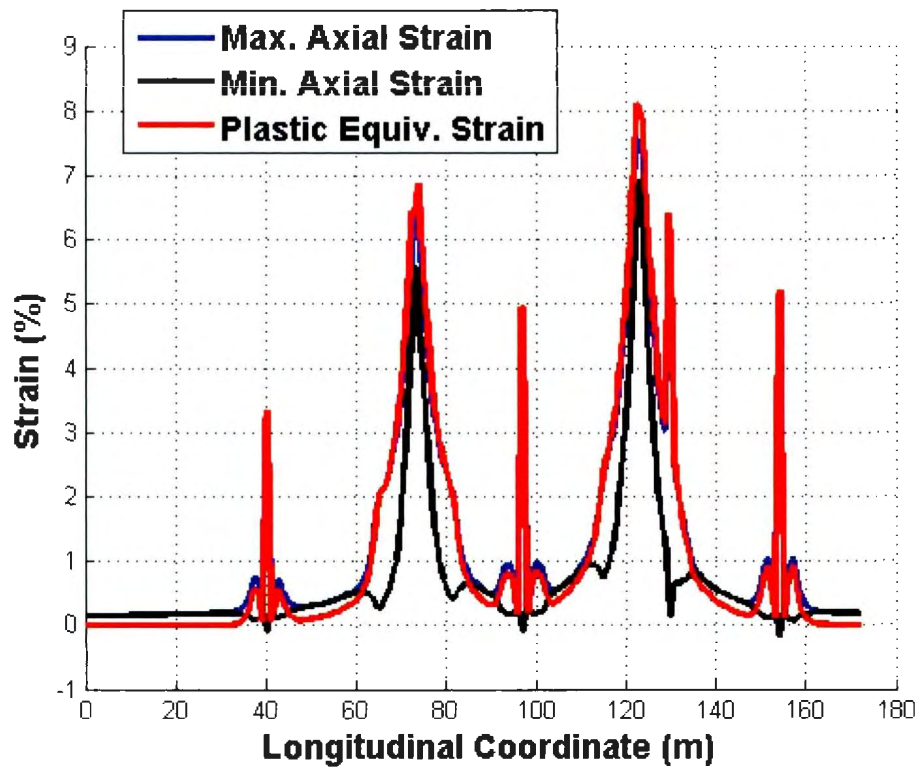


Figure B-13: Maximum, minimum axial strain and equivalent plastic strain in the pipe section when no interaction is considered.

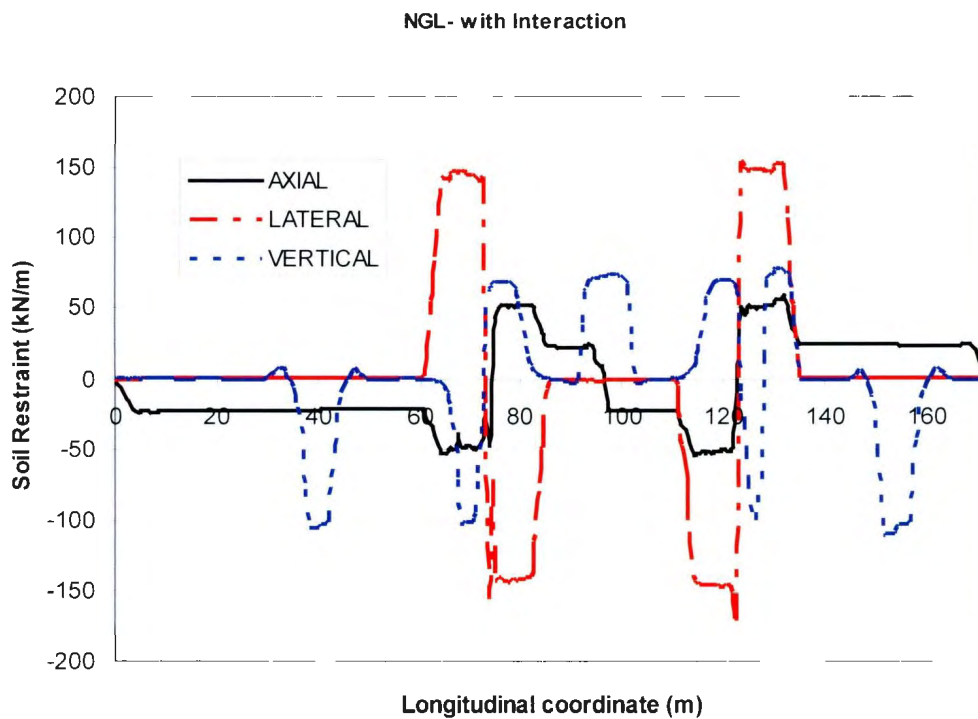


Figure B-14: Soil reaction forces on pipeline when interaction is considered.

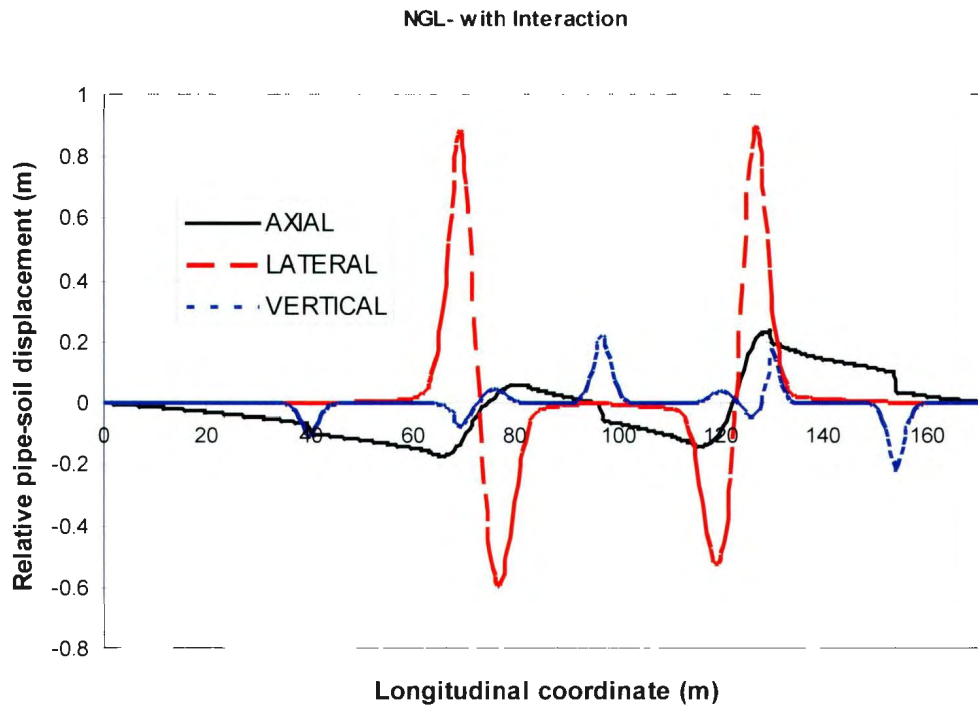


Figure B-15: Relative pipe/soil displacement when interaction is considered.

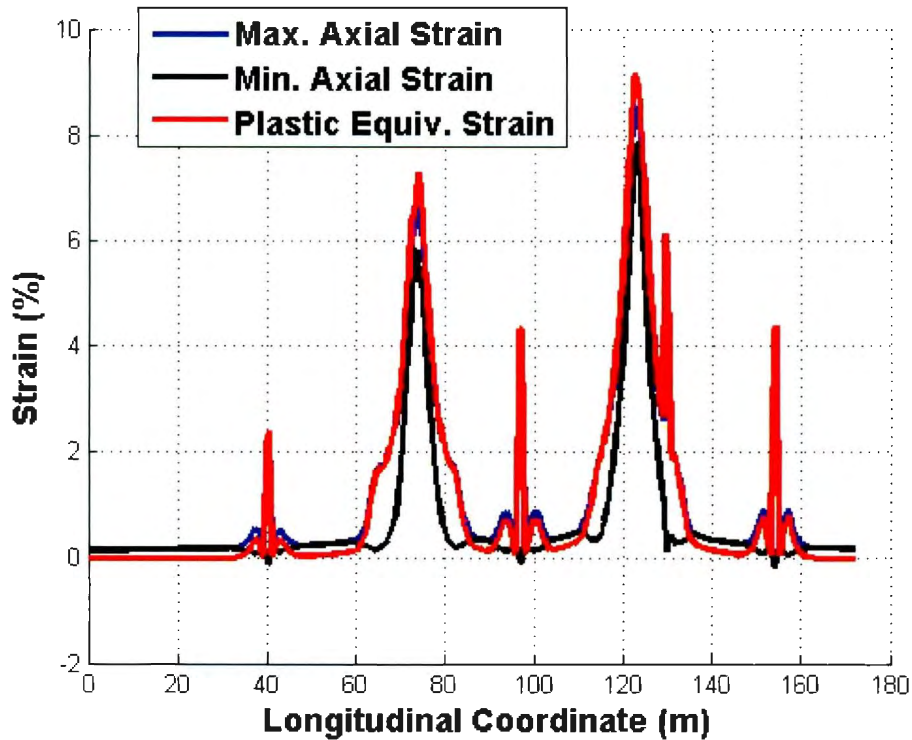


Figure B-16: Maximum, minimum axial strain and equivalent plastic strain in the pipe section when interaction is considered.

Comparison of Figures B-13 and B-16 shows because of higher flexibility of NGL pipeline, peak strains occur at all places of change in pipe elongation. By considering the interaction effect the maximum strains in the pipeline change in different ways. While the larger peaks in the strains increase by about 13%, the smaller peaks at the points of change in direction decrease by up to 33%. This observation may be attributed to the fact that the interaction effect varies for different relative displacement schemes (i.e. oblique angles) between soil and pipeline. For smaller oblique angles the axial ultimate soil restraint increases and the lateral soil restraint decreases while for larger oblique angles (close to pure lateral movements) the changes in the soil restraint are less significant.

The two examples discussed in this Appendix show the effect of axial-lateral pipe/soil interaction on the internal strains of pipelines can be significant. Depending on the pipeline geometry and the displacement pattern applied to the pipeline the internal strains may increase or decrease. This effect will be more important and more difficult to predict when a three-dimensional pipeline/soil relative displacement occurs. Therefore it is important to understand this interaction effect and consider it in the engineering guidelines. A method such as proposed by Cocchetti et al. (2009b) can be a practical tool to account for pipe/soil interaction effect in numerical structural modeling.

